Arne Fjeldstad

Modelling of Fatigue Crack Growth at Notches and Other Stress Raisers

Thesis for the degree philosophiae doctor

Trondheim, November 2007

Norwegian University of Science and Technology
Faculty of Engineering Science and Technology
Department of Engineering Design and Materials

NTNU

NTNU
Norwegian University of Science and Technology

Thesis for the degree philosophiae doctor

Faculty of Engineering Science and Technology
Department of Engineering Design and Materials

ISBN 978-82-471-5109-9 (printed version)
ISBN 978-82-471-5112-9 (electronic version)
ISSN 1503-8181

Doctoral theses at NTNU, 2007:231

Printed by NTNU-trykk

Preface

This thesis consists of an introduction and eight papers. Seven papers are either published or in the process of being published. The work has been carried out in close cooperation with colleagues at NTNU and SINTEF with supervision from Professor Gunnar Härkegård.

In Paper 1, the manuscript was developed together with Dr Bård Wathne Tveiten (SINTEF), while the statistical evaluation was carried out by me. In Paper 2 and Paper 5 to 8, manuscript and theory were done in cooperation with Anders Wormsen. In the development of the computer code P•FAT, the statistical work was largely implemented by Anders Wormsen (NTNU), while the crack growth modelling was largely implemented by me. This will to some extent reflect the individual contributions in Paper 6 and 7.

In Paper 2 and 3, I am the main author and solely responsible for the theory, the calculations and the manuscript.

Acknowledgement

This work has been made possible by the support from the Research Council of Norway and the Norwegian light metal industry through the NorLight project. The project was carried out at the department of Engineering Design and Materials at the Norwegian University of Science and Technology (NTNU). All contributing parties are greatfully acknowledged.

I wish to express my deepest gratitute to my supervisor Professor Gunnar Härkegård who throughout my doctoral studies has contributed with excellent scientific support and inspiration. I am also gratefull to my co-supervisor Dr Bård Wathne Tveiten for always taking keen interest in my work. I wish to thank my colleague and friend Anders Wormsen for the close collaboration. I really cherish all the endless discussions and your critical mind, which ulimately has lead to results we both can be proud of. I also wish to thank my former colleagues at NTNU: Dr Hans Jörg Huth and Dr Torsten Mann.

Furthermore, I wish to thank all my friends for all the support. A special thanks to my parents for always supporting me. Finally, I would like to thank my lovely wife Signe for waiting patiently.

Abstract

This thesis consists of an introduction and eight papers [1–8]. Paper 1 presents simple and flexible methods to enhance the fatigue life of welded aluminium components. The key element of the methods is to change residual stresses from tension to compression at locations vulnerable to fatigue crack growth. This is accomplished by mechanical pre-stressing using elastic pre-deformation or thermal pre-stressing using induction heating. Based on fatigue test results induction heating tuned out to be the most promising method.

In Paper 2, an approximate method based on asymptotic solutions for estimating the stress intensity factor for cracks at stress concentrations is presented. The proposed solution makes use of the near-notch and remote-notch solution to interpolate over the entire range from shallow to deep cracks. Paper 3 extends the theory presented in Paper 2 to cover through-cracked plates of finite width subjected to bending or tension. Paper 4 examines how a decreasing stress field influences the fatigue crack growth. Even though the stress generally decreases from a maximum at some critical point, fatigue crack growth analyses are often performed assuming a homogeneous stress state to avoid the difficulties related to crack growth analyses in complex components. The degree of conservatism has been determined by comparing the calculated fatigue life of cracks growing in a homogeneous stress field with the fatigue life of cracks growing in a gradient stress field. In Paper 5, an approximate method based on asymptotic solutions for estimating the stress intensity factor for cracked V-notched plates is presented. The proposed solutions make use of a reference solution to interpolate from shallow to deep cracks. The reference solution is obtained by considering the current crack emanating from the associated specimen with a sharp notch. It is showed how the proposed theory can be used for estimating the stress intensity factor for a crack located at the root of a weld toe in a T-joint.

Paper 6 and 7 presents the probabilistic fatigue assessment tool, P•FAT, for the fatigue analysis of arbitrary components. General concepts which have to be considered for the accomplishment of a 3D fatigue crack simulation by post-processing results from a standard finite element analysis are introduced. General features such as determination of the life controlling defect, fatigue strength and

fatigue life distribution, and probability of component failure, have been presented. Furthermore, a new short crack growth model that accounts for short crack growth is presented. In Paper 8, the short crack growth model is used to predict the arrest of cracks growing in stress gradient fields. The predictions have been compared with experimentally obtained data for notched specimens and found to agree well.

List of papers

This work comprises an introduction and eight papers:

1. B. W. Tveiten, A. Fjeldstad, G. Härkegård, O. R. Myhr and B. Bjørneklett: Fatigue life enhancement of aluminium joints through mechanical and thermal prestressing. *International Journal of Fatigue*, Vol. 28, 2006, pp. 1667-1676.

2. A. Wormsen, A. Fjeldstad and G. Härkegård: The application of asymptotic solutions to a semi-elliptical crack at the root of a notch: *Engineering Fracture Mechanics*, Vol. 73, 2006, pp. 1899-1912.

3. A. Fjeldstad, G. Härkegård and A. Wormsen: The stress intensity factor for a crack in a finite notched plate based on asymptotic solutions. Submitted for publication in *Engineering Fracture Mechanics*.

4. A. Fjeldstad, G. Härkegård and A. Wormsen: The influence of a stress gradient on the growth of a fatigue crack. Proceedings of the *International Fatigue Congress*, Atlanta, USA, 2006.

5. A. Fjeldstad, A. Wormsen and G. Härkegård: Approximate stress intensity factors for cracked V-notched specimens based on asymptotic solutions with application to T-joints. Accepted for publication in *Engineering Fracture Mechanics*.

6. A. Wormsen, A. Fjeldstad and G. Härkegård: A post-processor for fatigue crack growth analysis based on a finite element stress field. Accepted for publication in *Computer Methods in Applied Mechanics and Engineering*.

7. A. Fjeldstad, A. Wormsen and G. Härkegård: Simulation of fatigue crack growth in components with random defects. Accepted for publication in *Engineering Fracture Mechanics*.

8. A. Fjeldstad, A. Wormsen and G. Härkegård: A reanalysis of Frost's classical fatigue tests on self-arresting cracks at notches. Norwegian University of Science and Technology, 2007.

In addition, the paper [9] have been published but are not included in the thesis.

Contents

CHAPTER 1

Introduction

At a time when the industry is challenged to come up with better and less costly products, and this in even shorter cycles, all product development processes must undergo the same improvements, including fatigue design. This represents an enormous challenge for the engineers to continuously develop improved solutions. One example is the automotive industry where saving structural weight is of utmost importance in order to improve, e.g., the fuel efficiency. At the same time, the time to market has been drastically reduced. In order to comply with this development the use of computer simulations has been increasingly important. This is highly relevant for the fatigue process, where the need for tools that offers both fast and reliable solutions is evident.

Fatigue is a potential failure mode in virtually all mechanical components, e.g. turbines, automotive structures and pressure vessels. Regardless of production method, e.g. welding, forging or extrusion, fatigue failure is caused by the same physical process, namely a microscopical damage in the material that after continued cycling develops into a crack that finally leads to component failure. It is important to study the growth of fatigue cracks located in stress raisers and how the decreasing stress field influences the fatigue life. What makes this an important aspect in the assessment of fatigue damage is that fatigue failure in real components very often is caused by an initial flaw, in the proximity of a stress raiser, who ultimately grows to become critical. When assessing fatigue lives it is important that accurate solutions for the stress intensity factor, K, which is the main parameter to seek in fatigue crack growth calculations, are available. A large number of solutions has been proposed, but most have a general weakness of either being valid only for the near notch area, or that extensive preliminary analysis is required for establishing the stress intensity factor. Another important aspect is the growth of physically short cracks that must be taken into account since the crack during a majority of its lifetime is short.

The main scientific challenge to be addressed in this project is to establish a

robust description of crack growth that can be used in more precise fatigue lifetime models and simulations of fatigue behaviour. The key elements addressed in this thesis are

- estimation of the stress intensity factor for cracks at stress concentrations.
- increased fundamental understanding of the growth of physically short cracks.
- finite-element post-processor tool for estimating the fatigue life under service conditions for components and more complex structures.

The industrial benefit will be access to a reliable, fast and efficient tool for the fatigue assessment of critical structures.

CHAPTER 2

Stress intensity factor solutions

The stress intensity factor, K, is an important parameter for characterising the severity of the stress state and the size of the plastic zone at the crack tip. Linear elastic fracture mechanics states that the singular stress field ahead of a crack tip is proportional to the stress intensity factor. K is defined as

$$K = FS\sqrt{\pi a}, \tag{2.1}$$

where the geometry factor, F, is dependent on the geometry, crack size and loading. S is the applied stress and a is the crack depth. Fatigue failure is caused by repeated cyclic loading. Hence, when a structure is subjected to an alternating stress ΔS, it follows from equation (2.1) that the stress intensity range can be defined as

$$\Delta K = F\Delta S\sqrt{\pi a}. \tag{2.2}$$

The stress intensity range plays an important role in the analysis of fatigue crack growth [10–14]. It is therefore of crucial importance that robust and accurate methods for obtaining K is used when predicting the fatigue life of structures containing crack-like defects.

As long as the crack is located in a homogeneous stress field, K can be approximated with good accuracy, cf. [15,16]. However, for complex stress fields the K solution can be difficult to obtain. A large number of different methods for calculating the stress intensity factor for different cracked configurations exists [17]. In the following, two methods for calculating K are presented.

2.1 Asymptotic solutions

The initiation and growth of a fatigue crack often occurs from stress concentrations. If the crack grows in a gradient stress field, the procedure for obtaining the stress intensity factor is not necessarily straight forward. However, the use of

asymptotic solutions has shown that K can be calculated quite easily. Asymptotic solutions make use of the near-notch and the remote-notch solution of K to interpolate over the entire range from shallow to deep cracks. The near notch solution is obtained by means of the stress concentration factor. For cracks located in the remote stress field, K is obtained by considering the crack to be located in a smooth plate with a crack depth equal to the sum of the notch depth and the actual crack depth. Consider the cracked semi-infinite notched specimen in Fig. 2.1(a). For a crack in the notch stress field, the stress intensity factor solution is asymptotically the same as for a surface crack in a smooth solid, except that the remote stress is being amplified by the stress concentration factor $K_\mathrm{t} = \sigma_{\max}/S$, where $\sigma_{\max}$ is the maximum notch stress. As $a \to 0$,

$$K = FS\sqrt{\pi a} = F_0 K_\mathrm{t} S\sqrt{\pi a}, \tag{2.3}$$

i.e.,

$$F = F_0 K_\mathrm{t}, \tag{2.4}$$

where F_0 is the geometry factor for the current crack emanating from a smooth surface. When the crack grows beyond the notch stress field, the remote stress field dominates the stress intensity factor

$$K = F_0 S\sqrt{\pi(a+d)}, \tag{2.5}$$

where d denotes the notch depth. Identification with equation (2.1) yields

$$F = F_0\sqrt{1+\frac{d}{a}}. \tag{2.6}$$

When $a/d \gg 1$, F asymptotically approaches F_0. If the shallow and deep crack solution is known, K can be obtained by interpolating between the two solutions.

2.1.1 Equivalent crack depth

Jergéus [18] and Härkegård [19] introduced a solution for the stress intensity factor by considering the equivalence between the notched configuration and a smooth semi-infinite plate with a crack of depth D subjected to the same remote load. D must be of a certain length such that the two configurations yield the same K value, i.e.,

$$K = F_0 S\sqrt{\pi D}. \tag{2.7}$$

According to [18, 19] the equivalent crack depth can be estimated by

$$D = a + d\left[1 - \exp\left(-\frac{a}{a'}\right)\right], \tag{2.8}$$

where

$$a' = \frac{d}{K_\mathrm{t}^2 - 1}. \tag{2.9}$$

The transition crack depth, a', is defined as the crack depth at which the shallow crack asymptote and deep crack asymptote in equations (2.3) and (2.5), yield equal results. For a shallow crack the equivalent crack depth becomes

$$D = K_\mathrm{t}^2 a, \tag{2.10}$$

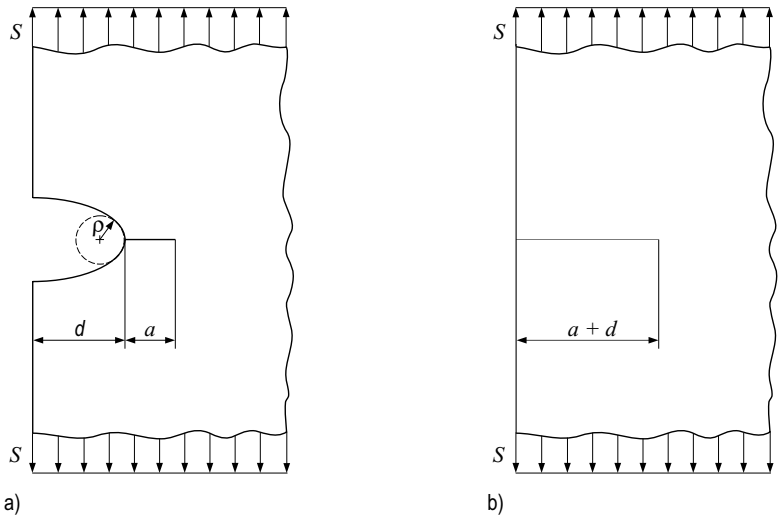

Figure 2.1: (a) Semi-infinite notched plate under uniform stress and (b) smooth semi-infinite plate with crack depth $a + d$.

and, for a deep crack,

$$D = a + d. \tag{2.11}$$

In Paper 2, it is showed that the same method can be used for obtaining K for semi-elliptic cracks located at the root of a semi-circular notch in a semi-infinite plate subjected to uniaxial tension. Paper 4 further uses the solution to estimate the degree of conservatism by replacing the notch root crack by a homogeneously stressed surface crack subjected to the maximum notch stress.

2.1.2 Normalised geometry factor

Calculating K by means of normalised geometry factors is a somewhat different approach. Here, the geometry factor F, for the current cracked configuration is normalised by means of a known reference solution, F_∞. For the notched configuration in Fig. 2.1(a), the smooth semi-infinite plate, in Fig. 2.1(b), with a crack of depth $a + d$ is used as a reference. Hence, F_∞ can be obtained from equation (2.6) where $F_\infty = F$. The shallow crack asymptote of the normalised geometry factor is given by

$$\frac{F}{F_\infty} = K_\mathrm{t}\sqrt{\frac{a}{d}}. \tag{2.12}$$

For deep cracks, the geometry factor of the cracked notch will approach a smooth plate solution with crack depth $a + d$, i.e., $F/F_\infty = 1$. In Paper 2 a simple expression was proposed which asymptotically agrees with the near notch and remote field estimates, i.e.

$$\frac{F}{F_\infty} = \sqrt{1 - \exp(-a/a^*)}, \tag{2.13}$$

where a^* denotes the transition crack depth at which the two asymptotes coincide. Hence, by setting equation (2.12) equal to unity yields

$$a^* = \frac{d}{K_{\mathrm{t}}^2}. \tag{2.14}$$

Paper 3 shows that equation (2.13) can be used also for obtaining K solutions for finite width through-cracked notched plates subjected to tension or bending.

The same method is used in Paper 5 to establish solutions for both through-cracks and semi-elliptic cracks in the root of a V-notched plate. The asymptotic solutions were further used for estimating K for a T-joint with a fillet-weld-shaped transition.

2.2 Weight functions

The use of asymptotic solutions has shown to give accurate approximations of K. However, it has a weakness of being applicable only for specific geometries and is not preferable for arbitrary geometries. Papers 6 and 7 deal with the principals behind the finite-element post-processor, P•FAT. For this purpose the theory of weight functions has shown to have the desired flexibility to handle cracks subjected to an arbitrary stress field by using the un-cracked stress field. The use of weight functions in crack mechanics was first proposed by Bueckner [20] and subsequently generalised by Rice [21].

Consider a two-dimensional crack located in an arbitrary elastic body subjected to the stress field $\sigma_{ij}(\mathbf{x})$. The weight function, $g(x', y')$, where x' and y' are local crack coordinates, is defined as the stress intensity factor value at the

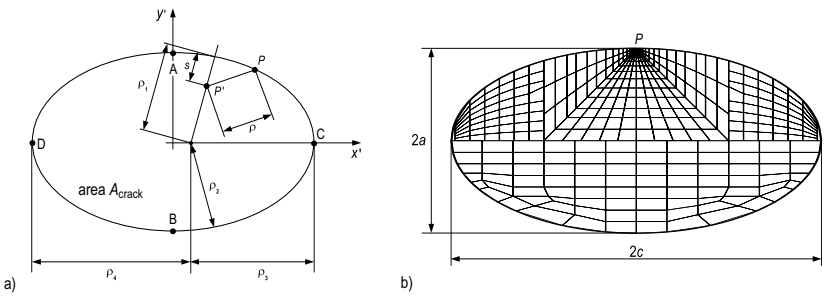

Figure 2.2: (a) Schematic drawing of an embedded elliptical crack and definition of parameters for obtaining the stress intensity factor. (b) Typical finite element mesh used for an embedded elliptical crack.

crack front point P, when a pair of symmetrical unit opening forces are applied at a point P' on the crack surface, cf. Fig. 2.2(a). The stress intensity factor is obtained by integrating the product of the weight function $g(x', y')$ and the stress distribution of the crack free solid $\sigma_{\mathrm{a}}(x', y')$ over the crack surface area A_{crack}:

$$K(\mathrm{P}) = \int_{A_{\mathrm{crack}}} \sigma_{\mathrm{a}}(x', y') g(x', y') \mathrm{d}A_{\mathrm{crack}}. \tag{2.15}$$

The integral in equation (2.15) is solved numerically in the finite-element post-processor by using Gauss-Legendre quadrature integration. An example of the integration mesh for an embedded crack is shown in Fig. 2.2(b). The finite-element post-processor can handle the growth of an embedded crack [22], surface crack [23] and a corner crack [24], see Fig. 2.3. A thorough presentation of weight functions is given in reference [25].

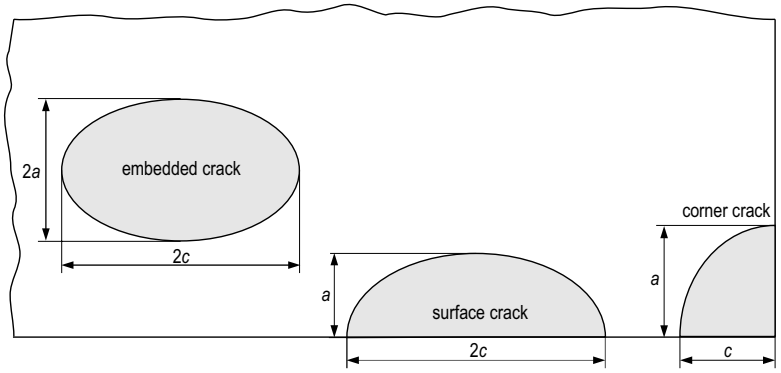

Figure 2.3: Crack configurations implemented in the finite-element post-processor.

CHAPTER 3

Defects causing fatigue failure

The fatigue lifetime largely depends on material defects, e.g., porosity and inclusions, which form as a natural part of the manufacturing process. A successful design must consider both the size and the number of large defects as well as the stress distribution arising from the geometry and loading of the component. A description of different inspection methods, such as non-destructive testing and optical microscopy is presented in [26].

3.1 Defect distributions

The reliability and performance of metallic components are greatly affected by the size of defects contained in the most highly stressed volume. Because defects are small and mostly inside the material, they are difficult to detect and measure. Observations using automated optical microscopy can, however, be made on polished plane regions (control areas), and the maximum defect size in a real component must be obtained by prediction based on some statistical analysis. There are two different approaches based on the statistics of extremes for estimating the sizes of large defects in a large volume from those of a small volume. The first approach, called the *block maximum* method, is based on the generalised extreme value distribution [27]. In this method, only the size of the largest defect in each of the k control areas is measured. The second approach is the *peak over threshold* method. Here, all defects with sizes above a certain high threshold are considered and fitted to a generalised Pareto distribution [27]. Both distributions can be used to predict the maximum defects size in a large volume.

In Papers 6 and 7, the process of predicting number, size and location of life controlling defects is described.

3.2 Crack growth law

The use of stress intensity factors was extended to fatigue problems by Paris and Erdogan [10], who suggested a power-law relationship between the crack growth rate $\mathrm{d}a/\mathrm{d}n$ and the stress intensity range ΔK, viz.,

$$\frac{\mathrm{d}a}{\mathrm{d}n} = C\Delta K^m, \tag{3.1}$$

where C and m are material parameters. Klesnil and Lukáš [11] extended Paris' law into the near threshold region by including the threshold stress intensity range, ΔK_{th}:

$$\frac{\mathrm{d}a}{\mathrm{d}n} = C(\Delta K^m - \Delta K_{\mathrm{th}}^m). \tag{3.2}$$

The fatigue tests by Kitagawa and Takahashi [28] clearly show that the fatigue limit of a cracked solid can be determined by means of the threshold of the stress intensity range for long cracks only. For short cracks, however, the fatigue limit asymptotically approaches the ordinary fatigue limit as determined by means of a smooth specimen. Fig. 3.1 shows a Kitagawa-Takahashi diagram with experimental data [29, 30]. Both the long and the short crack fatigue limits are satisfied by an equation initially proposed El Haddad et al. [31] for $F = 1$, and generalised by Härkegård [19] to an arbitrary geometry factor, F, viz.

$$\Delta\sigma = \frac{\Delta K_{\mathrm{th}}}{F\sqrt{\pi(a+a_0)}} = \frac{\Delta\sigma_{\mathrm{A}}}{\sqrt{1+a/a_0}}. \tag{3.3}$$

One may interpret a_0 as an 'intrinsic' crack length, which should be added to the length of the real crack to yield an 'effective' crack length.

By means of the theory proposed by ElHaddad et al. [31], the crack propagation law presented by Klesnil and Lukáš [11] can be rewritten as

$$\frac{\mathrm{d}a}{\mathrm{d}n} = C\Delta K_{\mathrm{th}}^m \left[\left\{ \left(\frac{\Delta K}{\Delta K_{\mathrm{th}}} \right)^2 + \left(\frac{\Delta\bar{\sigma}}{\Delta\sigma_{\mathrm{A}}} \right)^2 \right\}^{m/2} - 1 \right]. \tag{3.4}$$

Crack growth measurements reported in the literature [32, 33] have been reanalysed in Paper 7 in order to verify the above crack growth law.

3.3 Crack arrest

The short crack growth model in equation (3.4) can be used to predict the arrest of cracks. The stress field decreases rapidly ahead of a notch and may result in a decreasing crack growth rate for a propagating crack. Fig. 3.2 shows the normalised equivalent stress intensity factor, $\Delta K_{\mathrm{eq}}/\Delta K_{\mathrm{th}}$, against the normalised crack depth, a/d, for a circumferentially notched specimen subject to tension-compression loading. ΔK_{eq}, presented in Papers 7 and 8, is a quantity that includes the short crack behaviour. In Fig. 3.2, $\Delta K_{\mathrm{eq}}/\Delta K_{\mathrm{th}}$ has been presented for three different stress ranges. The upper curve illustrates a situation, where the

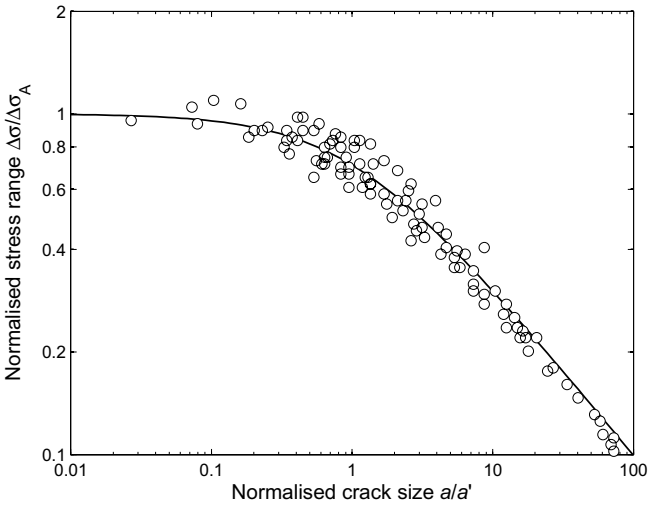

Figure 3.1: Normalised crack size versus normalised stress range. Data points have been gathered by Tanaka et al. [29] and Hertzberg [30].

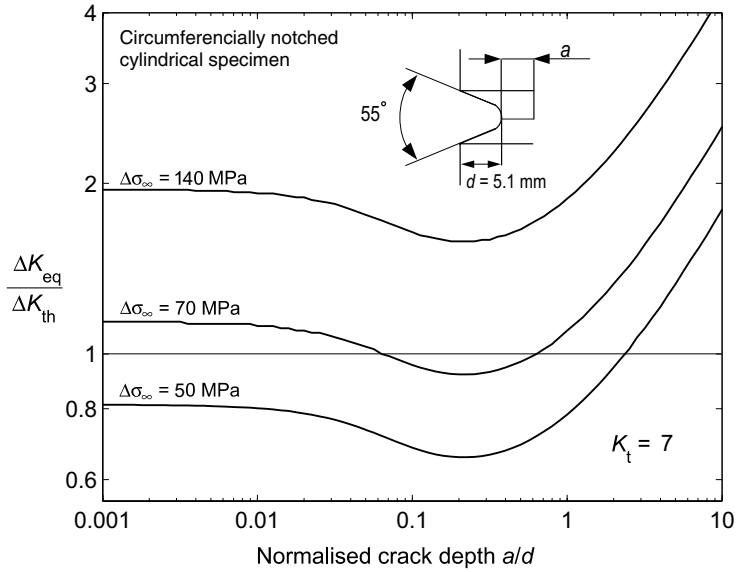

Figure 3.2: Principle graph of $\Delta K_{\mathrm{eq}}/\Delta K_{\mathrm{th}}$ versus a/d for three different load levels.

crack starts to grow from the notch root and continues to grow until final failure. The intermediate curve shows crack initiation and growth, until ΔK_{eq} falls below ΔK_{th} and the crack arrests. The lower curve corresponds to a situation, where no crack initiates.

In paper 8, the experimental data reported by Frost [34] of self-arresting cracks has been compared with predictions from equation (3.4) and found to be in good agreement.

CHAPTER 4

A post-processor for analysis of fatigue problems

4.1 P•FAT

P•FAT is designed as a stand-alone, finite-element post-processor with the component geometry and stresses given by a standard finite element program. Data needed for the computation are nodal coordinates, element topology and stresses. It has been developed to perform fatigue life predictions in arbitrary three-dimensional components.

There is a variety of approaches to the fatigue analysis of mechanical components. As emphasised in Chapter 1, all approaches are basically related to the same physical process, namely fatigue crack propagation. A majority of these approaches can be categorised according to Table 4.1. The implicit approaches make use of conventional $S - N$ data, where the number of cycles until failure, N, usually denotes the number of cycles required for the occurrence of a critical state, e.g. a defined crack size or a certain loss of the bearing capability. The explicit approaches, on the other hand, consider the actual growth of a fatigue crack from its initial size, a_{i}, to a final size, a_{f}. Standard methods for fatigue life predictions are deterministic by nature, i.e., material parameters are considered as predetermined quantities. On the other hand, the probabilistic approaches assume the material properties to be randomly distributed. Thus, the fatigue life distribution is obtained rather than a single fatigue lifetime value.

Table 4.1 shows the four types of fatigue assessment methods that have been implemented in P•FAT (Papers 6 and 7). In the two following Sections, a short description of the four fatigue assessment methods will be given.

Table 4.1: Different approaches to fatigue analysis, all related to fatigue crack growth.

Approaches to fatigue analysis	Deterministic	Probabilistic
Implicit	Local Stress	Weakest-Link
Explicit	Single Defect	Random Defect

4.2 Implicit fatigue assessment methods

The implicit approaches, i.e., local stress and weakest-link, use conventional $S-N$ data as a starting point, and the fatigue life, N, is usually defined as the number of load cycles required for a macroscopic crack to develop.

4.2.1 Local stress approach

The local stress approach is based on the assumption that the fatigue life or strength of an arbitrary component can be obtained by solely regarding the local stress state at some critical location. The analysis is performed on the basis of a $S-N$ curve from laboratory experiments of a standard smooth fatigue specimen. By assuming equivalence between the smooth fatigue specimen and the highly stressed point of a component, the fatigue life or strength can be determined by means of the $S-N$ curve. Hence, no fatigue damage occurs if

$$\sigma_{\mathrm{a,max}} \leq \sigma_{\mathrm{A}}, \tag{4.1}$$

where $\sigma_{\mathrm{a,max}}$ is the stress amplitude at the critical location and σ_{A} is the characteristic fatigue strength of a smooth reference fatigue test specimen. The local stress approach does not take into account the stress field or the component size.

Presented on generalised from, equation (4.1) can be expressed by means of the function f, i.e.,

$$f\left(\sigma_{ij}\right) \leq \lambda, \tag{4.2}$$

where σ_{ij} is the local stress tensor at a critical point and λ is the limiting value for fatigue to occur. Obviously, the function f is given by the selected criterion. A large number of multiaxial stress criteria has been proposed. Well known multiaxial criteria, such as Dang Van [35], McDiarmid [36], Sines [37], Findley [38], Crossland [39], Matake [40] and maximum principal stress have been implemented in P•FAT. A review of the presented criteria is given in [41, 42].

4.2.2 Weakest-link approach

A widely used analogy for the weakest-link model is by considering a chain consisting of several rings. Just as the chain is no stronger than the weakest-link,

an arbitrary component can be regarded likewise, i.e., that the component only survives if all small volume elements, which the component has been divided into, survives. By dividing the the component into infinitely small volumes, the probability of failure can be obtained from the two-parameter Weibull distribution [43, 44]:

$$P_{\mathrm{f}} = 1 - \exp\left[-\int_V \left(\frac{\sigma_a}{\sigma^*_{\mathrm{A0}}} \right)^{b_\sigma} \frac{\mathrm{d}V}{V_0} \right]. \tag{4.3}$$

Here, b_σ denotes the shape parameter and σ^*_{A0} the scale parameter. The shape parameter is a measure of the fatigue limit scatter. The scale parameter is the 63.2% quantile of the Weibull distribution and is often referred to as the characteristic fatigue strength. See Wormsen et al. [9] for a more detailed description of the weakest-link theory.

4.3 Explicit Fatigue Assessment Methods

The explicit approaches, i.e., single defect and random defect, consider the physical damage process. Hence, the fatigue life is determined based on the number of cycles necessary to propagate a crack from an initial size a_{i} to a final size a_{f}.

In order to perform a crack growth analysis at a reasonably low cost, the component geometry is often simplified so that a standard handbook solution can be used. This procedure is pursued in the programs NASGRO [45] and AFGROW [46]. When such simplifications cannot be justified, a fully three-dimensional analysis can be performed [47–50]. However, three-dimensional crack modeling has a drawback of being extremely time consuming. Therefore, it is desirable that an alternative method for standard crack growth analysis is used.

An alternative method used in P•FAT, which gives a CPU efficient post-processing tool, is to use results from a standard finite element stress analysis and account for a crack by using weight functions [20, 21]. The initial crack-like defect is regarded as an embedded, semi-elliptical, or a corner crack, depending on the location of the crack front relative to the free surface. Failure of a component occurs when a critical crack depth is reached, or when the stress intensity factor K has reached the fracture toughness.

4.3.1 Single defect approach

In the single defect approach a crack-like defect is inserted into the component geometry at a user defined location. The post-processor then calculates the fatigue life of the cracked component based on the stress field from a finite element stress analysis.

In Subsection 4.4 a practical example of the single defect approach is given.

4.3.2 Random defect approach

In the random defect approach the number, size and position of crack-like defects are obtained by 'drawing' from distribution functions. This process is repeated for a large number of nominally equal components ('Monte Carlo' simulation). The fatigue life distribution of the component can then be obtained. Consequently, one has a post-processing tool that can account for fatigue crack growth and calculate the probability of component failure in the same simulation. An important industrial case where this is relevant is for cast automotive components.

4.4 A practical example using P•FAT

As a practical example of the use of the finite-element post-processor, a welded aluminium rectangular hollow section T-joint, see Fig. 4.1(a), has been investigated. As reported in paper 1 the T-joint was tested in four-point bending with a constant stress ratio $R = \sigma_{\min}/\sigma_{\max} = 0.1$, resulting in a constant bending moment throughout the weld region. A welding simulation was carried out

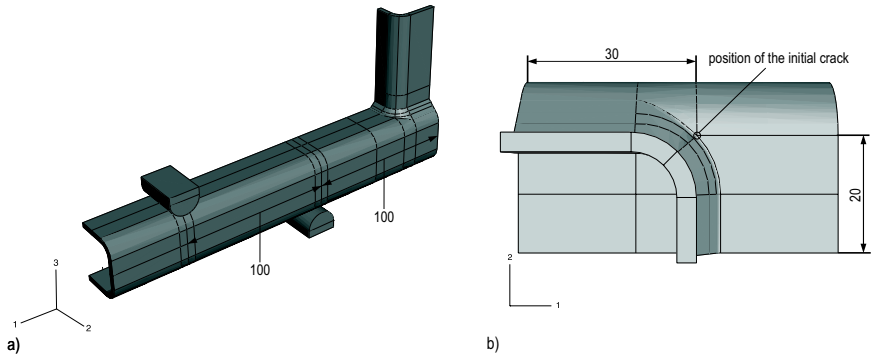

Figure 4.1: T-joint configuration: (a) global model and (b) submodel.

in Weldsim [51–53] in order to obtain the residual stress field. The operating stress field was found by using ABAQUS [54]. The T-joint was modeled using eight-noded brick elements with reduced integration. For reasons of symmetry, only one quarter of the T-joint had to be considered. The load was applied to the chord through cylindrical rods, see Fig. 4.1(a). A submodel with a highly refined mesh, see Fig. 4.1(b), was used to accurately capture the peak stress and the adjacent stress field. The boundary conditions imposed on the submodel are obtained from the global model. The submodel was meshed with twenty-noded brick elements with reduced integration. The weld was modeled with a weld angle of 45° and with a weld toe radius of 1 mm. The operating stress field from the submodel and the residual stress field from the weld simulation are combined in the finite-element post-processor to obtain the spatial distribution of the stress amplitude and the mean stress.

Fatigue crack growth calculations have been performed with a semi-elliptic surface crack of initial depth $a_{\mathrm{i}} = 50$ μm. The initial aspect ratio has been

assumed to be $a/c = 1$. The position of the initial crack is shown in Fig. 4.1(b). The fatigue crack growth analysis was terminated, when the crack had reached a depth of 95% of the wall thickness, i.e., 2.85 mm. The material properties for the aluminium alloy are given in Table 4.2. The predicted fatigue life curve is shown

Table 4.2: Mechanical properties of the 6082-T6 aluminium alloy.

Fatigue limit [55]	$\Delta\sigma_{\mathrm{A}}(R = 0) = 148$ MPa
Stress intensity threshold [56]	$\Delta K_{\mathrm{th}}(R = 0.1) = 2.08$ MPa$\sqrt{\mathrm{m}}$
Walker exponent [55]	$\gamma = 0.78$
Crack growth coefficient [55]	$C(R = 0.1) = 6.1 \cdot 10^{-12}$ m/cycle
Crack growth exponent [55]	$m = 5.1$

in Fig. 4.2 together with fatigue test results that have been reported in Paper 1. Even though the steepness of the predicted and the experimental $S - N$ curves are somewhat different, the overall agreement is good. The predicted curve is non-conservative at elevated stresses but approaches the experimental curve as the stress decreases. Eventually, the two curves crosses and the predicted fatigue limit for the T-joint is obtained at approximately 55 MPa. This is clearly a over prediction since some of the data points are below the predicted curve. It is worth mentioning that the fatigue limit of the T-joint is strongly dependent on the intrinsic fatigue limit of the material ($\Delta\sigma = 148$ MPa at $R = 0$). However, the intrinsic fatigue limit has been calculated based on the ultimate tensile strength [55], and thus, the fatigue limit of the T-joint is rather uncertain.

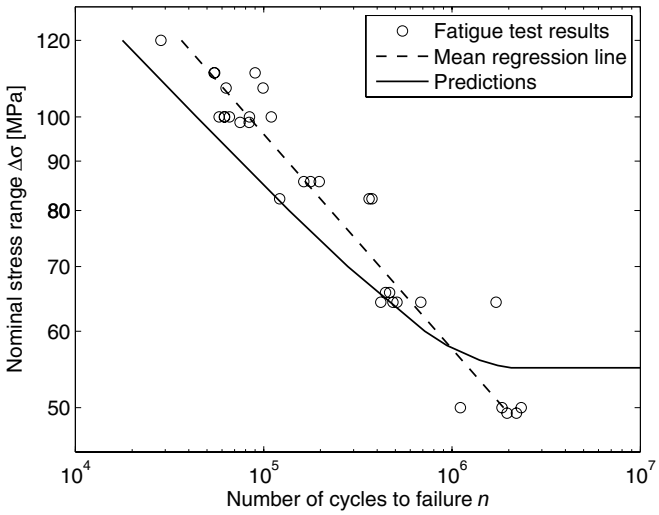

Figure 4.2: Fatigue test results for the considered T-joint configuration (Fig. 4.1) together with the finite-element post-processor based prediction curve.

CHAPTER 5

Suggestions for further work

The objective of this thesis has been to study the growth of cracks growing in gradient stress fields. Much effort has been put into establishing simple and robust K-solutions and to describe the growth of short cracks. Furthermore, a post-processor for the analysis of arbitrary components has been presented. However, there are still many issues that needs to be addressed. Some suggestions for further work are:

- Establish stress intensity factor solutions for semi-elliptic cracks in finite notched plates based on asymptotic solutions.
- Develop a methodology for calculating the J-integral based on asymptotic solutions.
- Perform crack growth measurements on physically short cracks in notches for validation of short crack growth model.
- Improve weight functions for surface cracks and near-surface cracks.
- Extend P•FAT to cover fatigue crack growth from initial defects that are not regarded as cracks.
- Increase the fundamental understanding of the relation between the size and density of material defects, and the forming of a fatigue crack.

Bibliography

[1] **Tveiten, B.W.**, **Fjeldstad, A.**, **Härkegård, G.**, **Myhr, O. R.**, and **Bjørneklett, B.** Fatigue life enhancement of aluminium joints through mechanical and thermal prestressing. *International Journal of Fatigue*, 28(12):1667–1676, 2006.

[2] **Wormsen, A.**, **Fjeldstad, A.**, and **Härkegård, G.** The application of asymptotic solutions to a semi-elliptical crack at the root of a notch. *Engineering Fracture Mechanics*, 73(13):1899–1912, 2006.

[3] **Fjeldstad, A.**, **Härkegård, G.**, and **Wormsen, A.** The stress intensity factor for a crack in a finite notched plate based on asymptotic solutions. Submitted for publication in Engineering Fracture Mechanics, 2007.

[4] **Fjeldstad, A.**, **Härkegård, G.**, and **Wormsen, A.** The influence of a stress gradient on the growth of a fatigue crack. In W. S. Johnson et al., editor, *Proceedings of the International Fatigue Congress 2006*, Atlanta, Georgia, USA, May 2006. Elsevier.

[5] **Fjeldstad, A.**, **Wormsen, A.**, and **Härkegård, G.** Approximate stress intensity factors for cracked V-notched specimens based on asymptotic solutions with application to T-joints. *Engineering Fracture Mechanics*, doi:10.1016/j.engfracmech.2007.04.028, 2007.

[6] **Wormsen, A.**, **Fjeldstad, A.**, and **Härkegård, G.** A post-processor for fatigue crack growth analysis based a finite element stress field. Accepted for publication in Computer Methods in Applied Mechanics and Engineering.

[7] **Fjeldstad, A.**, **Wormsen, A.**, and **Härkegård, G.** Simulation of fatigue crack growth in components with random defects. *Engineering Fracture Mechanics*, doi:10.1016/j.engfracmech.2007.04.006, 2007.

[8] **Fjeldstad, A.**, **Wormsen, A.**, and **Härkegård, G.** A reanalysis of frost's classical fatigue tests on self-arresting cracks at notches. Norwegian University of Science and Technology, 2007.

[9] **Wormsen, A.**, **Sjödin, B.**, **Härkegård, G.**, and **Fjeldstad, A.** Non-local stress approach for fatigue assessment based on weakest-link theory and statistics of

extremes. Accepted for publication in Fatigue & Fracture of Engineering Materials & Structures, 2007.

[10] **Paris, P. C.** and **Erdogan, F.** A critical analysis of crack propagation laws. *Journal of Basic Engineering*, 85:528–534, 1963.

[11] **Klesnil, M.** and **Lukáš, P.** Influence of strength and stress history on growth and stabilisation of fatigue cracks. *Engineering Fracture Mechanics*, 4(1):77–92, 1972.

[12] **Forman, R. G.**, **Kearney, V. E.**, and **Engle, R. M.** Numerical analysis of crack propagation in cyclic-loaded structures. *Journal of Basic Engineering*, 89:459–464, 1967.

[13] **Erdogan, F.** and **Ratwani, M.** Fatigue and fracture of cylindrical shells containing a circumferential crack. *International Journal of Fracture Mechanics*, 6(4):379–392, 1970.

[14] **Pugno, N.**, **Ciavarella, M.**, **Cornetti, P.**, and **Carpenteri, A.** A generalized paris' law for fatigue crack growth. *Journal of the Mechanics and Physics of Solids*, 54(7):1333–1349, 2006.

[15] **Newman, Jr. J. C.** and **Raju, I. S.** An empirical stress-intensity factor equation for the surface crack. *Engineering Fracture Mechanics*, 15(1-2):185–192, 1981.

[16] **Tada, H.**, **Paris, P. C.**, and **Irwin, G. R.** *The stress analysis of cracks handbook.* Professional Engineering Publishing Limited, Bury St. Edmunds and London, 3rd edition, 2000.

[17] **Rooke, D. P.**, **Baratta, F. I.**, and **Cartwright, D. J.** Simple methods of determining stress intensity factors. *Engineering Fracture Mechanics*, 14(2):397–426, 1981.

[18] **Jergéus, H. Å.** A simple formula for the stress intensity factors of cracks in side notches. *International Journal of Fracture*, 14:R113–116, 1978.

[19] **Härkegård, G.** An effective stress intensity factor and the determination of the notched fatigue limit. In J. Bäcklund, A. F. Blom, and C. J. Beevers, editors, *Fatigue thresholds: fundamentals and engineering applications, volume II*, pages 867–879. Engineering Materials Advisory Services Ltd, 1982.

[20] **Bueckner, H. F.** A novel principel for the computation of stress intensity factors. *Z. Agenwandte Math. Mech.*, 50:529–546, 1970.

[21] **Rice, J. R.** Some remarks on elastic crack-tip stress fields. *International Journal of Solids and Structures*, 8(6):751–758, 1972.

[22] **Wang, X.**, **Lambert, S. B.**, and **Glinka, G.** Approximate weight functions for embedded elliptical cracks. *Engineering Fracture Mechanics*, 59(3):381–392, 1998.

[23] **Shen, G.** and **Glinka, G.** Weight functions for a surface semi-elliptical crack in a finite thickness plate. *Theoretical and Applied Fracture Mechanics*, 15(3):247–255, 1991.

[24] **Zheng, X. J.**, **Glinka, G.**, and **Dubey, R. N.** Stress intensity factors and weight functions for a corner crack in a finite thickness plate. *Engineering Fracture Mechanics*, 54(1):49–61, 1996.

[25] **Fett, T.** and **Munz, D.** *Stress intensity factors and weight functions.* International series on advances in fracture. Computational Mechanics Publications, Southampton, 1997.

[26] **Atkinson, H. V.** and **Shi, G.** Characterization of inclusions in clean steels: a review including the statistics of extreme methods. *Progress in Materials Science*, 48:457–520, 2003.

[27] **Coles, S.** *An Introduction to Statistical Modeling of Extreme Values.* Springer Series in Statistics, London, 3rd edition, 2001.

[28] **Kitagawa, H.** and **Takahashi, S.** Applicability of fracture mechanics to very small cracks or the cracks in early stage. In *Proceedings of the Second International Conference on the Mechanical Behaviour of Materials*, pages 627–631, Boston, Ma., 1976.

[29] **Tanaka, K.**, **Nakai, Y.**, and **Yamashita, M.** Fatigue growth threshold of small cracks. *International Journal of Fracture*, 17(5):519–533, 1981.

[30] **Hertzberg, R. W.** *Deformation and Fracture Mechanics of Engineering Materials.* John Wiley & Sons, Inc., 4th edition, 1996.

[31] **El Haddad, M. H.**, **Topper, T. H.**, and **Smith, K. N.** Prediction of non-propagating cracks. *Engineering Fracture Mechanics*, 11(3):573–584, 1979.

[32] **Breat, J. L.**, **Murdy, F.**, and **Pineau, A.** Short crack propagation and closure effects in A508 steel. *Fatigue of Engineering Materials & Structures*, 6(4):349–358, 1983.

[33] **Mann, T.**, **Härkegård, G.**, and **Stärk, K.** Short fatigue crack growth in aluminium alloy 6082-T6. *International Journal of Fatigue*, doi: 10.1016/j.ijfatigue.2007.01.002, 2007.

[34] **Frost, N. E.** A relation between the critical alternating propagation stress and crack length for mild steels. *Proceedings of the Institution of Mechanical Engineers*, 173:811–827, 1959.

[35] **Dang Van, K.** Macro-micro approach in high-cycle multiaxial fatigue. In D. L. McDowell and R. Ellis, editors, *Advances in Multiaxial Fatigue*, pages 120–130, Philidelphia, USA, 1993. American Society for Tesing and Materials, ASTM STP 1191.

[36] **McDiarmid, D. L.** A general criterion for high cycle multiaxial fatigue failure. *Fatigue and Fracture of Engineering Materials and Structures*, 14(4):429–453, 1991.

[37] **Sines, G.** *Metal fatigue*, chapter 'Behaviour of metals under complex static and alternating stresses', pages 145–169. McGraw-Hill, New York, 1959.

[38] **Findley, W. N.**, **Coleman, J. J.**, and **Hanley, B. C.** Theory for combined bending and torsion fatigue with data for SAE 4340 steel. In *Proceedings of the International Conference on Fatigue of Metals*, pages 150–156, London, 1956. Institute of Mechanical Engineers.

[39] **Crossland, B.** Effect of large hydroststic pressures on the torsional fatigue strength of an alloy steel. In *Proceedings of International Conference on fatigue of Metals*, pages 138–149, London, 1956. Institution of Mechanical Engineers.

[40] **Matake, T.** An explanation on fatigue limit under combined stress. *Bulletin of the Japan Society of Mechanical Engineers*, 20(141):257–263, 1977.

[41] **Socie, D. F.** and **Marquis, G. B.** *Multiaxial fatigue.* Warremdale, Pa.: Society of Automotive engineers, 2000.

[42] **Norberg, S.** *Prediction of the fatigue limit – accuracy of post-processing methods.* Licentiate thesis, Royal Institute of Technology, 2006.

[43] **Weibull, W.** A statistical theory of the strength of materials. *Ingeniörsvetenskapsakademiens handlingar*, 151:1–14, 1939.

[44] **Weibull, W.** The phenomenon of rupture in solids. *Ingeniörsvetenskapsakademiens handlingar*, 153:1–55, 1939.

[45] *NASA: Fatigue Crack Growth Computer Program 'NASGRO', version 3.0, 2000*, (Reference Manual, JSC-22267B, Engineering Directorate, National Aeronautics and Space Administration, Lyndon B. Johnson Space Center, Houston).

[46] *AFGROW: Users Guide and Thecnical Manual*, Air Vehicles Directorate, Air Force Laboratory, Wright-Patterson Air Force Base, Ohio.

[47] Cornell Fracture Group. *FRANC3D 2.6 Concepts and user guide*, Cornell University, Ithaca, New York, 2003.

[48] *BEASY User Guide, Computational Mechanics BEASY Ltd., 2001*, (Ashurst Lodge, Ashurst, Southampton, Hampshire, SO40 7AA, UK).

[49] **Schöllmann, M.**, **Fulland, M.**, and **Richard, H. A.** Development of a new software for adaptive crack growth simulations in 3d structures. *Engineering Fracture Mechanics*, 70(2):249–263, 2003.

[50] **Fulland, M.** and **Richard, H. A.** Application of the fe-method to the simulation of fatigue crack growth in real structures. *Steel Research*, 74(9):584–590, 2003.

[51] **Myhr, O. R.**, **Klokkehaug, S.**, **Fjær, H. G.**, **Grong, Ø.**, and **Kluken A. O.** Modelling of microstructure evolution, residual stresses and distortions in 6082-T6 aluminium weldments. *Welding Journal*, 77(7):286–292, 1998.

[52] **Myhr, O. R.**, **Grong, Ø.**, **Klokkehaug, S.**, **Fjær, H. G.**, and **Kluken, A. O.** Modelling of the microstructure and strength evolution during ageing and welding of Al-Mg-Si alloys. In *6th International Seminar on Numerical Analysis of Weldability*, Graz-Seggau, Austria, October 1-3 2001.

[53] **Fjær, H. G.**, **Myhr, O. R.**, **Klokkehaug, S.**, and **Holm, S.** Advances in aluminium weld simulations applying WeldSim. In *11th International Conference on Computer Technology in Welding*, Columbus, Ohio, USA, December 2001.

[54] Abaqus/Standard, User's manual, version 6.5-1. *(Hibbit, Karlsson and Sorensen, Pawtucket, Rhode Island)*, 2005.

[55] **Mann, T.** *Fatigue assessments methods for welded structures and their application to an aluminium T-joint.* PhD thesis, NTNU, Trondheim, Norway, 2006.

[56] **Borrego, L. P.**, **Ferreira, J. M.**, and **Costa, J. M.** Fatigue crack growth and crack closure in an AlMgSi alloy. *Fatigue & Fracture of Engineering Materials & Structures*, 24(4):255–265, 2001.

Paper 1

Available online at www.sciencedirect.com
ScienceDirect
International Journal of Fatigue 28 (2006) 1667–1676
International Journal of Fatigue
www.elsevier.com/locate/ijfatigue

Fatigue life enhancement of aluminium joints through mechanical and thermal prestressing

Bård Wathne Tveiten [a,*], Arne Fjeldstad [b], Gunnar Härkegård [b], Ole Runar Myhr [c], Børge Bjørneklett [c]

[a] SINTEF Materials and Chemistry, N-7465 Trondheim, Norway
[b] Norwegian University of Science and Technology (NTNU), N-7491 Trondheim, Norway
[c] Hydro Aluminium Structures, N-2830 Raufoss, Norway

Received 17 January 2005; received in revised form 26 January 2006; accepted 30 January 2006
Available online 22 March 2006

Abstract

This paper presents some simple and flexible methods to enhance the fatigue life of welded aluminium components. Besides enhancing the fatigue life, the proposed methods can easily be implemented into manufacturing processes. The key element of the methods is to change residual stresses from tension to compression at locations vulnerable to fatigue. This is accomplished by mechanical prestressing using elastic pre-deformation or by thermal prestressing using induction heating. The specimens tested are welded aluminium rectangular hollow section T-joints. Prior to fatigue testing, welding FE-simulations were carried out to verify the magnitude and pattern of the residual stress fields (through process modeling). Fatigue testing was later carried out on four different batches. One batch was produced using elastically pre-deformed chords, two batches were treated by means of thermal prestressing (induction heating), and one batch was "as welded" representing a "reference case". Based on statistical evaluation of *S–N* data, the introduction of superimposed compressive stress fields results in a significantly improved fatigue life. Among the different batches, induction heating turned out to be the most promising method with a fatigue strength improvement factor of 1.5 on stress, compared to "as welded" components.

Keywords: Fatigue testing; Induction heating; Residual stress; Weld geometry; Welding simulation

1. Introduction

It is well established that manipulations of residual stress fields will influence the fatigue life either by retarding (superimposed compressive stress field) or by accelerating (superimposed tensile stress field) fatigue crack growth.

Residual stresses are defined as those stresses existing in a structure or a part of a structure in the absence of externally applied loads. Residual stresses can be categorised as short-range or long-range stresses. Short-range stresses exist in the weld metal and the heat affected zone (HAZ) of welded components and are self-equilibrating over the cross section of the local member. They are caused by inhomogeneous thermal expansion and contraction of the material in the weld and HAZ region. It is generally assumed that short-range stresses in welded built-up members may reach a level not far from yield stress both parallel and transverse to the weld. Long-range stresses are uniform throughout structural members, but not self-balanced within local members. They are generally small compared to the yield stress and exhibit small stress gradients. In small-scale welded specimens typical of *S–N* testing, only short-range residual stresses are present.

Various methods to enhance the fatigue life by introducing favourable residual stresses have been suggested in the literature, e.g. peening, overload, and thermal methods [1]. However, common to these methods are that they are generally time-consuming, costly, and labour-intensive. Thus, they are not feasible in high-volume productions, e.g.

* Corresponding author. Tel.: +47 73593890; fax: +47 73592931.
E-mail address: Bard.W.Tveiten@sintef.no (B.W. Tveiten).

0142-1123/$ - see front matter © 2006 Elsevier Ltd. All rights reserved.
doi:10.1016/j.ijfatigue.2006.01.006

engine cradles, or in an early stage of the design process of single, large structures, e.g. ships, bridges. The methods are rather used as a last resort against poor fatigue design at the end of the manufacturing process, when no other options are available.

This paper suggests some simple and flexible methods that can be integrated directly into the manufacturing process in order to enhance the fatigue strength of aluminium structures. The basic idea is to change the residual stresses at locations vulnerable to fatigue from tension to compression, by elastic pre-deformation of chord members during welding, or by application of induction heating at some carefully selected positions. In the case of the thermal prestressing, the analysis scheme is based on FE-simulations where the intensity and duration of the heat treatment are varied systematically. In the case of the mechanical prestressing, different degrees of elastic bending of the chord are examined through numerical simulations in order to optimise the welding with respect to the residual stresses. The manipulation of the manufacturing process is not straightforward, as the method requires exact information about the effect of the external manipulations, which is not known a priori. Thus, the method requires an accurate tool for the prediction of residual stresses resulting from the welding process, as well as for the subsequent induction heat treatment.

The governing factors affecting the fatigue life of welded structures can be categorised as:

- macro-geometrical features and concentrated loads,
- notch effects (local geometrical features),
- weld defects,
- residual stress field.

The objective of this study is to enhance the fatigue life of aluminium components by means of superimposed residual stress fields. The paper demonstrates how improvement methods can be combined with "through process modeling" (TPM). In order to quantify the significance of the imposed residual stress field on the fatigue life, other influencing factors must be accounted for. Thus, influencing factors like notch effects determined by weld toe radius, weld toe angle and weld leg length, and weld defects have been quantified during the experiments.

Various methods for fatigue assessment such as the hot spot stress approach, or other such as the nominal stress range approach, or crack growth assessment using fracture mechanics are not within the scope of this paper. These issues will be dealt with in subsequent studies.

2. Test specimen preparation

2.1. Residual stress simulation

The FE based simulation program WeldSim was used to simulate the residual stress distribution resulting from welding and subsequent local induction heating. The simulation tool is described in Myhr et al. [2,3] and Fjær et al. [4]. No details regarding the FE-model will be given here. However, details can be found in Myhr et al. [5] and Tveiten [6]. WeldSim is a microstructure based FE-program which consists of three components that are sequentially coupled, viz. a numerical heat flow model, a microstructural model and a mechanical model. The temperature field calculated by the thermal model influences both the microstructural evolution at each material point of the solution domain as well as the stress–strain fields. At the same time, there is a link between the microstructural model and the mechanical model to take into account the important effect of softening due to dissolution of hardening particles as the temperature increases during welding or heat treatment.

2.2. Test specimen manufacturing description

The rectangular hollow section (RHS) T-joint tested in this study was produced by means of four different manufacturing processes. Batch 1 was manufactured without any treatment, representing the "as-welded" condition. It was tested mainly to establish a reference to the proposed treatments. In accordance with the WeldSim analysis of batch 1, the residual stress pattern is dominated by tensile stresses at the weld toe region. As opposed to batch 1, the residual stress pattern experienced in batches 2–4 is dominated by compressive stresses at the weld toe region.

The batches are produced according to the following procedures (obtained by TPM simulations) as illustrated in Fig. 1:

- Batch 1: Brace and chord welded without clamping or pre-deformation.
- Batch 2: Brace and chord welded with the chord clamped at both ends and with an elastic pre-deformation of the chord member with a maximum deformation at mid-span of 4 mm.
- Batch 3: Brace and chord welded without any clamping or pre-deformation (production identical to batch 1) and the chord heated locally at four locations close to the weld after the welding.
- Batch 4: Brace and chord welded without any clamping or pre-deformation (production identical to batch 1) and chord heated locally at 12 locations close to the weld after the welding.

Chord and brace elements of batches 1–3 were taken from the same extrusion, while those of batch 4 were from another extrusion series. However, both extrusions were produced with the same aluminium alloy (6082-T6) under comparable conditions at the same production facility.

3. Experimental test program

3.1. Introduction

A total of 41 test specimens were included in the test program. Twelve specimens from each of batches 1 and

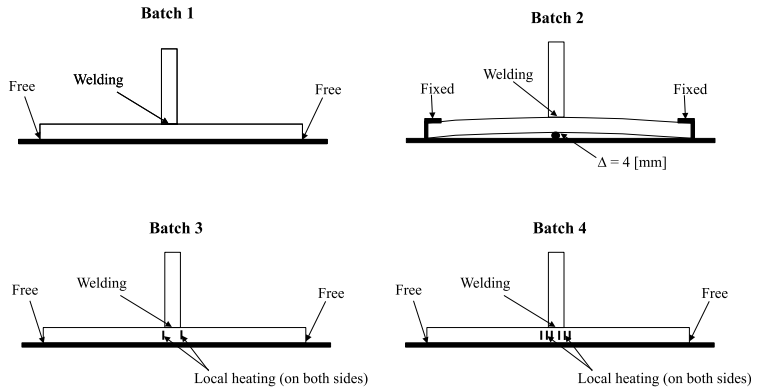

Fig. 1. Description of the different manufacturing methods of the RHS T-joints tested.

2, 9 specimens from batch 3, and 8 specimens from batch 4. The welded specimens consist of two identical aluminium RHS profiles. The dimensions of the profiles are 40 mm × 60 mm with a length of 500 mm and a wall thickness of 3 mm. The end of one profile is welded against the flat side of the other using fully automatic welding. The welding was carried out along the circumference of the tube at a travelling speed between 9 and 12 mm/s. After welding and local heating, the test specimens were stored at room temperature for more than a month before the fatigue test program was started. As the start and stop positions on the weld are characterised by a rather irregular and unfavourable weld geometry, the start and stop positions were placed on the long sides of the RHS (parallel to the load direction, Fig. 2). With respect to the applied loading (4-point bending, see Section 3.3), this was assumed to be an optimum location where possible irregular weld geometry (and possible weld defects) would not adversely influence the fatigue strength of the test specimens.

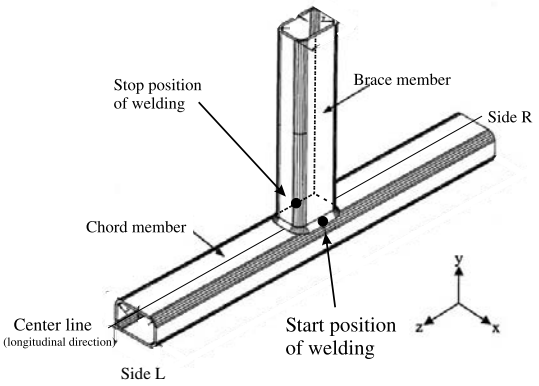

Fig. 2. RHS T-joint.

3.2. Weld characteristics

In order to quantify the notch effects of the four batches, weld geometry features such as the weld toe radius, ρ, weld toe angle, ϕ, and weld leg length, l, were measured (see Table 1). A local two-parameter description (with ρ and ϕ) has been shown to provide a satisfactory description of the local weld notch effects [7,8]. The current investigation also measures the weld leg length l as it has been shown that this may as well influence the notch effect [6]. Structured light was used to measure the weld geometry [9].

The measurements were performed at three weld cross-sections (at the centre line $x = 0$, Fig. 2, and at locations $x = \pm 10$ mm) for some randomly selected components from each batch. In order to determine the characteristics of the weld geometry, definitions of weld toe angle and radius have been established (Fig. 3). The definition is based on a circle drawn over the weld toe, which is fixed at the transition point between the weld and chord, point A. The circle radius is altered until it fits the weld toe geometry. A second point is defined as the point where the circle leaves the weld toe contour, point B. Two vectors are established from the centre of the circle to each of the two points. The weld toe angle is then defined as the angle between the two vectors. The radius is defined as the vector length.

The weld geometry and weld defects were measured using structured light [9], which makes it possible to detect crack depths down to 50 μm. The mean values and the standard deviation of the measured values have been present in Table 1.

Statistical analyses of the weld geometry parameters ρ, ϕ and l were carried out on all four batches according to Walpole et al. [10]. The parameters were assumed to follow a normal distribution. At a significance level of 95%, there is no difference between the batches regarding the mean values of the weld toe radius. Regarding the weld toe angle, no significant difference was seen between batches 1, 3, and

Table 1
Measured weld toe characteristics, weld toe radius, ρ; weld leg length, l; and weld toe angle, ϕ

		Side R						Side L					
		Radius, ρ (mm)		Weld leg length (mm)		Angle, ϕ (°)		Radius, ρ (mm)		Weld leg length (mm)		Angle, ϕ (°)	
		Mean value	STDV	Mean value	STDV	Mean value	STDV	Mean value	STDV	Mean value	STDV	Mean value	STDV
Batch 1 (4 welds)	−10 mm	1.9	0.5	7.4	0.4	48	15	2.0	0.3	7.1	0.5	48	3
	Centre line	1.6	0.7	7.3	0.4	53	7	4.9	1.3	8.2	0.6	39	3
	+10 mm	1.7	0.2	6.6	0.5	62	9	4.7	0.6	7.5	0.2	43	4
Batch 2 (5 welds)	−10 mm	2.1	0.7	6.8	0.4	59	3	1.5	0.6	6.3	0.4	57	5
	Centre line	1.8	0.6	6.6	0.6	56	5	1.7	0.6	6.4	0.4	55	10
	+10 mm	1.8	0.6	6.3	0.7	58	5	1.9	0.5	6.0	0.6	59	9
Batch 3 (4 welds)	−10 mm	1.1	0.7	6.0	0.3	72	1	1.9	1.0	7.1	0.3	48	10
	Centre line	1.0	0.3	6.0	0.1	64	6	2.8	1.0	7.2	0.5	42	12
	+10 mm	1.0	0.4	5.5	0.1	69	7	2.8	0.6	6.6	0.1	45	10
Batch 4 (5 welds)	−10 mm	2.4	0.9	7.2	0.5	46	7	1.7	0.2	7.4	0.2	47	3
	Centre line	1.4	0.5	7.2	0.6	49	16	3.1	1.2	7.5	0.4	32	10
	+10 mm	1.1	0.1	6.7	0.4	56	10	2.6	1.7	6.7	0.6	36	9

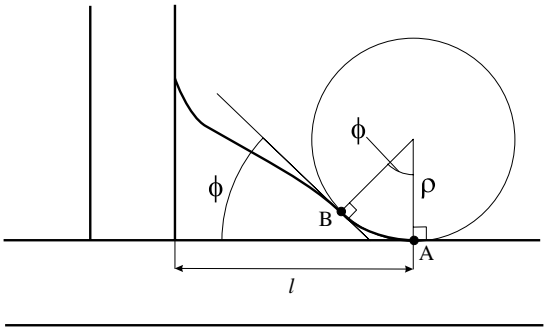

Fig. 3. Weld geometry definition, weld toe radius, ρ; weld toe angle, ϕ; and weld leg length, l.

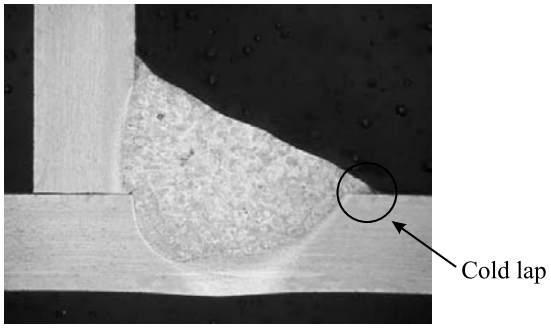

Fig. 4. Example of macro graph, batch 1.

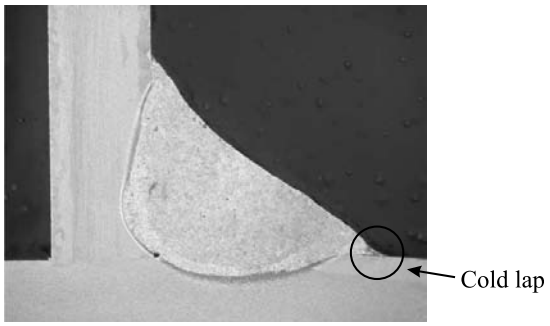

Fig. 5. Example of macro graph, batch 2.

4. However, there is a significant difference between the weld at side L (see Fig. 2 for definition of sides) where the weld toe angle of batch 2 is significantly larger than that of the other batches. Thus, larger weld toe angles (increased notch effects) at side L of batch 2 may adversely affect the fatigue strength of batch 2 compared to the other batches.

In addition to the geometrical measurements presented above, possible detectable weld defects were quantified by means of macro-graphs (examples given in Figs. 4 and 5).

From each of the batches 1, 2 and 4, one test specimen was cut and macro-graphs were produced. The macro-graphs were taken at several locations along the fillet weld. Examining the macro-graphs, a lack of fusion can be seen at the weld toe (also referred to as cold laps). Similar cold laps were also detected at previously tested RHS T-joints [11]. Cold laps of aluminium welds are often caused by a surface oxide layer, which has a considerable higher temperature of fusion than metallic aluminium (2050 and 650 °C, respectively). Since the temperature at the rim of the weld bead during welding is somewhat lower than the temperature inside the weld bead, the temperature is probably not sufficient to break down the oxide layer in order to obtain complete fusion at the weld toe. As seen from the macro-graphs, all batches of test specimens experience cold

laps, with a tendency for the largest to appear in batch 2. Actually, similar features are normally seen in aluminium production welds, even though the welds meet the specifications.

In a study on welded cruciform steel joints, cold laps have been shown to reduce the fatigue strength [12], since cold laps act as sites for fatigue crack initiation. It has been shown that a crack growing from a cold lap rapidly reaches a vertical orientation [13]. Thus, as observed for numerical simulations and fatigue tests, it is assumed that the observed cold laps will reduce the fatigue strength of the test specimens. However, it is assumed that even though the cold laps are adversely influencing the fatigue strength, the effect is the same for all batches. It is therefore likely that the observed cold laps will not distinctly influence the comparison between the different production methods. Indeed, as cold laps at the weld toes seem to be an inherent feature of aluminium production welds, one should ask the question whether the fatigue strength of aluminium joints may be considerably improved by new welding methods that can eliminate lack of fusion at the weld toes. However, this is beyond the scope of this study.

After welding batch 2, possible weld defects were observed by means of visual inspection along the fusion line of the welded RHS T-joints [6]. Fig. 6 shows an example of the observed weld defects along the weld toe of a specimen in batch 2. Similar weld defects were not observed visually for batches 1, 3, and 4. The weld defects were also detected in the structured light measurements of batch 2, whereas no weld defects were detected for batches 1, 3 and 4.

The visible, large weld defects observed for batch 2 may be a result of the presence of Mg_2Si near the fusion line [14]. Mg_2Si reaches solid state at a lower temperature than the weld and base material. Thus, at a point in time during cool-down, a layer of liquid Mg_2Si is present at grain boundaries close to the fusion line, while the weld and base material have already solidified. This leads to cracks forming at, or near the fusion line. The phenomenon affects all batches. However, since batch 2 is prestrained at the upper surface, and is therefore experiencing a large tension field at the weld, the weld defects will grow larger. These weld defects will, as mentioned, also appear in the other batches, but are assumed to be smaller. Thus, it is concluded that even though the welding process of batch 2 will introduce compressive stresses along the fusion line, which will enhance the fatigue life, the process will also introduce rather large weld defects, which are likely to reduce the fatigue life of the RHS T-joint.

Based on the discussion above, the following points are noted:

- larger weld toe angles (increased notch effects) at side L of batch 2 may affect the fatigue strength of batch 2 compared with the other batches,
- as seen from the macro-graphs, all batches show cold laps,
- the specimens of batch 2 show large weld defects along the fusion line, which will most likely affect the fatigue life.

3.3. Test rig arrangement

The four different batches of the aluminium RHS T-joints (Fig. 2) were tested in 4-point bending, with a constant bending moment throughout the weld region (Fig. 7). The axial loading was provided by a servo-hydraulic actuator. Sinusoidal constant amplitude loading was applied at $R = 0.1$ and the fatigue testing was performed in laboratory air at ambient temperature with a loading frequency ranging from 5 to 10 Hz depending on the applied load level.

In order to verify the actual stress-state experienced in the test rig and the validity of elastic beam theory applied to the RHS T-joints, strain gauge measurements were carried out for one welded specimens from each of batches 1 and 4, and one unwelded RHS chord member (without brace). The measured strain values are presented relative to elastic beam theory predictions ($\Delta\epsilon_{zz}/\Delta\epsilon_{beam}$) in

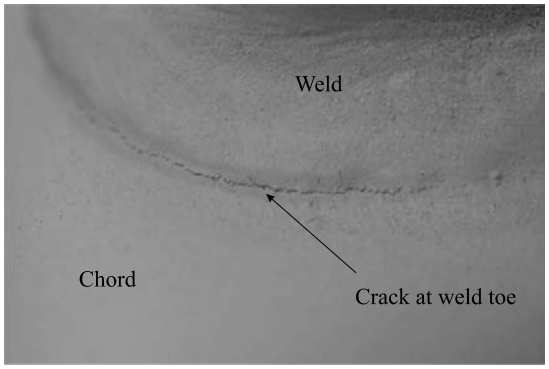

Fig. 6. Close-up of the weld defect observed along the fusion line, batch 2.

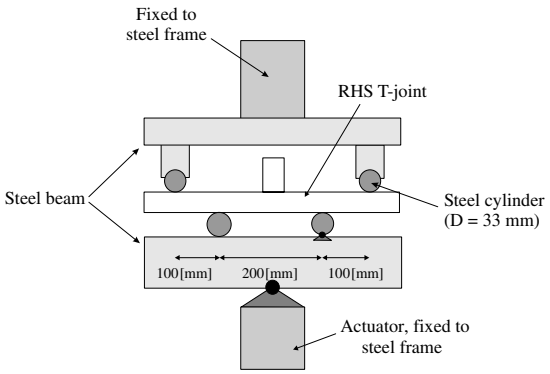

Fig. 7. Schematic outline of test rig.

longitudinal direction (see Figs. 8 and 9) both at the centre line and at the sides (approximately 10 mm from the centre line, x-direction) of the RHS profile. Due to the irregular geometry at the weld toe and the size of the strain gauges, these could not be placed closer to the weld toe location than about 1 mm.

As should be expected from the brace geometry and the local notch effects, the strain will increase close to the weld toe as seen in Figs. 8 and 9. The concentrated loads (steel cylinders, Fig. 7) from the test rig applied to the chord explains the localised peak strain observed within 50 mm from the applied load. The strain measurements performed

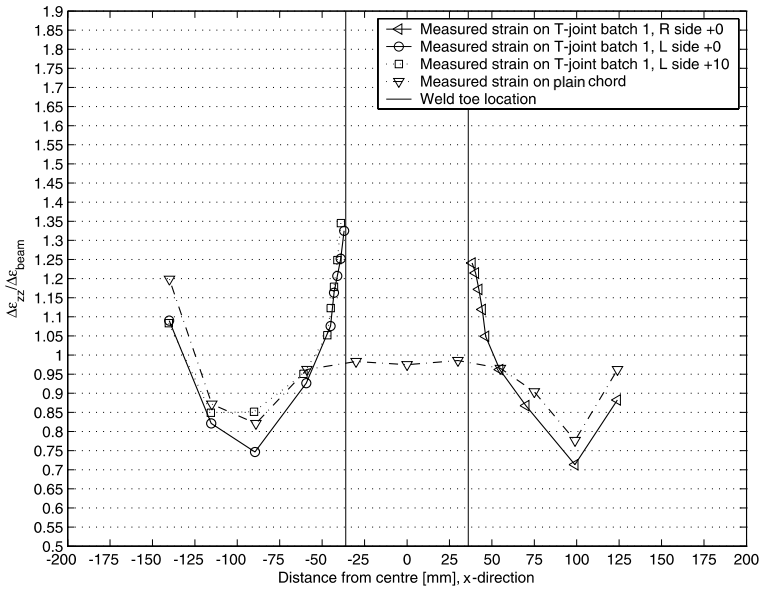

Fig. 8. Strain gauge measurements from T-joint (batch 1) and plain chord member relative to elastic beam theory predictions.

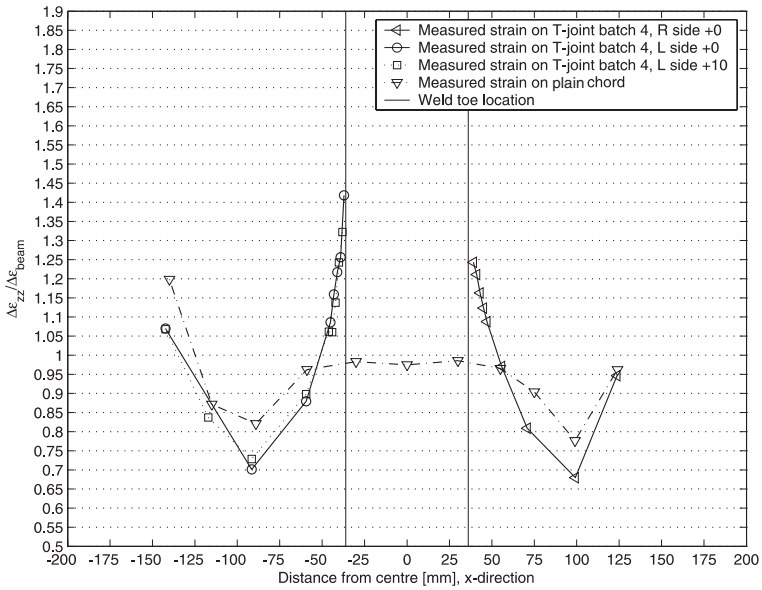

Fig. 9. Strain gauge measurements from T-joint (batch 4) and plain chord member relative to elastic beam theory predictions.

on the unwelded chord shows that concentrated loads from the steel cylinders will not influence the stress field near the weld of the T-joint. A difference of less than 2.5% is seen between the measures stains and beam theory. Inhouse experience shows that differences of this magnitude is normally expected from strain gage measurements on welded joints. No significant difference in strain is observed between the two batches that were produced from different extrusion series.

Based on the strain gage measurements, it is concluded that:

- the concentrated loads from the test rig not will influence the state of stress near the weld toe,
- the test rig arrangement provides a constant bending moment over the gauge length,
- elastic beam theory is valid for representing the strains.

4. Fatigue test results

4.1. Introduction

Macro-geometrical features and concentrated loads, notch effects, weld defects and local compressive or tensile stress fields are factors affecting the fatigue life. The relative influence on the fatigue life of welded structures will, however, be highly case sensitive depending on, e.g. the complexity of the joint, the workmanship and the loading pattern. However, as a general trend, macro-geometrical features (e.g. brace attachments), irregular geometry (small weld toe radii, ρ, and large weld toe angles, ϕ), existing weld defects (e.g. undercut and cold lap), and local tensile stress fields will adversely affect the fatigue strength of welded structures.

4.2. Fatigue test results

The fatigue test results obtained from the fatigue experiments of the four different batches are shown in Fig. 10. In order to increase the population of batch 1, results from fatigue tests performed by Haavi [11] and Edvardsen and Trandum [15] were included in the statistical analysis of the S–N data. In [11,15] corresponding tests were performed on "as welded" specimens under comparable laboratory conditions. The three test series were subjected to extensive statistical analyses based on methods described by Rausand [16] and Guttman et al. [17] in order to verify if it is statistically reasonable to treat the results as one pooled population. The analysis showed that given a 95% significance level, the samples could be regarded as one population. The test S–N data are plotted using the number of cycles, N, to a complete loss of the load-bearing capacity of the RHS T-joint versus the nominal stress range, $\Delta\sigma$, obtained by means of elastic beam theory. The S–N data were analysed using a linear S–N curve on a log-log scale, given by

$$\log N = \beta \log \Delta\sigma + \alpha, \tag{1}$$

where the intercept parameter α and slope parameter β were determined through a statistical regression analysis (see Table 2 for linear regression parameters). Due to shear lag effects, maximum longitudinal stress is experienced at the side corners. The welded RHS T-joint tested in this

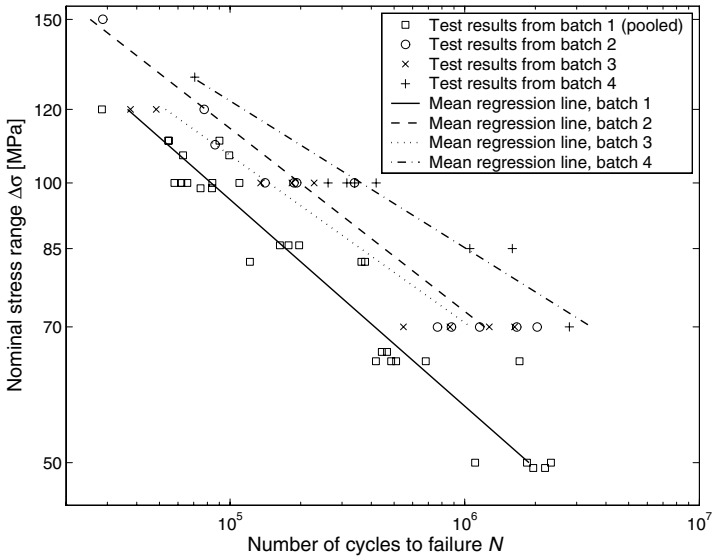

Fig. 10. Fatigue results of batches 1–4.

Table 2
Linear regression parameters

	Number of specimens, n	Slope of S–N curve, β	Intercept of $\log(N)$-axis, α	Correlation, R^2	Standard deviation, $\mathrm{STDV}_{\log N}$	Characteristic strength (MPa) at $N = 10^6$
Batch 1	12	−4.6	14.1	0.98	0.11	57
Batch 2	12	−5.1	15.5	0.94	0.15	73
Batch 3	9	−5.6	16.3	0.93	0.17	71
Batch 4	8	−6.3	18.2	0.96	0.11	85

study has two locations (side L and R, Fig. 2), where fatigue failure may initiate subjected to the same nominal stress state (see Section 3.3) and environment.

The statistical comparison of batches 1–4 was performed according to methods presented by [16,17]. It is required that the variances of the data sets subjected to analysis are equal. The variances of the four batches were tested and found to be equal with a 95% significance level. The "coefficient of variance" (COV) for the entire test was found to be 0.3, and this is within what is usually seen for constant amplitude tests of welded aluminium joints (see e.g. [18,19,20] where values between 0.23 and 0.33 were found). Based on a statistical evaluation of the test S–N data, the introduction of superimposed compressive stresses into the weld and HAZ has been shown to enhance the fatigue strength. Fig. 11 shows the 95% confidence region of the parameters α and β for all four batches. According to [16,17], the confidence region is obtained from the following expression:

$$\frac{n(\hat{\alpha}-\alpha)^2 + 2(\hat{\alpha}-\alpha)(\hat{\beta}-\beta)\sum_{i=1}^{n}\Delta\sigma_i + (\hat{\beta}-\beta)^2\sum_{i=1}^{n}\Delta\sigma_i^2}{2S^2} > f_{\epsilon,2,n-2}, \tag{2}$$

where f_{ϵ,v_1,v_2} denotes the upper ϵ percentile of the Fisher distribution with v_1 and v_2 degrees of freedom and S is the sample standard deviation. $\hat{\alpha}$ and $\hat{\beta}$ are estimates for the current population with sample size n. It is seen from Fig. 11 that the slopes of batches 2–4 are significantly different from that of batch 1. Thus, as can be seen from Fig. 10, all prestressing methods presented in this paper result in an increased fatigue life. Comparing the batches subjected to mechanical and thermal treatment, batch 4 is significantly different from batches 2 and 3, while no significant difference can be seen between batches 2 and 3 due to the overlap in confidence regions. The most effective treatment regarding the fatigue life is achieved through the thermal prestressing preformed on batch 4 with a 50% higher characteristic strength at $N = 1 \times 10^6$ cycles than that of batch 1. The corresponding values for batches 2 and 3 are 29% and 25%, respectively.

Studying the crack surfaces in a scanning electron microscope (SEM), it is possible to locate the site of crack initiation. The origin of crack initiation is found by tracing the striations backwards. As expected, crack initiation always takes place at one of the corners (see Fig. 12), which are experiencing the highest stresses. The crack first develops in an elliptic manner, while subsequent cracks initiate

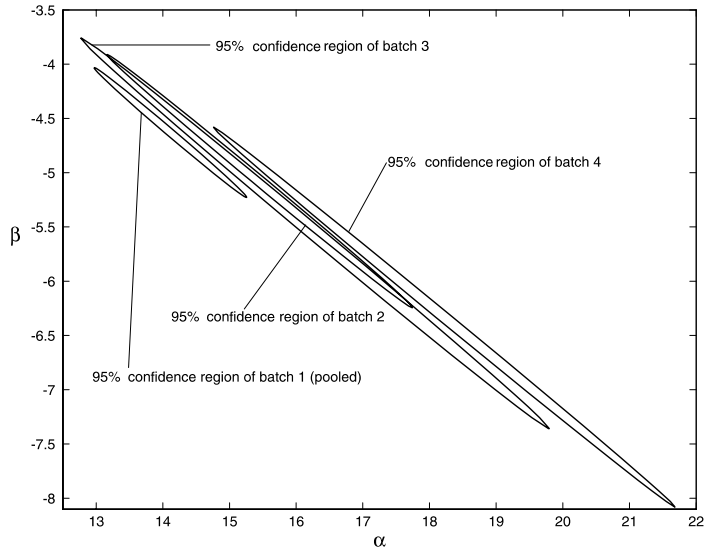

Fig. 11. The 95% confidence region for the intercept parameter α and the slope parameter β for all four batches.

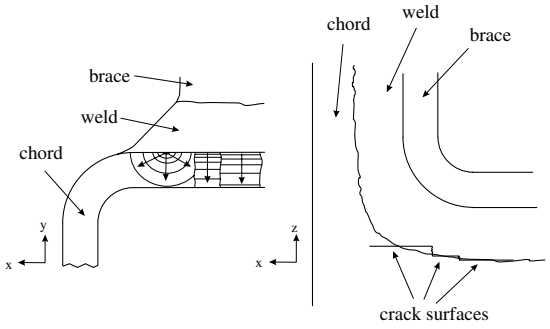

Fig. 12. Sketch of the crack surface showing the crack growth behaviour.

along the weld toe beside the elliptic crack. As opposed to the initial elliptical crack growth, these cracks grow in a straight crack front (y-direction).

The TPM analyses using WeldSim show residual stresses that are all-tensile for batch 1, all compressive for batches 2 and 4, and compressive for batch 3 with some areas of low tensile stresses. Knowing that batch 2 experiences large weld defects due to the cooling process, which takes place under large tensile stresses, the general trend of the fatigue life (Fig. 10) is highly consistent with the predicted residual stress fields. Thus, the results show that it is possible to realise methods for the enhancement of fatigue life based on TPM simulations.

The fatigue tests presented in this study have been based on constant amplitude loading. However, for "real structures", it is observed that the magnitude of the residual stresses can decrease during the load sequence when subjected to variable amplitude loading. The decay is due to local shake down, i.e. local plastic deformations caused by peak loads during the cyclic loading which modifies the local stress distribution [21]. Thus, definitive conclusions regarding the success of FE-simulations together with optimised prestressing methods under various service-like loadings need to be confirmed by further testing. However, the uncertainties related to the long term effect of the fatigue strength improvement by means of residual stress methods is also relevant for existing weld improvement methods.

5. Conclusions

Based on a statistical evaluation of the S–N data of the RHS T-joints, the introduction of superimposed residual stress fields by manipulating the manufacturing process will improve the fatigue life of the welded aluminium RHS T-joints. The manufacturing process have been based on FE-simulations taking into account microstructural and mechanical models (through process modeling, TPM). Other factors influencing fatigue life were monitored, and were found not to play a significant role. Thus, the fatigue life enhancement seen in this study is solely a consequence of the superimposed residual stress fields.

Even though the method of modifying residual stresses by means of elastic pre-deformation of the chord shows an improvement of the fatigue strength by a factor of 1.3, the method is not considered practicable, since welding introduces large defects along the fusion line. However, the induction heating procedures used in this study have great potential, since a fatigue strength improvement of a factor of 1.5 on stress for the RHS T-joint has been demonstrated.

The following main points are noted:

- The fatigue strength of welded aluminium RHS T-joints can be enhanced by manipulating the residual stresses.
- The fatigue strength of batch 2 is affected by a large number of weld defects, caused by the subsequent cooling process under a large tensile stress field.
- The fatigue strength of all batches is adversely affected by a large number of cold laps.
- The difference in fatigue life among the batches can be solely explained by variation in the residual stress field (except for batch 2 where a large number of defects is seen). Other factors affecting the fatigue life are assumed to influence all batches equally.
- Methods for fatigue life enhancement of welded aluminium joints can be obtained and optimised by means of through process modeling (TPM).

Acknowledgements

The authors gratefully acknowledge the research support for this work provided by The Research Council of Norway – Norges forskningsråd (NFR) and the industrial participants within the NorLight project.

References

[1] Haagensen PJ, Maddox SJ. Recommendations on post weld improvement of steel and aluminum structures. Technical Report IIW Doc. No. XIII-1850-00, International Institute of Welding; 1999.
[2] Myhr OR, Klokkehaug S, Fjær HG, Grong Ø, Kluken AO. Modelling of microstructure evolution, residual stresses and distortions in 6082-T6 aluminium weldments. Welding J 1998;77(7):286–92.
[3] Myhr OR, Grong Ø, Klokkehaug S, Fjær HG, Kluken AO. Modelling of the microstructure and strength evolution during ageing and welding of Al–Mg–Si alloys. In: Proceedings of the sixth international seminar on numerical analysis of weldability, Graz-Seggau, Austria, October 1–3; 2001.
[4] Fjær HG, Myhr OR, Klokkehaug S, Holm S. Advances in aluminium weld simulations applying WeldSim. In: Proceedings of the 11th international conference on computer technology in welding, Columbus, OH, USA, December; 2001.
[5] Myhr OR, Tveiten BW, Fjær HG, Bjørneklett B. Through process modelling in manufacturing of aluminium structures for automotive applications. In: Proceedings of the TMS global innovations symposium, USA; 2005.
[6] Tveiten BW. The Fatigue Strength of RHS T-joints – NFR Kompetanseprosjekt – KMB 144004/213 – Fatigue and Durability. Technical Report STF24 A03220, SINTEF, Trondheim, Norway; 2003.

[7] Engesvik KM. Analysis of uncertainties in the fatigue capacity of welded joints. PhD Thesis, Department of Marine Technology, The Norwegian Institute of Technology (NTH), University of Trondheim, Norway; 1981.
[8] Almar-Næss A. Fatigue handbook. Trondheim, Norway: Tapir Forlag; 1985.
[9] Couweleers F, Skotheim Ø, Tveiten BW. Optical measurement of weld toe geometry with structured light. In: Proceedings of the eighth international symposium on measurement and quality control in production, Erlangen, Germany, October 12–15; 2004.
[10] Walpole RE, Myers RH, Myers SL. Probability and statistics for engineers and scientists. sixth ed. Englewood Cliffs, NJ, USA: Prentice-Hall International; 1998.
[11] Haavi T. Fatigue of welded joints in extruded aluminium hollow section profiles. Master's Thesis, Norwegian University of Science and Technology, Trondheim, Norway; 1998.
[12] Samuelsson J. Cold laps and weld quality acceptance limits. In: Samuelsson J, editor. Design and analysis of welded high strength steel structures. Stockholm, Sweden: EMAS Ltd.; 2002. p. 151–61.
[13] Martinsson J. Fatigue strength of welded cruciform joint with cold laps. In: Samuelsson J, editor. Design and analysis of welded high strength steel structures. Stockholm, Sweden: EMAS Ltd.; 2002. p. 163–84.
[14] Grong Ø. Metallurgical modelling of welding. second ed. The Institute of Materials; 1997.
[15] Edvardsen RM, Trandum R. Fatigue of welded rectangular aluminium hollow section joints (in Norwegian). Master's Thesis, Norwegian University of Science and Technology, Trondheim, Norway; 1996.
[16] Rausand M. Statistical analysis of fatigue test data. Technical Report STF18 A81047, SINTEF, Trondheim, Norway; 1981.
[17] Guttman I, Wilks SS, Hunter S. Introductory engineering statistics. second ed. Wiley; 1971 [chapter 15.2–15.4, p. 341–50].
[18] Tveiten BW. Fatigue Assessment of Welded Aluminium Ship Details. PhD Thesis, Department of Marine Structures, The Norwegian University of Science and Technology; 1999.
[19] Aabø S, Paauw AJ, Engh B, Solli O. Utmatting av Sveiste Aluminiumsforbindelser. Technical Report STF34 A85024, SINTEF, Trondheim, Norway; 1985.
[20] Partanen T, Niemi E. Hot spot *S–N* curves based on fatigue tests of small mig welded aluminium specimens. Technical Report IIW-XIII-1636-96, The International Institute of welding, Cambridge, United Kingdom; 1996.
[21] Bogren J, Martinez LL. Spectrum fatigue testing and residual stress measurements on non-load carrying fillet welded test specimen. London, United Kingdom: Cameleon Press Ltd.; 1993.

Paper 2

Available online at www.sciencedirect.com
SCIENCE DIRECT®
Engineering Fracture Mechanics 73 (2006) 1899–1912
Engineering Fracture Mechanics
www.elsevier.com/locate/engfracmech

The application of asymptotic solutions to a semi-elliptical crack at the root of a notch

A. Wormsen *, A. Fjeldstad, G. Härkegård

Department of Engineering and Design and Materials, Norwegian University of Science and Technology, Richard Birkelandsevi 2B, NO-7491 Trondheim, Norway

Received 4 June 2005; received in revised form 27 January 2006; accepted 10 February 2006
Available online 18 May 2006

Abstract

This paper presents an approximate method based on asymptotic solutions for estimating the stress intensity factor K for semi-elliptic surface cracks at stress concentrations. The proposed equation for estimating K makes use of the near-notch and remote-notch solution to interpolate over the entire range from shallow to deep cracks. The near-notch solution is obtained by means of the stress concentration factor. For cracks located in the remote stress field, K is obtained by considering the crack to be located in a smooth plate with a crack depth equal to the sum of the notch depth and the actual crack depth. The accuracy of the predictions is assessed using numerical calculations and solutions found in the literature.

Keywords: Stress intensity factor; Geometry factor; Asymptotic solution; Shallow crack; Deep crack; Notch

1. Introduction

For a real component the stress is generally decreasing from a maximum at some critical point at the surface, e.g. in the case of notches or components subjected to bending or torsion. For simplicity and to ensure conservatism, crack growth analyses are often performed assuming a homogeneous stress field based on the maximum stress acting on the surface. This local stress approach yields acceptable results provided that the stress decreases slowly, i.e. the stress gradient is small. However, for steep stress gradients, a crack growth analysis based on the local stress will lead to over-conservative predictions. Since crack growth prediction requires the stress intensity factor K to be known, it is of great practical interest to establish simple formulae for estimating K for a semi-elliptical crack at the root of a notch.

While approximate K estimation procedures are well established for cracks emanating from a smooth surface, the situation is much less satisfactory, when it comes to cracks at the root of a notch. Thus, the present work focuses on through-cracks and semi-elliptical cracks at the root of a surface notch in a semi-infinite plate. Systematic computational efforts over the last 50 years have lead to stress intensity factor solutions for many

* Corresponding author. Tel.: +4773597098.
E-mail address: anders.wormsen@ntnu.no (A. Wormsen).

0013-7944/$ - see front matter
doi:10.1016/j.engfracmech.2006.02.006

Nomenclature

A	deepest point of crack front
a	crack depth
a',a^*	transition crack depth between shallow and deep crack asymptotes
BEA	boundary element analysis
C	intersection between crack front and free surface
c	half the surface crack length
D	equivalent surface crack depth
d	notch depth
E	Young's modulus
E_2	complete elliptic integral of the second kind
F	geometry factor
F_0	geometry factor for a crack emanating from a smooth surface
F_A	geometry factor at point A
F_C	geometry factor at point C
F_∞	reference geometry factor $= F_0\sqrt{1+d/a}$
FEA	finite element analysis
g	Green's function
J	J integral
K	stress intensity factor $= F\sigma_\infty\sqrt{\pi a}$
K_t	stress concentration factor $= \sigma_{max}/\sigma_\infty$
w	width of plane specimen
δ_i	coefficient of ith order term of $\sigma_y(x)$
ν	Poisson's ratio
ξ	dimensionless co-ordinate $= x/a$
ρ	notch root radius
σ_y	normal stress in y-direction
σ_{max}	maximum stress
σ_∞	remote stress
ϕ	angle defining location on semi-elliptical crack front
χ	relative stress gradient

different crack geometries [1], but these are often restricted to a few simple stress fields. For more complex stress fields, only few empirical solutions exist [2–4]. These are mainly given in terms of a set of empirical equations established by means of curve fitting to numerical results.

The objective of the present investigation is to present simplified solutions for the stress intensity factor K for semi-infinite notched plates. These formulae make use of asymptotic solutions to interpolate over the entire range from shallow to deep cracks. Although only semi-infinite notched plates have been considered, these formulae should be equally applicable to other notched components, since the component geometry does not markedly affect the stress intensity values for relatively shallow cracks, provided that the stress field in the vicinity of the crack is the same [4,5]. The present paper shows that asymptotic solutions provide a useful basis for the analysis of cracked notched solids.

2. Linear crack analysis, general equations

For an arbitrary body with a semi-elliptic surface crack of depth a under uniaxial remote tension σ_∞ perpendicular to the plane of the crack, K can be written as

$$K = F\sigma_\infty\sqrt{\pi a}, \tag{1}$$

where F is a dimensionless function of the geometry of the body and the crack. For a crack in the notch stress field, the stress intensity solution is asymptotically the same as for a surface crack in a smooth solid, except that the remote stress is being amplified by the stress concentration factor $K_t = \sigma_{max}/\sigma_\infty$ (see Fig. 1). Thus, as $a \to 0$,

$$K = F\sigma_\infty\sqrt{\pi a} = F_0 K_t \sigma_\infty \sqrt{\pi a}, \tag{2}$$

where F_0 is the geometry factor for the current surface crack emanating from a smooth surface. Well known solutions for a surface crack in a finite plate under tension or bending have been presented by Newman and Raju [6]. For a semi-infinite plate, the geometry factors for tension and bending coincide. For a semi-elliptic surface crack with aspect ratio a/c (cf. Fig. 3(b)), the geometry factor at the deepest point of the crack front A$(a;0)$ can be estimated as

$$F_0(\phi = \pi/2;\, a/c) = F_{A,0} = \frac{1.13 - 0.09\frac{a}{c}}{E_2(a/c)}. \tag{3}$$

Similarly, at the intersection between the crack front and the free surface, C$(0;c)$, the geometry factor can be estimated as

$$F_0(\phi = 0;\, a/c) = F_{C,0} = \frac{1.243 - 0.099\frac{a}{c}}{E_2(a/c)}\sqrt{\frac{a}{c}}. \tag{4}$$

In Eqs. (3) and (4), the aspect ratio, a/c, is limited to the range from 0 to 1, where the complete elliptic integral of the second kind, $E_2(a/c)$, can be approximated by

$$E_2(a/c) \approx \sqrt{1 + 1.464\left(\frac{a}{c}\right)^{1.65}}, \quad 0 \leqslant a/c \leqslant 1. \tag{5}$$

For an edge through-crack, Eq. (3) reduces to

$$F_0 = F_{A,0} = 1.13, \tag{6}$$

in good agreement with the more precise solution $F_0 = 1.122$ [1].

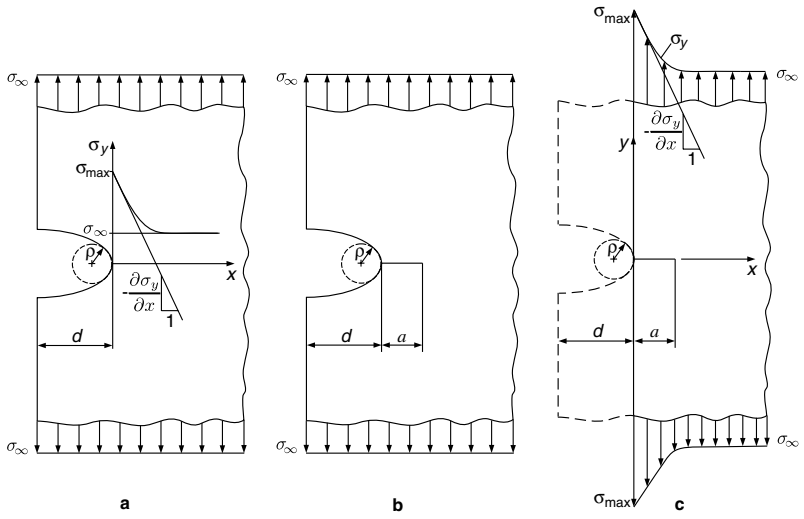

Fig. 1. Semi-infinite notched plate under uniform remote stress σ_∞: (a) stress concentration and stress gradient, (b) through-crack at the root of a surface notch, (c) un-notched cracked plate subjected to the notch stress field $\sigma_y(x)$.

For a crack located in the notch stress field, the asymptotic solution for the geometry factor F becomes

$$F = F_0 K_t. \tag{7}$$

When the crack grows beyond the notch stress field, the remote stress field dominates the stress intensity factor, which may now be estimated by

$$K = F_0 \sigma_\infty \sqrt{\pi(a+d)}, \tag{8}$$

where d denotes the notch depth. Identification with Eq. (1) yields

$$F = F_\infty = F_0 \sqrt{1 + \frac{d}{a}}, \tag{9}$$

where F_∞ denotes a reference geometry factor. When $a/d \gg 1$, F asymptotically approaches the constant value

$$F = F_0. \tag{10}$$

The two preceding asymptotic solutions, i.e. Eqs. (7) and (10), give the upper and lower bound values for the geometry factor F. By using these asymptotic solutions, simple formulae can be established for the geometry factor F of an arbitrarily sized semi-elliptic crack emanating from the root of a notch.

In the next section, geometry factors are presented for through-cracks at the root of a notch. Semi-elliptical cracks will be treated in Section 4.

3. Through-crack at the root of a notch

The configuration considered is a notched semi-infinite plate subjected to a remote stress σ_∞ perpendicular to the symmetry plane of the notch. The notch is characterised by its depth d, its root radius ρ and its elastic stress concentration factor $K_t = \sigma_{max}/\sigma_\infty$. Along with the stress concentration comes a stress field with its largest gradient at the notch root, as illustrated in Fig. 1(a). At the root of the notch, a through-crack of depth a is located as shown in Fig. 1(b). It should be noted that $F_0 = 1.122$ for a through-crack.

3.1. Geometry factors

Several methods are available for determining stress intensity factors [7,8]. In the following, only approximate methods using the 'nominal' stress field equal to the 'local' stress field of the crack-free specimen (in the plane of the subsequent crack) are considered.

3.1.1. Green's function

One of these methods is based on the solution of an edge through-crack of depth a, where the crack surfaces are subjected to a pair of symmetrical point forces, the so-called *Green function*. Once the stress in the plane of the subsequent crack and the appropriate Green function are known, determination of the geometry factor F is reduced to a simple integration procedure.

Consider now an edge through-crack of depth a located in a smooth semi-infinite plate subjected to the notch stress field $\sigma_y(x)$, see Fig. 1(c). The geometry factor F can then be estimated according to

$$F = \frac{1}{\pi} \int_0^1 \frac{\sigma_y(a\xi)}{\sigma_\infty} g(\xi) \mathrm{d}\xi, \tag{11}$$

where $g(\xi)$ is the Green function and $\xi = x/a$. According to Hartranft and Sih [9], the Green function for a crack of depth a subjected to a pair of symmetrical point forces in a semi-infinite plate is given by

$$g(\xi) = \frac{2(1+f(\xi))}{\sqrt{1-\xi^2}}, \tag{12}$$

$$f(\xi) = (1-\xi^2)(0.2945 - 0.3912\xi^2 + 0.7685\xi^4 - 0.9942\xi^6 + 0.5094\xi^8). \tag{13}$$

3.1.2. Stress gradient method

Another method for estimating the F value for a shallow crack at the root of a notch [10,11] is based on work by Benthem and Koiter [12]. For an edge-cracked semi-infinite plate subjected to a linear distribution of stress, one obtains

$$F = F_0(1 + 0.609\chi a). \tag{14}$$

If x denotes the distance below the surface, the relative stress gradient χ is defined as (cf. Fig. 1(c))

$$\chi = \frac{1}{\sigma_{\max}}\left(\frac{\partial \sigma_y(x)}{\partial x}\right)_{x=0}. \tag{15}$$

For a plate of width w subjected to pure bending, the relative stress gradient is given by

$$\chi = -\frac{2}{w}. \tag{16}$$

Eq. (14) may be compared with the geometry factor of a single-edge-cracked plate of width w subjected to bending [1]:

$$F = \frac{\sqrt{\frac{2w}{\pi a}\tan\frac{\pi a}{2w}}}{\cos\frac{\pi a}{2w}}\left[0.923 + 0.199\left(1 - \sin\frac{\pi a}{2w}\right)^3\right]. \tag{17}$$

It turns out that Eq. (14) is accurate for shallow cracks only, and that it should not be extrapolated beyond $a/w = 0.05$.

If a shallow crack at the root of a notch is subjected to the same stress gradient, χ, as the semi-infinite edge-cracked plate loaded by a linear distribution of stress, the geometry factors should be asymptotically equal. Thum et al. [13] found that the relative stress gradient at the root of a semi-elliptic surface notch of root radius ρ could be well approximated by

$$\chi = -\frac{2}{\rho}. \tag{18}$$

Eq. (14) then reduces to

$$F = F_0 K_t\left(1 - 1.218\frac{a}{\rho}\right). \tag{19}$$

According to [14], the stress concentration factor for a semi-infinite notched plate subjected to tension can be estimated by

$$K_t = 1 + \left(\frac{0.1}{d/\rho} + \frac{0.13}{(d/\rho)^{1.25}}\right)^{-0.5}. \tag{20}$$

As can be seen from Eqs. (19) and (20), the asymptotic geometry factor, F, for an edge-crack at the root of a notch is only dependent on the ratios a/ρ and d/ρ.

3.1.3. Lukáš and Klesnil's method

For a shallow through-crack at the root of a notch, Lukáš and Klesnil [15] presented a simple formula for the geometry factor, viz.

$$F = \frac{F_0 K_t}{\sqrt{1 + 4.5(a/\rho)}}. \tag{21}$$

Again, ρ denotes the notch root radius. As $a/\rho \to 0$, Eq. (21) simplifies to the shallow crack asymptote $F = F_0 K_t$. Normalising Eq. (21) with respect to the geometry factor, F_∞, for an edge through-crack in a smooth plate with the total crack depth $a + d$, cf. Eq. (9), yields

$$\frac{F}{F_\infty} = \frac{K_t}{\sqrt{1 + d/a + 4.5(a/\rho) + 4.5(d/\rho)}}. \tag{22}$$

3.2. Geometry factors based on asymptotic solutions

3.2.1. 'Equivalent' surface crack depth

For a through-crack located at the root of a notch, the geometry factor F is bounded by a lower and an upper asymptote, so that $1 \leqslant F/F_0 \leqslant K_t$. Jergéus [16] and Härkegård [17] introduced an equation for F, which asymptotically agrees with the near and remote field estimates. Thus, they suggested that the geometry factor be written as

$$F = F_0\sqrt{\frac{D}{a}}, \tag{23}$$

where D is an 'equivalent' surface crack depth, which can be estimated by

$$D = a + d\left[1 - \exp\left(-\frac{a}{a'}\right)\right], \tag{24}$$

and

$$a' = \frac{d}{K_t^2 - 1}. \tag{25}$$

The transition crack depth a' is defined as the crack depth at which the asymptotic Eqs. (2) and (8) for the stress intensity factors of shallow and deep cracks, respectively, yield equal results.

For a shallow crack, i.e. $a \ll a'$, the equivalent surface crack depth becomes

$$D = K_t^2 a, \tag{26}$$

and, for a deep crack, i.e. $a \gg a'$,

$$D = a + d. \tag{27}$$

Hence, Eq. (23) is in complete agreement with the asymptotic Eqs. (7) and (9).

3.2.2. Normalised geometry factors

For shallow cracks, $a/d \ll 1$, the ratio F/F_∞ is dominated by the stress field from the notch root, and F approaches the shallow crack asymptote, see Eq. (7). For a through-cracked notched plate subjected to uniaxial tension σ_∞ (cf. Fig. 1), the ratio becomes

$$\frac{F}{F_\infty} = \frac{K_t}{\sqrt{1 + \frac{d}{a}}}, \tag{28}$$

which simplifies to

$$\frac{F}{F_\infty} = K_t\sqrt{\frac{a}{d}}, \tag{29}$$

when $a' \ll d$.

For deep cracks, the geometry factor of the cracked notch will approach that of a smooth plate with a crack depth equal to the sum of the notch depth and the actual crack depth.

A simple expression, which asymptotically agrees with the near and remote field estimates is given by

$$\frac{F}{F_\infty} = \sqrt{1 - \exp(-a/a^*)}, \tag{30}$$

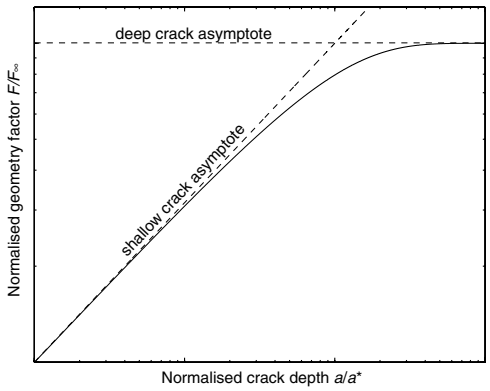

Fig. 2. Principle graph of F/F_∞ against the normalised crack depth a/a^*: logarithmic scales.

where a^* denotes the transition crack depth between the shallow and deep crack asymptotes, defined by the crack depth at which the two asymptotes coincide (cf. Fig. 2). Hence, a^* is determined by setting Eq. (29) equal to unity, which yields

$$a^* = \frac{d}{K_t^2}. \tag{31}$$

It can be shown that Eq. (30) satisfies the asymptotic expressions for shallow and deep cracks. Eq. (30) is depicted in Fig. 2 as a solid line.

4. Semi-elliptic crack at the root of a surface notch

Next, a semi-elliptic crack located at the root of a semi-circular edge notch in a semi-infinite plate subjected to uniaxial tension σ_∞ perpendicular to the symmetry plane of the notch is considered. The cracked configuration is shown in Fig. 3(a). The crack is characterised by its depth a and its surface length $2c$, as shown in Fig. 3(b).

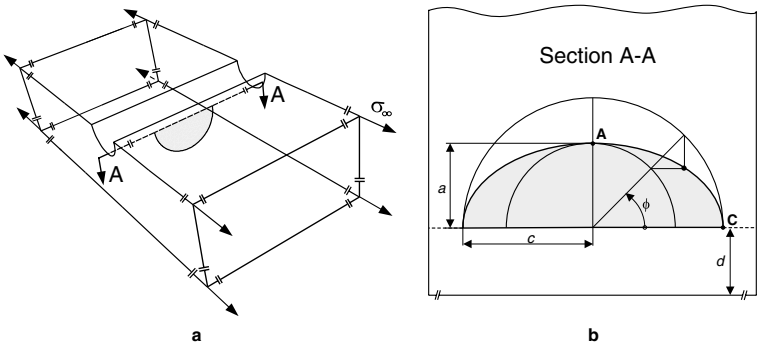

Fig. 3. Schematic drawings of a semi-elliptic crack emanating from the notch root: (a) three-dimensional view and (b) two-dimensional view of the cracked section A–A.

4.1. Geometry factors

4.1.1. Pommier, Sakae and Murakami

Using the body force method [18], Pommier et al. [3] have derived numerical solutions for the geometry factor F of a semi-elliptic surface crack located in a semi-infinite plate subjected to mode I loading. The crack aspect ratio is limited to the interval $0.5 \leqslant a/c \leqslant 2$. Their solution is given by a set of empirical equations, which allow the stress field of the crack-free plate to be fitted to a third-order polynomial.

For the semi-infinite plate, shown in Fig. 1, the normal stress in the y-direction varies with the x-coordinate only. The normal stress $\sigma_y(x)$ is approximated by the third-order polynomial [19]

$$\sigma_y(x) = \sum_{i=0}^{3} \delta_i \cdot (x/d)^i \cdot \sigma_\infty, \tag{32}$$

where δ_i is the coefficient of the ith order term of $\sigma_y(x)$. If Eq. (32) were an exact representation of $\sigma_y(x)$, then $\delta_0 = K_t$.

The empirical equations due to Pommier et al. [3] yield the geometry factor at the deepest point of the crack front A$(a;0)$ (cf. Fig. 3(b))

$$F_A = \sum_{i=0}^{3} \delta_i \cdot (a/d)^i \cdot F_i(\phi = \pi/2;\, a/c), \tag{33}$$

and at the intersection between the crack front and the free surface C$(0;c)$

$$F_C = \sum_{i=0}^{3} \delta_i \cdot (a/d)^i \cdot F_i(\phi = 0;\, a/c). \tag{34}$$

F_i is the geometry factor corresponding to the ith order unit stress field.

4.1.2. Lukáš method for semi-elliptical cracks

Based on work by Grandt and Kullgren [20], Lukáš [21] found that Eq. (21) for a through-crack at the root of a notch could be generalised to a semi-elliptic crack with an arbitrary aspect ratio a/c. It is only necessary to replace F_0 by the geometry factor $F_{A,0}$ for the deepest point of a semi-elliptic crack emanating from a smooth surface and having the same aspect ratio as the crack at the notch root. Thus Lukáš estimated the geometry factor of a semi-elliptic notch crack to be

$$F_A = \frac{F_{A,0} K_t}{\sqrt{1 + 4.5(a/\rho)}}. \tag{35}$$

4.2. Asymptotic solution

Based on work by Jergéus [16] and Härkegård [17], cf. Eq. (23), it is suggested that the geometry factor at the deepest point of the crack front A$(a;0)$ can be written in terms of the crack depth a and the equivalent crack depth D_A as

$$F(\phi = \pi/2;\, a/c) = F_A = F_{A,0}\sqrt{\frac{D_A}{a}}, \tag{36}$$

where $F_{A,0}$ is given by Eq. (3), and $D_A = D$ according to Eq. (24). As for the through-cracked specimens, Eq. (36) asymptotically satisfies the shallow and deep crack estimates $F_{A,0}K_t$ and $F_{A,0}$.

Similar to the deepest point A$(a;0)$, the geometry factor at the surface point C$(0;c)$ is characterised by a shallow and a deep crack asymptote. For shallow cracks, i.e. $a/d \ll 1$, the asymptote is given by

$$F_C = F_{C,0} K_t, \tag{37}$$

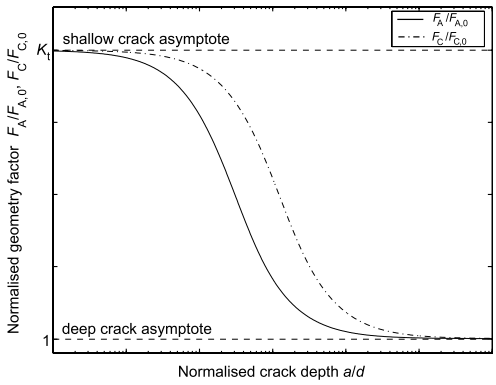

Fig. 4. Principal graph of $F_A/F_{A,0}$ and $F_C/F_{C,0}$ versus the normalised crack depth a/d.

where $F_{C,0}$ is the corresponding geometry factor of a crack in a smooth plate, which can be found by means of Eq. (4). While the surface point C$(0;c)$, regardless of the crack depth, is influenced by the elevated stress at the notch root, it may not be obvious that F_C asymptotically approaches a 'deep crack' solution. However, as the crack grows deeper, a decreasing part of the crack front will be influenced by the notch stress field. The influence decreases until the notch depth becomes insignificant compared with the dimensions of the crack. This can then be regarded as a semi-elliptical surface crack of depth $a+d$ located in a smooth plate. Hence, as the crack grows deeper, the ratio $F_C/F_{C,0}$ asymptotically approaches unity. Based on numerical results, it will be shown in Section 5 that the geometry factor F_C converges more slowly towards its 'deep crack' solution than F_A. Thus, a suitable expression for the equivalent notch depth turns out to be

$$D_C = a + 4d\left[1 - \exp\left(-\frac{a}{4a'}\right)\right]. \tag{38}$$

With this equivalent notch depth, the geometry factor at the surface point can be estimated as

$$F(\phi = 0; a/c) = F_C = F_{C,0}\sqrt{\frac{D_C}{a}}. \tag{39}$$

Fig. 4 shows a principle graph of the normalised geometry factors $F_A/F_{A,0}$ and $F_C/F_{C,0}$ versus the normalised crack depth a/d. As can be seen, both F_A and F_C satisfy the asymptotic solutions for shallow and deep cracks.

5. Numerical analysis

5.1. Through-cracked specimens

5.1.1. Finite element modelling and evaluation procedures

Linear elastic analyses of the finite element models were performed using the finite element program ABAQUS [22]. Fig. 5(a) illustrates a typical finite element mesh employed in the present work. The local mesh in the crack tip region was identical for all models, with 16 elements around the crack tip. Eight-noded isoparametric second-order plane strain elements with reduced integration (2×2 Gauss points; element type CPE8R in ABAQUS [22]) were applied. The finite element models contained 1100–1600 elements. The applied mesh assured sufficient accuracy in all cases investigated. In these analyses, Poisson's ratio was chosen to be $\nu = 0.3$, and small displacement theory was assumed throughout.

5.1.2. Geometry factors

The through-crack configuration considered is shown in Fig. 1. The notch is assumed to be semi-circular, i.e. $d/\rho = 1$. According to Eq. (20), and verified by FEA, the stress concentration factor $K_t = 3.1$ for the

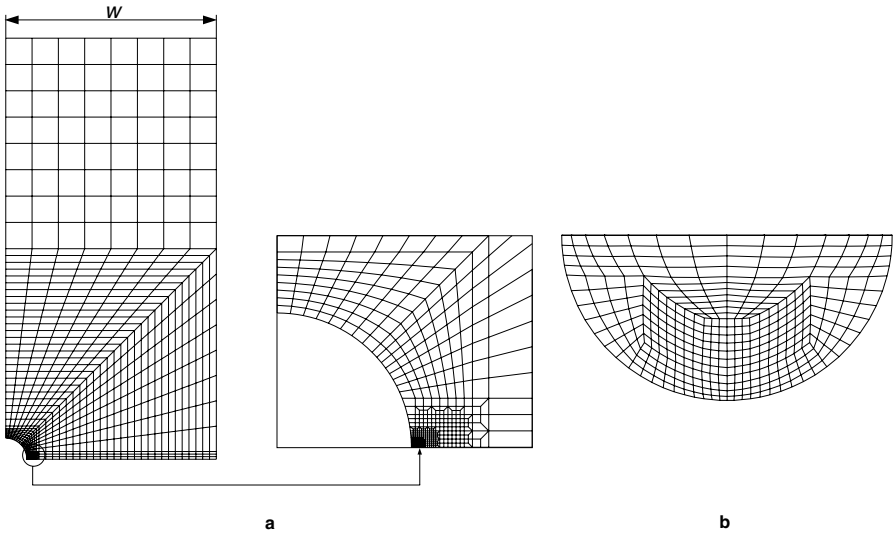

Fig. 5. (a) Finite element mesh for a through-cracked notched specimen ($d/\rho = 1$ and $\rho/w = 0.1$) with a magnified view of the notch root region. The mesh contains 4804 nodes, forming 1527 elements. (b) Boundary element mesh of a semi-circular crack ($a/c = 1$). The mesh contains 403 nodes forming 374 elements.

notched configuration. Subsequently, the different solutions for the geometry factor presented in Section 3 are compared.

Geometry factors, F, have been plotted against the normalised crack depth, a/d, in Fig. 6. Fig. 6 shows the FEA graph of F against a/d together with curves based on asymptotic solutions and Green function. For very shallow cracks, say $a/d < 0.001$, the geometry factor assumes the constant value F_0K_t. As a/d increases, F decreases in a regular fashion. As the crack grows beyond the notch root stress field, the remote stress field

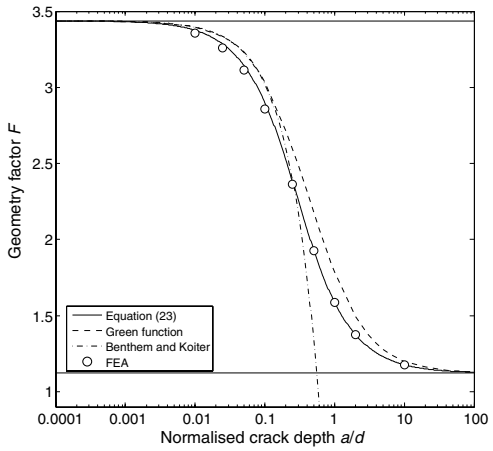

Fig. 6. Geometry factors due to FEA for an edge through-cracked notched plate ($d/\rho = 1$, Fig. 1(b)) with $K_t = 3.1$, together with results obtained from the solutions based on Jergéus and Härkegård, Green's function and Benthem and Koiter.

becomes dominating, and F asymptotically approaches the constant value F_0. The expression for the solid line is given by Eq. (23). As can be seen, the solution is in excellent agreement with the finite element results. The result obtained with Green function is drawn as a dashed curve, the asymptote of which agrees with those predicted by Eq. (23). For intermediate crack depths, the Green function yields values of the geometry factor exceeding those obtained with Eq. (23) by less than 13%.

In Fig. 6, Eq. (19) based on work by Benthem and Koiter [12] is shown as a dash-dotted line. For $a/d < 0.1$, F values generated by the Benthem and Koiter formula are slightly to conservative. For somewhat deeper edge cracks, the Benthem and Koiter values of F fall below the FEA results, since only the tangent of the stress field at the notch root is used. The difference between the FEA results and Eq. (19) is due to the uncertainties related to the determination of the relative stress gradient χ. The χ value from FEA is found to be slightly greater than Eq. (18). Hence, geometry factors from Eq. (19) exceeds those obtained from FEA.

5.1.3. Normalised geometry factors

In Fig. 7 the finite element F values have been normalised with respect to F_∞ for an edge through-crack in a semi-infinite smooth plate with the total crack depth $D = a + d$. The abscissa is the normalised crack depth a/a^*. The solid line is given by Eq. (30). The finite element results have been obtained from three notched plates ($d = 0.1w$) under remote tension with $d/\rho = 0.27$, 0.93 and 1.96. According to Eq. (20), and verified by FEA, the stress concentration factors for these specimens are $K_t = 2$, 3 and 4, respectively. As can be seen from Fig. 7, Eq. (30) is in excellent agreement with the finite element results. For comparison, the results obtained from Eq. (22) according to Lukáš and Klesnil [15] have been depicted as dashed lines in the same figure. For $a/a^* < 1$ the two solutions nearly coincide. For deeper cracks, Eq. (22) gives non-conservative values for the geometry factor. This occurs since Eq. (22) does not fulfil the deep crack asymptotic behaviour.

5.2. Semi-elliptically cracked specimens

5.2.1. Boundary element modelling and evaluation procedures

Fig. 5(b) shows the boundary element mesh of a semi-elliptical crack employed in the present work. The local mesh of the semi-elliptical cracks was similar for all a/c ratios analysed and consisted of 42 elements around the crack front. Four-noded first-order elements were applied.

Elastic analyses of the boundary element models were performed using the boundary element program FRANC3D [23–26]. In this program, the stress intensity factor is evaluated at discrete points at the crack front according to a displacement based method given by Chan et al. [27]. Furthermore, plane strain conditions are assumed all along the crack front.

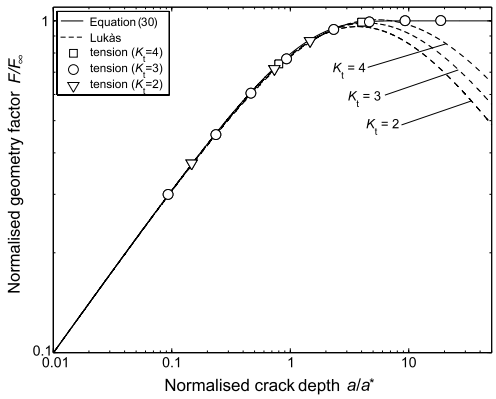

Fig. 7. Geometry factors as functions of the normalised crack depth a/a^* for through-cracked notched plates subjected to remote uniaxial tension (Fig. 1(b)).

5.2.2. Geometry factors

The cracked configuration considered is shown in Fig. 3 and has been analysed under remote uniaxial stress σ_∞. The notch is assumed to be semi-circular, i.e. $d/\rho = 1$. The stress concentration factor $K_t = 3.2$ at the center of the notch. It should be noted that the stress in the three-dimensional case varies from the surface to the center.

In Figs. 8 and 9, the geometry factors F_A and F_C have been plotted against the normalised crack depth a/d. The geometry factors have been obtained by means of the asymptotic solutions for semi-elliptic cracks (Eqs. (36) and (39)), the solution by Pommier et al. [3] and by Lukáš method (Eq. (35)). Along with these solutions, finite element results presented by Lin and Smith [28] and boundary element results are shown.

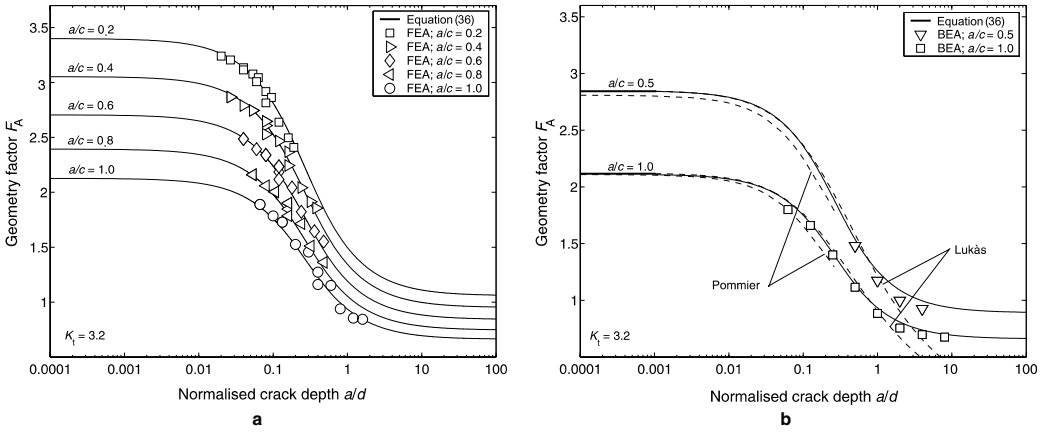

Fig. 8. Geometry factors F_A for the deepest point A$(a;0)$ due to (a) FEA results [28] and (b) BEA results for a semi-elliptically cracked notched plate ($K_t = 3.2$, $d/\rho = 1$) (Fig. 3(a)).

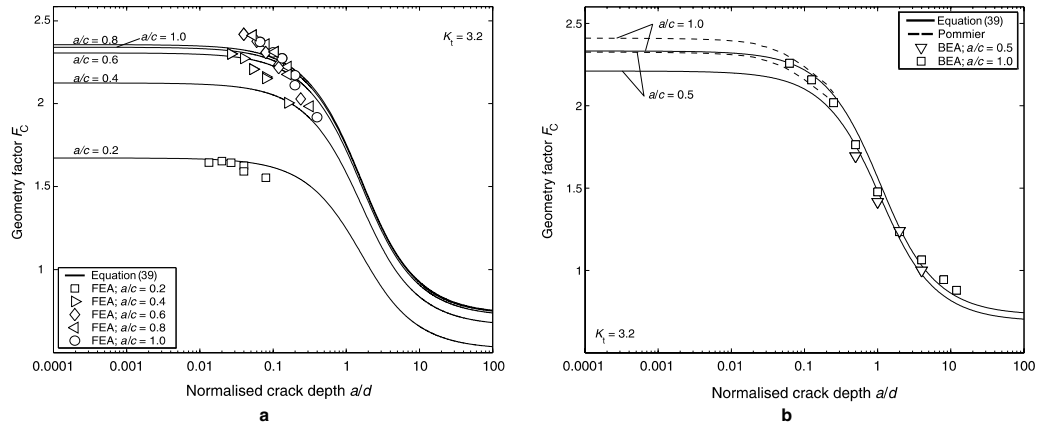

Fig. 9. Geometry factors F_C for the surface point C$(0;c)$ due to (a) FEA [28] and (b) BEA results for a semi-elliptically cracked notched plate ($K_t = 3.2$, $d/\rho = 1$) (Fig. 3(a)).

5.2.3. Geometry factors for the deepest point at the crack front

Fig. 8(a) shows the geometry factor F_A for the deepest point, A(a;0), for the aspect ratios $a/c = 0.2$, 0.4, 0.6, 0.8 and 1.0. The expression for the solid lines is given by Eq. (36). As can be seen, the solution is in good overall agreement with the finite element results presented by Lin and Smith [28].

Fig. 8(b) shows the geometry factors, F_A, generated by means of the asymptotic solutions, Eq. (36), Pommier et al. and Lukáš method for crack aspect ratios $a/c = 0.5$ and 1.0 together with boundary element results. As can be seen, Eq. (36) is in good overall agreement with the boundary element results. For $a/d > 1$, the boundary element results fall slightly below the F_A values from Eq. (36).

For $a/d \leqslant 1$, F_A values generated by Lukáš solution, i.e. Eq. (35), follow the asymptotic solution. For somewhat deeper cracks, Lukáš solution falls below the deep crack asymptote.

The solution due to Pommier et al. is shown in Fig. 8(b) as a dashed curve and is discontinued at $a/d = 0.25$, since this is the maximum range, where the uncracked stress field can be fitted to a third-order polynomial. For $a/c = 0.5$, the F_A values generated from the Pommier solution fall below those of Eq. (36) even for very shallow cracks. This occurs since the $F_{A,0}$ value due to Pommier for $a/c = 0.5$ falls below $F_{A,0}$ due to Newman–Raju. For deeper cracks, values based on Pommier's solution fall slightly below BEA data.

5.2.4. Geometry factors for the crack front surface point

In the previous subsection, results of F_A were presented. This subsection presents geometry factors, F_C, for the crack front surface point C(0;c).

Finite element results in Fig. 9(a) are from Ref. [28]. The solid lines are given by Eq. (39). For shallow cracks, say $a/d < 0.1$, the FEA results exceed the shallow crack asymptote, except for $a/c = 0.2$. FEA results tend to fall below those of Eq. (39), but within acceptable limits.

In Fig. 9(b), geometry factors, F_C, from Eq. (39) and the Pommier et al. solutions are shown for crack aspect ratios $a/c = 0.5$ and 1.0 along with boundary element results. As can be seen, Eq. (39) is in good overall agreement with the boundary element results. For crack depths $a/d < 0.01$ and $a/c = 0.5$ and 1.0, the F_C values generated by the Pommier solution exceed the asymptotic values. This occurs since the Newman–Raju $F_{C,0}$ value is below the corresponding Pommier value.

In the present paper, the proposed asymptotic method has been used in conjunction with Newman and Raju's [6] solution for a surface crack in a finite plate under tension. As can be seen in Fig. 9(b), the Newman–Raju $F_C = K_t F_{C,0}$ value is below the corresponding Pommier value. If the Pommier $F_{C,0}$ value is used, a better agreement is achieved between the present approach and the FE-based results of [28]. In addition, Lin and Smith [28] notes that their F_C values might not be sufficiently accurate for shallow and deep cracks due to the finite element mesh used.

6. Conclusions

Notched specimens with through-cracks or semi-elliptic cracks emanating from the root of the notch have been analysed by means of the finite element and boundary element methods. Simplified solutions for the stress intensity factor K have been presented. These solutions use the stress field ahead of the crack-free notch as the boundary load of an un-notched cracked specimen.

For the through-crack specimens, the solution by Jergéus [16] and Härkegård [17], Eq. (23), is found to be in excellent agreement with the finite element results. The geometry factors generated by means of Green function exceed the FEA values by less than 13%. For $a/d < 0.2$, geometry factors from Eq. (19) slightly exceeds those obtained from FEA.

A simple equation has been proposed for the geometry factor of a through-crack specimen based on a reference solution F_∞. The equation satisfies the shallow and deep crack asymptotes. This solution has been compared with a solution presented by Lukáš and Klesnil [15]. It is found that the two solutions are in good agreement for shallow cracks.

For a semi-elliptic crack at the root of a notch, it has been shown that the geometry factors F_A and F_C are both bounded by a shallow and a deep crack asymptote. The solution by Jergéus and Härkegård for edge through-cracks has been extended to semi-elliptically cracked specimens. Their solution is found to be in good agreement with finite element and boundary element results for both F_A and F_C. For the deepest point A(a;0)

of a shallow crack ($a/d \ll 1$) it has been found that the proposed solution is in good agreement with solutions by Pommier et al. [3] and Lukáš [21]. The solution by Pommier et al. for F_C was also found to be in good agreement with the proposed solution for shallow cracks.

Acknowledgments

The authors gratefully acknowledge the research support for this work provided by GE Energy (Norway) AS, the Research Council of Norway – Norges forskningsråd (NFR) and the industrial participants within the NorLight project. The authors also express their gratitude to Dr. Hans-Jörg Huth for the permission to use a computer code for fatigue crack growth based on the work of Pommier et al.

References

[1] Tada H, Paris PC, Irwin GR. The stress analysis of cracks handbook. 3rd ed. Bury St. Edmunds and London: Professional Engineering Publishing Limited; 2000.
[2] Nilsson L. Stress intensity factors for semi-elliptical surface cracks in plates subjected to a complex stress field. SAQ/FoU-Report 98/10, SAQ KONTROLL AB, Stockholm, Sweden, 1998.
[3] Pommier S, Sakae C, Murakami Y. An empirical stress intensity factor set of equations for a semi-elliptical crack in a semi-infinite body subjected to a polynomial stress distribution. Int J Fatigue 1999;21(3):243–51.
[4] Carpinteri A, Brighenti R, Huth HJ, Vantadori S. Fatigue growth of a surface crack in a welded T-joint. Int J Fatigue 2005;27(1):59–69.
[5] Huth HJ. Fatigue design of hydraulic turbine runners. Ph.D. Thesis, Norwegian University of Science and Technology, Trondheim, Norway, 2005.
[6] Newman Jr JC, Raju IS. An empirical stress-intensity factor equation for the surface crack. Engng Fract Mech 1981;15(1–2):185–92.
[7] Rooke DP, Baratta FI, Cartwright DJ. Simple methods of determining stress intensity factors. Engng Fract Mech 1981;14(2): 397–426.
[8] Bloom JM, Van Der Sluys WA. Determination of stress intensity factors for gradient stress field. J Press Ves Technol-Trans ASME 1977;99(3):477–84.
[9] Hartranft RJ, Sih GC. Alternating method applied to edge and surface crack problems. Methods of analysis and solutions of crack problems. Mechanics of fracture. Leyden: Noordhoff; 1973 [chapter 4].
[10] Karlsson A, Bäcklund J. Summary of SIF graphs for cracks emanating from circular holes. Int J Fract 1978;14:585–96.
[11] Schijve J. The stress intensity factor of small cracks at notches. Fatigue Engng Mater Struct 1982;5(1):77–90.
[12] Benthem JP, Koiter WT. Asymptotic approximations to crack problems. Mechanics of fracture, vol. 1. Noordhoff; 1973. p. 137–78.
[13] Thum A, Petersen C, Svenson O. Verformung, Spannung und Kerbwirkung. Eine Einführung. Düsseldorf: VDI-Verlag; 1960.
[14] Beitz W, Grothe K-H, editors. Dubbel – Taschenbuch für den Maschinenbau. 20th ed. Berlin: Springer-Verlag; 2001. p. E103 [chapter E].
[15] Lukáš P, Klesnil M. Fatigue limit of notched bodies. Mater Sci Engng 1978;34(1):61–6.
[16] Jergéus HÅ. A simple formula for the stress intensity factors of cracks in side notches. Int J Fract 1978;14:R113–6.
[17] Härkegård G. An effective stress intensity factor and the determination of the notched fatigue limit. In: Bäcklund J, Blom AF, Beevers CJ, editors. Fatigue thresholds: fundamentals and engineering applications, vol. 2. Engineering Materials Advisory Services Ltd.; 1982. p. 867–79.
[18] Murakami Y. Analysis of stress intensity factors of mode I, II and III for inclined surface cracks of arbitrary shape. Engng Fract Mech 1985;22(1):101–4.
[19] Härkegård G, Huth HJ, Faanes S. FEA-based fatigue assessment methodology for hydraulic turbine runners. In: Strang A, Banks WM, Conroy RD, McColvin GM, Neal JC, Simpson S, editors. Proceedings of the 5th international Charles Parsons turbine conference. London, July 2000, p. 1005–118. IOM Communications Ltd.
[20] Grandt Jr AF, Kullgren TE. Tabulated stress intensity factor solutions for flawed fastener holes. Engng Fract Mech 1983;18(2):435–51.
[21] Lukáš P. Stress intensity factor for small notch-emanated cracks. Engng Fract Mech 1987;26(3):471–3.
[22] Abaqus/standard, User's manual, version 6.4, Hibbit, Karlsson and Sorensen, Pawtucket, Rhode Island, 2003.
[23] Carter BJ, Chen C-S, Ingraffea AR, Wawrzynek PA. A topology based system for simulating 3D crack growth in solid and shell structures. In: Karihaloo BL, Mai YW, Ripley MI, Ritchie RO, editors. Advances in fracture research, ICF5, vol. 4, 1997, p. 1923–34.
[24] Carter BJ, Wawrzynek PA, Ingraffea AR. Automated 3-D crack growth simulation. Int J Numer Meth Engng 2000;47(1):229–53.
[25] Cornell Fracture Group. FRANC3D 2.6. Concepts and user guide. Cornell University, Ithaca, New York, 2003.
[26] Cornell Fracture Group. FRANC3D 2.6. Menu and dialog reference. Cornell University, Ithaca, New York, 2003.
[27] Chan SK, Tuba IS, Wilson WK. On the finite element method in linear fracture mechanics. Engng Fract Mech 1970;2(1):1–17.
[28] Lin XB, Smith RA. Stress intensity factors for semi-elliptical surface cracks in semicircularly notched tension plates. J Strain Anal Engng Des 1997;32(3):229–36.

Paper 3

The stress intensity factor for a crack in a finite notched plate based on asymptotic solutions

A. Fjeldstad*, G. Härkegård and A. Wormsen
Norwegian University of Science and Technology, Trondheim, Norway.

Abstract

An approximate method for determining the stress intensity factor K for an edge through-crack at the root of a notched plate of finite width subjected to tension or bending is presented. The method is an extension of a previously proposed solution for notched semi-infinite plates subjected to a remote uniaxial stress field. The K solution makes use of the near-notch and the remote-notch solution to interpolate over the entire range from shallow to deep cracks. The near-notch solution is obtained by means of the stress concentration factor. The remote-notch solution is obtained by considering the crack to be located in the corresponding smooth plate with a crack depth equal to the sum of the notch depth and the actual crack depth. The proposed solution includes the finite width effect. The accuracy of the solution is assessed using finite element calculations.

Keywords: stress intensity factor, asymptotic solution, geometry factor, shallow crack, deep crack.

NOTATION

a	crack depth
a^*	transition crack depth between shallow and deep crack asymptotes
d	notch depth
DENT	double-edge-notched tension
F	geometry factor
F_∞	reference geometry factor
F_P	geometry factor for a surface crack in a finite plate
F_N	notch factor
FEA	finite element analysis
K	stress intensity factor $= FS\sqrt{\pi a}$
K_t	stress concentration factor $= \sigma_{\max}/S$
S	remote stress
SENB	single-edge-notched bending
SENT	single-edge-notched tension
w	width of plane specimen
α	normalised crack depth
ρ	notch root radius
$\sigma_{\max}$	maximum stress at the notch root

1 Introduction

The estimation of stress intensity factors for cracks located in a notch stress field is a problem of significant engineering importance. A great number of solutions [**1**–**10**] has been proposed, but most have a general weakness of either being valid only for the near notch area, or that extensive preliminary analysis is required for establishing K [**11**]. Hence, it is still desirable to develop robust methods that can offer solutions over the entire range from shallow to deep cracks. Wormsen et al. [**12**] proposed such a solution for through-cracks and semi-elliptic cracks at the root a notch. However, the method only covers semi-infinite specimens under remote uniaxial tension. It would therefore be of considerable practical interest to extend the solution in [**12**] to cover finite notched specimens under tension or bending.

The objective of the present investigation is to present a simplified method for obtaining K for notched plates of finite width. It is emphasised that only easily accessible values, such as the stress concentration factor of a notched plate and the stress intensity factor solution of an un-notched cracked plate [**1, 2**], are needed. Thus, a minimum of preliminary work is necessary for obtaining K. In the current study, stress intensity factor solutions are presented for through-cracked specimens. Based on the work carried out by Wormsen et al. [**12**], it is reasonable to believe that the proposed methodology may also be used for calculating K for a semi-elliptic crack in a notched finite plate. However, this will not be investigated here.

*Corresponding author: Department of Engineering Design and Materials, Norwegian University of Science and Technology, Richard Birkelandsvei 2B, Trondheim, NO-7491 , Norway; email: Arne.Fjeldstad@ntnu.no

2 Linear elastic crack mechanics

2.1 Stress intensity factor

The stress intensity range, ΔK, is the main parameter to seek when performing fatigue crack growth calculations. K may be written as

$$K = FS\sqrt{\pi a}, \tag{1}$$

where the geometry factor F is a dimensionless function of the geometry and the loading. S is the remote stress, e.g., due to a tensile load or a bending moment. According to Fjeldstad et al. **[13]**, F can be written in terms of the geometry factor, F_{P}, for the associated crack emanating from the edge of a smooth finite plate, and a notch field factor, F_{N}, which takes the notch stress field into account. Hence,

$$F = F_{\mathrm{P}}F_{\mathrm{N}}. \tag{2}$$

For a smooth plate, cf. Fig. 1(a), the notch factor $F_{\mathrm{N}} = 1$.

2.2 Notched specimens

Consider now a notched plate of finite width, w, with notch radius ρ and notch depth d, as shown in Fig. 1(b). For a shallow crack located in the notch stress field, the stress intensity factor is asymptotically the same as for a cracked smooth semi-infinite plate, except that the remote stress is amplified by the stress concentration factor $K_{\mathrm{t}} = \sigma_{\max}/S$, where $\sigma_{\max}$ is the maximum notch stress. As the crack depth a approaches zero,

$$K = FS\sqrt{\pi a} = 1.122K_{\mathrm{t}}S\sqrt{\pi a}, \tag{3}$$

that is,

$$F = F_{\mathrm{P}}F_{\mathrm{N}} = 1.122K_{\mathrm{t}}. \tag{4}$$

As the crack grows beyond the notch stress field, the remote stress field dominates the stress intensify factor, and the cracked configuration can be regarded as a smooth plate with crack depth $a + d$, as illustrated in Fig 1(c). K can then be obtained as

$$K = F_{\mathrm{P}}S\sqrt{\pi(a + d)}. \tag{5}$$

Identification with equations (1) and (2) yields

$$F = F_{\mathrm{P}}F_{\mathrm{N}} = F_{\mathrm{P}}\sqrt{1 + \frac{d}{a}}. \tag{6}$$

When $a/d \gg 1$, F_{N} asymptotically approaches the constant value

$$F_{\mathrm{N}} = 1. \tag{7}$$

The two preceding asymptotic solutions, i.e., equations (4) and (7), give the upper and lower bound for the notch factor, i.e., $K_{\mathrm{t}} \geq F_{\mathrm{N}} \geq 1$. By using these asymptotes, simple formulae **[12,14–16]** have been established for the geometry factor for different cracked configurations.

3 Normalised geometry factors based on asymptotic solutions

Before normalised geometry factors are presented, it is convenient to introduce the reference geometry factor, F_∞.

3.1 Reference geometry factor F_∞

The reference geometry factor is obtained by considering a crack of depth $a+d$ in a smooth plate subjected to the same remote stress field, see Fig. 1(c). Hence, $F_\infty = F$ according to equation (6). This is an appropriate reference, since the geometry factor F for a crack at the root of a notch converges towards F_∞, when the crack is sufficiently deep compared with the notch depth. Furthermore, smooth plate solutions are easily accessible, e.g., in stress intensity factor handbooks **[1, 2]** . According to Tada et al. **[1]**, F_{P} is given by

$$F_{\mathrm{P}} = 0.265(1-\alpha)^4 + \frac{0.857 + 0.265\alpha}{(1-\alpha)^{3/2}}, \tag{8}$$

$$F_{\mathrm{P}} = \left(1 + 0.122\tan^4\frac{\pi\alpha}{2}\right)\sqrt{\frac{2}{\pi\alpha}\tan\frac{\pi\alpha}{2}}, \tag{9}$$

and,

$$F_{\mathrm{P}} = \sqrt{\frac{2}{\pi\alpha}\tan\frac{\pi\alpha}{2}}\left[\frac{0.923 + 0.199(1-\sin\frac{\pi\alpha}{2})^4}{\cos\frac{\pi\alpha}{2}}\right], \tag{10}$$

for single-edge-crack tension plates, double-edge-crack tension plates and single-edge-crack bending plates, respectively. Here,

$$\alpha = \frac{a+d}{w}. \tag{11}$$

Equations (8) to (10) will be used in the numerical examples presented in Section 4.

3.2 Semi-infinite plates

A crack located in a semi-infinite plate will evidently not be affected by finite width effects, i.e. $F_{\mathrm{P}} = 1.122$. Hence, according to equation (6) the reference geometry factor is given by

$$F_\infty = 1.122\sqrt{1 + \frac{d}{a}}. \tag{12}$$

For shallow cracks, i.e., $a \ll d$, F is obtained from equation (4). The normalised geometry factor

$$\frac{F}{F_\infty} = \frac{K_{\mathrm{t}}}{\sqrt{1 + \frac{d}{a}}}, \tag{13}$$

or, since $a \ll d$

$$\frac{F}{F_\infty} = K_{\mathrm{t}}\sqrt{\frac{a}{d}}. \tag{14}$$

For deep cracks, F/F_∞ approaches unity.

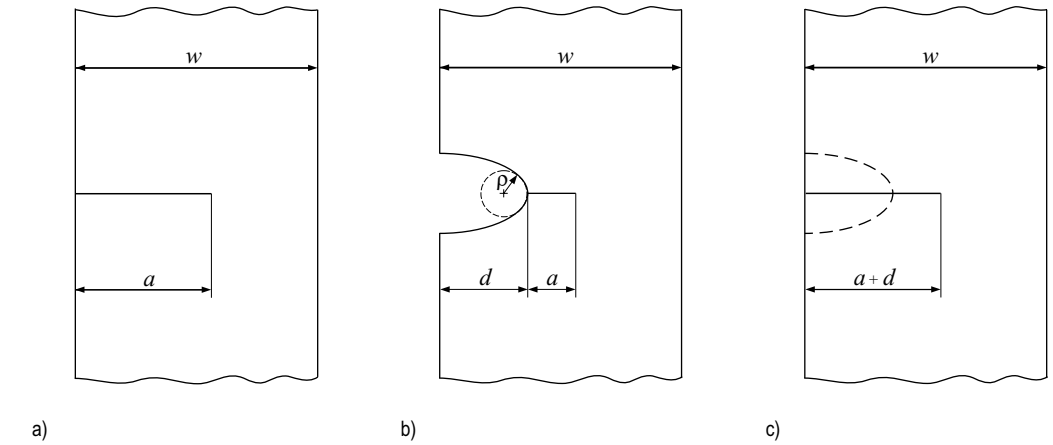

Figure 1: (a) smooth plate with crack depth a, (b) notched plate with a crack of depth a located in the root of the notch, and (c) reference plate with crack depth $a + d$.

In [**12**], Wormsen et al. presented a solution for the normalised geometry factor. A simple expression that asymptotically agrees with the two asymptotes is given by

$$\frac{F}{F_\infty} = \sqrt{1 - \exp\left(-\frac{a}{a^*}\right)}, \tag{15}$$

where a^* denotes the transition crack depth, at which the two asymptotes intersect (see Fig. 2). a^* is obtained by setting equation (14) equal to unity, which yields

$$a^* = \frac{d}{K_\mathrm{t}^2}. \tag{16}$$

In Fig. 2, equation (15) has been plotted as a solid line.

3.3 Finite plates

For plates of finite width, the shallow crack solution of F is still given by equation (4), and F_∞ is obtained from equation (6). Hence, as a approaches zero the shallow crack solution becomes

$$\frac{F}{F_\infty} = \frac{1.122}{F_\mathrm{P}\left(\frac{d}{w}\right)} K_\mathrm{t} \sqrt{\frac{a}{d}}. \tag{17}$$

As for a semi-infinite plate, F tends to F_∞ as the crack grows beyond the notch stress field, and thus, the normalised geometry factor approaches unity. Again, the transition crack depth is obtained where the two asymptotes intersect, i.e., by setting equation (17) equal to unity:

$$a^* = \left(\frac{F_\mathrm{P}\left(\frac{d}{w}\right)}{1.122}\right)^2 \frac{d}{K_\mathrm{t}^2}. \tag{18}$$

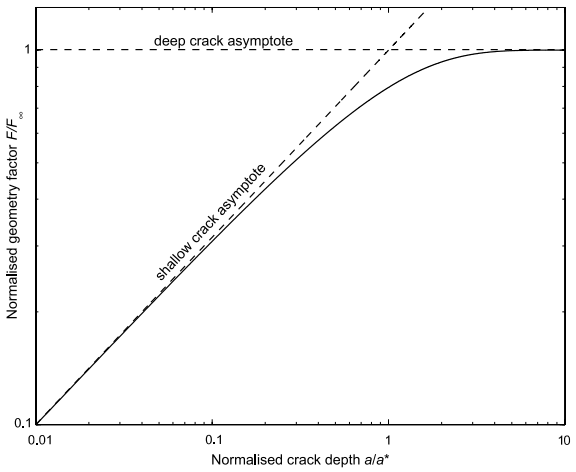

Figure 2: Principle graph of F/F_∞ against the normalised crack depth a/a^*: logarithmic scales.

When $w \gg d$, equation (18) agrees completely with equation (16). Hence, the solution presented in the previous Subsection can be regarded as a special case of the general solution presented here. The expression presented in equation (15) is used for describing the ratio F/F_∞ for the entire range from shallow to deep cracks.

4 Numerical analysis

The accuracy of the interpolation function given by equation (15) will now be assessed by finite element analysis of three basic through-cracked configurations, see Fig. 3:

a. single-edge-notched tension (SENT) plate.

b. double-edge-notched tension (DENT) plate.

c. single-edge-notched bending (SENB) plate.

The notch is described by its depth d and root radius ρ. A majority of the cracked configurations was modelled with crack depths around the transition crack depth, a^*, in order examine the accuracy of equation (15) in the transition between the two asymptotes. A variety of notched geometries were modelled in order to assess the accuracy of the interpolation function.

4.1 Finite element modelling

Linear elastic finite element analyses were performed by means of ABAQUS [**17**]. Fig. 4 illustrates a typical finite element mesh employed in the present work. The local mesh in the crack tip region was identical for all models, with 16 elements around the crack tip. Eight-noded isoparametric second-order plane strain elements with reduced integration (2×2 Gauss points; element type CPE8R in ABAQUS [**17**]) were applied. The finite element models contained 1100-1600 elements. The applied mesh assured sufficient accuracy in all cases investigated. In these analyses, Poisson's ratio was chosen to be $\nu = 0.3$, and small displacement theory was assumed throughout.

4.2 Normalised geometry factors

Fig. 5 shows the normalised geometry factor, F/F_∞, plotted against the normalised crack depth, a/a^*, for the three configurations. As anticipated, F/F_∞ closely follows the shallow crack asymptote as long as a/a^* is small. As a approaches the transition crack depth, the normalised geometry factor deviates from the shallow crack asymptote and approaches that of a deep crack. Finally, when $a/a^* \gg 1$, the deep crack asymptote dominates and the geometry factor closely agrees with a smooth plate with crack depth $a + d$. The expression for the solid curve in Fig. 5 is given by equation (15). The figure clearly shows that the proposed interpolation function is in excellent agreement with the finite element results. The data of Fig. 5 have been tabulated in Table 1. The results show that predictions based on equation (15) deviate by less than 3.5% from the finite element results, and the majority of the predictions by less than 2%. It is worth mentioning that the estimated geometry factors are generally on the conservative side.

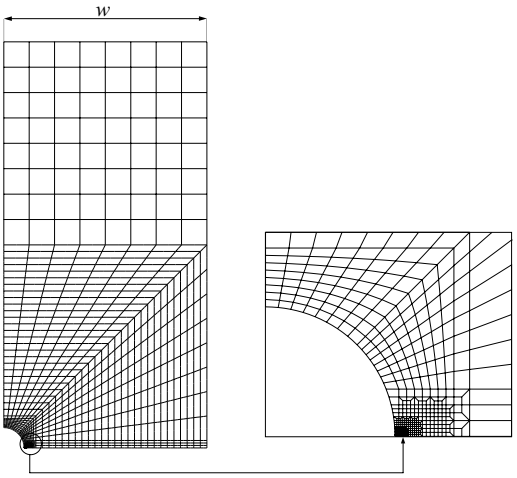

Figure 4: Finite element mesh for a through-cracked notched specimen ($d/\rho = 1$ and $\rho/w = 0.1$) with a magnified view of the notch root region.

5 Conclusions

SENT, DENT and SENB plates with an edge through-crack located at the root of the notch, have been investigated. A solution, originally proposed by Wormsen et al. [**12**] for obtaining the geometry factor, F, for semi-infinite specimens under homogeneous stress, has been extended to cover finite-width plates under tension or bending. The method only requires the stress concentration factor of the notch and the stress intensity factor of an edge crack in a smooth plate plate subjected to the same remote stress field to be known. Predictions based on the proposed formulae have been compared with finite element analyses and found to be in excellent agreement.

ACKNOWLEDGMENTS

The authors gratefully acknowledge the research support for this work provided by the Research Council of Norway and the industrial participants within the NorLight project.

Table 1: Results for the geometry factor F obtained from FEA along with predictions of F/F_∞ according to equation(15).

	d/w	ρ/d	K_t	a/d	a/a^*	F (FEA)	$F_\mathrm{P}^\dagger$	$\sqrt{1+\frac{d}{a}}$	F_∞	F/F_∞	Equation (15)	Deviation [%]
SENT:	0.003	3.4	2.0	0.034	0.14	2.25	1.12	5.48	6.15	0.365	0.359	-1.8
	0.003	3.4	2.0	0.172	0.69	2.09	1.12	2.61	2.93	0.713	0.705	-1.1
	0.003	3.4	2.0	0.345	1.38	1.89	1.12	1.97	2.22	0.854	0.864	1.2
	0.02	0.5	4.0	0.5	0.78	3.74	1.13	4.58	5.20	0.720	0.737	2.3
	0.02	0.5	4.0	0.25	3.92	2.46	1.14	2.24	2.44	0.970	0.990	2.1
	0.02	1	3.06	0.1	0.92	2.86	1.13	3.32	3.76	0.760	0.775	2.0
	0.02	1	3.06	0.5	4.59	1.93	1.14	1.73	1.97	0.976	0.995	1.9
	0.02	1	3.06	1.0	9.18	1.61	1.15	1.41	1.62	0.989	1.0	1.0
	0.02	1	3.06	2.0	18.4	1.39	1.16	1.22	1.43	0.976	1.0	2.4
	0.1	1	3.28	0.1	0.92	3.10	1.22	3.32	4.05	0.765	0.777	1.5
	0.1	1	3.28	0.3	2.77	2.46	1.25	2.08	2.60	0.946	0.968	2.3
	0.1	1	3.28	0.5	4.62	2.22	1.28	1.73	2.22	1.0	0.995	-0.5
	0.3	1	4.98	0.033	0.38	5.22	1.70	5.57	9.46	0.552	0.560	1.3
	0.3	1	4.98	0.1	1.13	4.73	1.78	3.32	5.89	0.804	0.822	2.3
	0.3	1	4.98	0.233	2.63	4.24	1.95	2.30	4.49	0.946	0.963	1.8
	0.6	1	16.0	0.0033	0.066	17.8	4.06	17.3	70.4	0.254	0.254	0.0
	0.6	1	16.0	0.033	0.66	16.6	4.37	5.57	24.3	0.683	0.697	2.1
	0.6	1	16.0	0.067	1.33	15.9	4.76	4.0	19.0	0.836	0.858	2.6
	0.6	1	16.0	0.167	3.33	16.4	6.35	2.65	16.8	0.978	0.982	0.4
	0.9	1	260	0.011	0.79	297	40.7	9.54	388	0.766	0.739	-3.4
	0.9	1	260	0.022	1.58	295	48.6	6.78	330	0.893	0.891	-0.2
DENT:	0.3	1	3.05	0.033	0.31	3.20	1.12	5.57	6.24	0.513	0.517	0.7
	0.3	1	3.05	0.1	0.93	2.86	1.12	3.32	3.72	0.768	0.779	1.5
	0.3	1	3.05	0.233	2.18	2.41	1.13	2.30	2.59	0.93	0.94	1.2
	0.6	1	3.55	0.0033	0.035	3.96	1.23	17.3	21.3	0.186	0.186	0.0
	0.6	1	3.55	0.033	0.35	3.75	1.24	5.57	6.93	0.542	0.544	0.4
	0.6	1	3.55	0.067	0.70	3.56	1.26	4.0	5.06	0.704	0.710	0.8
	0.6	1	3.55	0.167	1.76	3.20	1.34	2.65	3.55	0.90	0.91	1.1
	0.9	1	10.7	0.011	0.36	11.7	2.22	9.54	21.2	0.555	0.549	-1.1
	0.9	1	10.9	0.022	0.72	11.5	2.34	6.78	15.9	0.726	0.716	-1.4
SENB:	0.1	1	2.81	0.01	0.092	3.10	1.04	10.1	10.5	0.296	0.296	0.0
	0.1	1	2.81	0.1	0.92	2.64	1.04	3.32	3.44	0.766	0.775	1.1
	0.1	1	2.81	0.3	2.75	2.07	1.03	2.08	2.15	0.961	0.968	0.6
	0.1	1	2.81	0.5	4.59	1.78	1.03	1.73	1.78	1.0	0.995	-0.6
	0.3	1	3.14	0.033	0.34	3.29	1.11	5.57	6.17	0.533	0.539	1.0
	0.3	1	3.14	0.1	1.03	2.94	1.13	3.32	3.75	0.785	0.802	2.2
	0.3	1	3.14	0.233	2.41	2.58	1.18	2.30	2.72	0.946	0.954	0.8
	0.6	1	7.27	0.0033	0.032	8.08	1.91	17.3	33.1	0.244	0.244	0.0
	0.6	1	7.27	0.033	0.62	7.46	2.02	5.57	11.2	0.664	0.678	2.2
	0.6	1	7.27	0.067	1.23	7.11	2.16	4.0	8.63	0.824	0.842	2.1
	0.6	1	7.27	0.167	3.08	6.99	2.72	2.65	7.19	0.972	0.977	0.5
	0.9	1	103	0.011	0.95	107	14.5	9.54	139	0.771	0.784	1.7
	0.9	1	103	0.022	1.90	107	17.2	6.78	117	0.916	0.923	0.7

† SENT: equation(8), DENT: equation(9), SENB: equation(10).

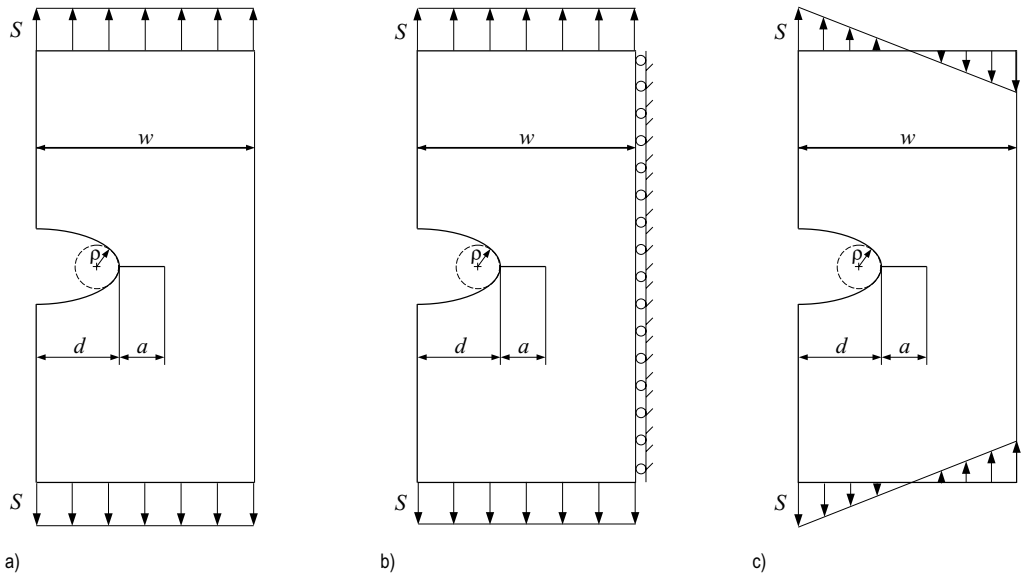

Figure 3: Boundary conditions applied to the cracked specimens: (a) SENT, (b) DENT, and (c) SENB.

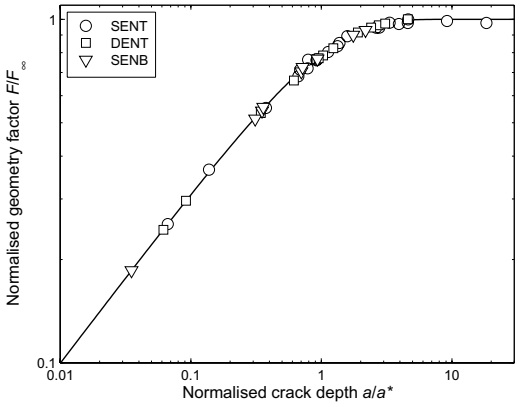

Figure 5: Normalised geometry factors as functions of the normalised crack depth a/a^* for through-cracked configurations.

References

[1] **Tada, H.**, **Paris, P. C.**, and **Irwin, G. R.** *The stress analysis of cracks handbook*. Professional Engineering Publishing Limited, Bury St. Edmunds and London, 3rd edition, 2000.

[2] **Murakami, Y.**, editor. *Stress intensity factors handbook*. Pergamon Press, Oxford, 2001.

[3] **Fett, T.** and **Munz, D.** *Stress intensity factors and weight functions*. International series on advances in fracture. Computational Mechanics Publications, Southampton, 1997.

[4] **Hartranft, R. J.** and **Sih, G. C.** *Alternating method applied to edge and surface crack problems*, chapter 4 of 'Methods of analysis and solutions of crack problems'. Mechanics of fracture. Nordhoff, Leyden, 1973.

[5] **Schijve, J.** Stress intensity factors of small cracks at notches. *Fatigue of Engineering Materials and Structures*, 5(1):77–90, 1982.

[6] **Benthem, J. P.** and **Koiter, W. T.** *Asymptotic approximations to crack problems*, chapter 3 of 'Methods of analysis and solutions of crack problems', pages 137–178. Mechanics of fracture, vol. 1. Nordhoff, 1973.

[7] **Lukáš, P.** and **Klesnil, M.** Fatigue limit of notched bodies. *Materials Science and Engineering*, 34(1):61–66, 1978.

[8] **Lukáš, P.** Stress intensity factor for small notch-emanated cracks. *Engineering Fracture Mechanics*, 26(3):471–473, 1987.

[9] **Pommier, S.**, **Sakae, C.**, and **Murakami, Y.** An empirical stress intensity factor set of equations for a semi-elliptical crack in a semi-infinite body subjected to a polynomial stress distribution. *International Journal of Fatigue*, 21(3):243–251, 1999.

[10] **Carpinteri, A.**, **Brighenti, R.**, **Huth, H. J.**, and **Vantadori, S.** Fatigue crack growth of a surface crack in a welded T-joint. *International Journal of Fatigue*, 27(1):59–69, 2005.

[11] **Rooke, D. P.**, **Baratta, F. I.**, and **Cartwright, D. J.** Simple methods of determining stress intensity factors. *Engineering Fracture Mechanics*, 14(2):397–426, 1981.

[12] **Wormsen, A.**, **Fjeldstad, A.**, and **Härkegård, G.** The application of asymptotic solutions to a semi-elliptical crack at the root of a notch. *Engineering Fracture Mechanics*, 73(13):1899–1912, 2006.

[13] **Fjeldstad, A.**, **Härkegård, G.**, and **Wormsen, A.** The influence of a stress gradient on the growth of a fatigue crack. In W. S. Johnson et al., editor, *Proceedings of the International Fatigue Congress 2006*, Atlanta, Georgia, USA, May 2006. Elsevier.

[14] **Jergéus, H. Å.** A simple formula for the stress intensity factors of cracks in side notches. *International Journal of Fracture*, 14:R113–116, 1978.

[15] **Härkegård, G.** An effective stress intensity factor and the determination of the notched fatigue limit. In J. Bäcklund, A. F. Blom, and C. J. Beevers, editors, *Fatigue thresholds: fundamentals and engineering applications, volume II*, pages 867–879. Engineering Materials Advisory Services Ltd, 1982.

[16] **Fjeldstad, A.**, **Wormsen, A.**, and **Härkegård, G.** Approximate stress intensity factors for cracked V-notched specimens based on asymptotic solutions with application to T-joints. *Engineering Fracture Mechanics*, doi:10.1016/j.engfracmech.2007.04.028, 2007.

[17] Abaqus/Standard, User's manual, version 6.5-1. *(Hibbit, Karlsson and Sorensen, Pawtucket, Rhode Island)*, 2005.

Paper 4

ORAL REFERENCE: FT254

THE INFLUENCE OF A STRESS GRADIENT ON THE GROWTH OF A FATIGUE CRACK

A. Fjeldstad*, G. Härkegård and A. Wormsen

Department of Engineering Design and Materials, Norwegian University of Science and Technology, Trondheim, Norway

ABSTRACT

This paper examines how a decreasing stress field influences the fatigue crack growth. Even though the stress generally decreases from a maximum at some critical point at the surface for real components, fatigue crack growth analyses are often performed assuming a homogeneous stress state to avoid the difficulties related to crack growth analyses in complex components. By comparing the calculated fatigue life of cracks growing in a homogeneous stress field with the fatigue life of cracks growing in a gradient stress field, the degree of conservatism has been determined for several stress gradients. It has been found that a high stress gradient has a significant influence on the fatigue life of a component. Hence, using a homogeneous stress field based on the maximum stress on the surface to calculate the lifetime may lead to overconservative predictions. Stress gradients lead to more conservative predictions for edge through-cracks than for semi-elliptical cracks located in the same stress field.

KEYWORDS

Fatigue crack growth, Stress gradient, Paris' law, Lifetime prediction

INTRODUCTION

For simplicity and to ensure conservatism, crack growth analyses are often performed assuming a homogeneous stress field based on the maximum stress acting at the surface. This simplified approach yields acceptable results provided that the stress decreases slowly, i.e. the stress gradient is low. However, for high stress gradients, a crack growth analysis based on the maximum stress will lead to overconservative predictions. It is therefore of great practical interest to determine under which circumstances it is permissible to replace the gradient stress field with a homogeneous stress field when calculating the fatigue life of a real component.

Both an un-notched semi-infinite specimen subjected to a linearly decreasing stress field and a notched semi-infinite specimen under a remote uniform stress will be treated. Assuming Paris' law to be valid, crack growth analyses of edge through-cracks and semi-elliptical surface cracks located in a semi-infinite body will be carried out to predict the influence of a stress gradient on the number of cycles N required to propagate a crack from $a = a_i$ to $a = a_f$. The dependence of the normalised lifetime N/N_0, where N_0 denotes the lifetime of a homogeneously stressed fatigue specimen, on the relative stress gradient, $(d\sigma/dx)/\sigma_{max,}$ and the notch curvature, $1/\rho$, will be examined.

GENERAL EQUATIONS

For an arbitrary body with a surface crack of depth a under remote stress σ perpendicular to the plane of the crack, the stress intensity factor, K, can be written as

$$K = F\sigma\sqrt{\pi a}\,, \tag{1}$$

where σ denotes the remote nominal stress. In equation (1), F denotes the geometry factor and is a dimensionless function of the geometry and the type of loading. Based on work by Benthem and Koiter [1], F can be written in terms of the geometry factor F_0 for a crack emanating from a smooth surface and F_χ, referred to as the gradient factor, which takes into account the influence of the stress gradient field:

$$F = F_0 F_\chi. \tag{2}$$

For a cracked specimen subjected to a homogeneous stress field, $F_\chi = 1$. The characteristics of F_χ will be treated in the subsequent Sections. F_0 is determined by means of the well known solution of Newman and Raju [2] for smooth finite plates under tension or bending. For a semi-infinite plate, i.e. $a/t \to 0$, the geometry factors for tension and bending are both equal to F_0. For a semi-elliptical surface crack with a crack aspect ratio a/c (cf. Figure 1), the geometry factor at the deepest point of the crack front $\mathrm{A}(a;0)$ can be estimated as [2]

$$F_0\left(\phi=\pi/2; a/c\right) = F_{\mathrm{A},0} = \frac{1.13 - 0.09\dfrac{a}{c}}{\sqrt{1+1.464\left(\dfrac{a}{c}\right)^{1.65}}},\ 0 \le a/c \le 1. \tag{3}$$

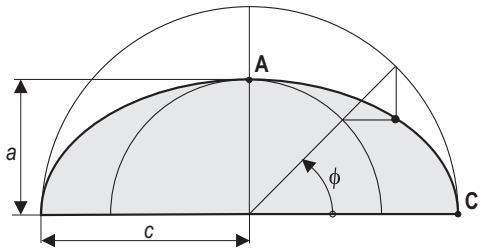

Figure 1: Two-dimensional view of a semi-elliptical crack.

In the case of an edge through-crack, i.e. $a/c = 0$, equation (3) reduces to $F_0(\phi = \pi/2;\ 0) = 1.13$, in good agreement with the more precise solution $F_0 = 1.122$ [3]. At the intersection between the crack front and the free surface C(0;c), $F_{\mathrm{C},0}$ can be estimated as

$$F_0\left(\phi=0; a/c\right) = F_{\mathrm{C},0} = \frac{1.243 - 0.099\dfrac{a}{c}}{\sqrt{1+1.464\left(\dfrac{a}{c}\right)^{1.65}}}\sqrt{\frac{a}{c}},\ 0 \le a/c \le 1. \tag{4}$$

In the two following Sections, the gradient factor F_χ will be presented for surface cracks growing in a linearly decreasing stress field and a notch stress field, respectively.

CRACKS IN LINEARLY DECREASING STRESS FIELDS

A smooth semi-infinite specimen with a surface crack of depth a is considered. The specimen is subjected to a linearly decreasing stress field with the maximum stress σ_{max} at the surface as shown in Figure 2.

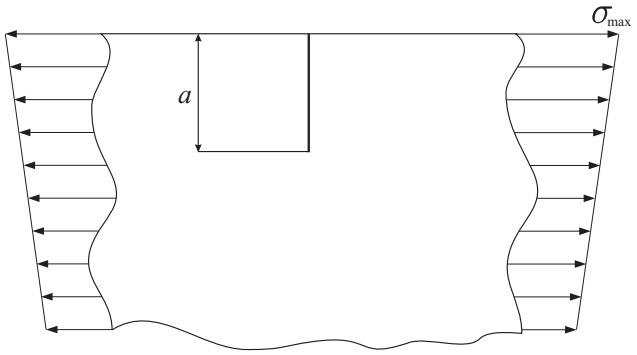

Figure 2: Semi-infinite notched plate with a surface crack of depth a subjected to a linearly decreasing stress field.

Edge through-cracks

For an edge through-crack in a semi-infinite body subjected to a linearly decreasing stress field, Benthem and Koiter [1] obtained

$$F_{\chi} = 1 + 0.61 \frac{1}{\sigma_{max}} \frac{\mathrm{d}\sigma}{\mathrm{d}x} a \,, \tag{5}$$

where x denotes the distance below the surface, $d\sigma/dx$ the constant stress gradient.

Semi-elliptical cracks

For semi-elliptical cracks, the empirical solutions proposed by Newman and Raju [2] are applied. Newman and Raju [2] presented a solution for specimens with finite thickness. Assuming the crack to be shallow, the expression for $F_{A,\chi}$ simplifies to:

$$F_{\chi}\left(\phi = \pi/2; a/c\right) = F_{A,\chi} = 1 - \left(1.22 + 0.12 \frac{a}{c}\right) \frac{a}{t} . \tag{6}$$

For a plate subject to pure bending, the relative stress gradient is implicitly known through the plate thickness and the maximum surface stress.

$$\frac{\mathrm{d}\sigma}{\mathrm{d}x} = -\sigma_{max} \frac{2}{t} . \tag{7}$$

Hence, by substituting the thickness t in equation (6) by means of equation (7), the gradient factor $F_{A,\chi}$ is obtained as a function of the relative stress gradient. Thus, the use of equation (7) allows the empirical K solutions by Newman and Raju [2] to be applied to semi-infinite specimens subjected to a linearly decreasing stress field. Introducing equation (7) into equation (6) yields

$$F_{A,\chi} = 1 + \left(0.61 + 0.06 \frac{a}{c}\right) \frac{1}{\sigma_{max}} \frac{\mathrm{d}\sigma}{\mathrm{d}x} a \,. \tag{8}$$

If $a/c = 0$, which corresponds to an edge through-crack, equation (8) is in full agreement with equation (5).

According to Newman and Raju [1], the gradient factor $F_{C,\chi}$ at the intersection between the crack front and the free surface C(0;c) can be written as

$$F_\chi\left(\phi=0;a/c\right)=F_{C,\chi}=1-\left(0.34+0.11\frac{a}{c}\right)\frac{a}{t}, \tag{9}$$

if the crack is assumed to be shallow. Substitution of equation (7) yields

$$F_{C,\chi}=1+\left(0.17+0.055\frac{a}{c}\right)\frac{1}{\sigma_{\max}}\frac{\mathrm{d}\sigma}{\mathrm{d}x}a\,. \tag{10}$$

As observed from equations (8) and (10), the gradient factors will decrease more rapidly with higher stress gradients. This supports the argument that fatigue life predictions based on maximum stresses are increasingly conservative for higher stress gradients.

CRACKS IN NOTCHED SPECIMENS

A notched semi-infinite specimen with notch depth d and notch radius ρ loaded by a nominal stress, σ_∞, is considered. The stress concentration factor of the notch is K_t. A crack of depth a is located at the root of a notch, as shown in Figure 3.

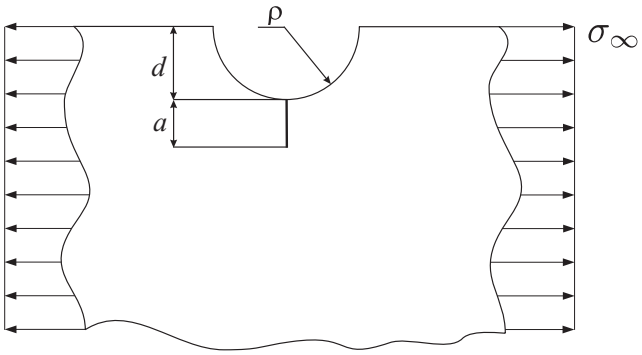

Figure 3: Semi-infinite notched plate with a crack of depth a at the root of the notch subjected to a uniform remote stress σ_∞.

Edge through-cracks

The gradient factor solution for the current problem is based on work by Jergéus [4] and Härkegård [5]. By introducing an equivalent crack depth, D, the gradient factor may be written as

$$F_\chi=\sqrt{\frac{D}{a}},\ 1\le F_\chi\le K_t, \tag{11}$$

for the entire range of crack depths. The equivalent crack depth is given by

$$D=a+d\left[1-\exp\left(-\frac{a}{a'}\right)\right], \tag{12}$$

and

$$a' = \frac{d}{K_t^2 - 1}. \tag{13}$$

The transition crack depth a' is defined as the crack depth at which the asymptotic stress intensity factors of shallow and deep cracks become equal.

Semi-elliptical cracks

Wormsen et al. [6] extended the above asymptotic solution for through-cracks to semi-elliptical surface cracks at the root of the notch. As for edge through-cracks, it was found that the gradient factor F_χ could be expressed in terms of the crack depth a and an equivalent crack depth D_A as

$$F_{A,\chi} = \sqrt{\frac{D_A}{a}}, \tag{14}$$

where $D_A = D$ according to equation (12). Even though the surface point C(0;c) is located in the notch stress field, Wormsen et al. [6] were able to show that $F_{C,\chi}$ approaches unity as the crack becomes sufficiently deep, i.e. $a >> d$. Similar to $F_{A,\chi}$, $F_{C,\chi}$ was found to be in the range $K_t \geq F_{C,\chi} \geq 1$. The gradient factor at the surface point can be written as

$$F_{C,\chi} = \sqrt{\frac{D_C}{a}}, \tag{15}$$

where the equivalent crack depth D_C is given by

$$D_C = a + 4d\left[1 - \exp\left(-\frac{a}{4a'}\right)\right]. \tag{16}$$

Due to the somewhat different expressions for the equivalent crack depths D, the gradient factor $F_{C,\chi}$ converges more slowly towards the deep crack asymptote than $F_{A,\chi}$. However, due to the far field solutions, where both $F_{A,\chi}$ and $F_{C,\chi} \rightarrow 1$, the semi-elliptical crack eventually will behave as a crack in a homogeneous stress field.

NUMERICAL CRACK GROWTH ANALYSIS

Crack growth analyses of a smooth specimen with a linearly decreasing stress field and a specimen with a semi-circular notch ($d = \rho$) loaded by a remote nominal stress are performed. Two cases are considered where the number of cycles, N, required to propagate a crack from an initial crack depth of a_i = 0.015mm and a_i = 0.15mm, respectively, to a critical crack depth of a_f = 1.5mm is calculated. The lifetimes are normalised by means of the lifetime N_0 of a homogeneously stressed semi-infinite specimen with corresponding initial and critical crack depths. The homogeneous stress is equal to the maximum stress acting on the surface (σ_{max} and $K_t\sigma_\infty$, respectively). All the semi-elliptical cracked configurations have an initial crack aspect ratio a/c = 1.

Numerical integration routine

The fatigue life estimation is performed by means of Paris' law [7], which describes the relationship between the crack growth rate da/dN and the stress intensity range ΔK, viz,

$$\frac{\mathrm{d}a}{\mathrm{d}N} = C\left(\Delta K\right)^m . \tag{17}$$

The constants C and m are crack growth parameters. According to equation (17), the fatigue lifetime is obtained through the following expression

$$N = k\int_{a_\mathrm{i}}^{a_\mathrm{f}} \frac{\mathrm{d}a}{F\left(a, a/c\right)^m a^{m/2}}, \tag{18}$$

where all quantities independent of a are represented by the constant k, given by

$$k = \frac{1}{\pi^{m/2} C \Delta\sigma^m}. \tag{19}$$

Since both N and N_0 are obtained from equation (18), it can be shown that N/N_0 is independent of the applied nominal stress range, $\Delta\sigma$, and the crack growth parameter C.

The numerical integration is performed by means of Simpson's rule, where the integration intervals are defined by

$$a_j = a_\mathrm{i} 10^{(j/\lambda)},\ 0 \le j \le \log\left(a_\mathrm{f}/a_\mathrm{i}\right)\lambda . \tag{20}$$

The parameter λ states the number of integration intervals for each decade. In this study, λ is set to 1000, which has proven to be sufficient for achieving convergence of the fatigue life N.

Crack growth analyses are performed for both the deepest point of the crack front A(0;c) and the surface point C(0;c). The integration intervals of a are already determined through equation (20). Thus, by applying the already known incremental growth of a, the incremental growth of c is determined through the following expression

$$\Delta c = \Delta a\left(\frac{\Delta K_\mathrm{C}}{\Delta K_\mathrm{A}}\right)^m = \Delta a\left(\frac{F_\mathrm{C}}{F_\mathrm{A}}\right)^m . \tag{21}$$

Normalised lifetimes for specimens with linearly decreasing stress fields

A large number of crack growth analyses has been performed with different stress gradients. Figure 4 shows the normalised lifetimes against the relative stress gradient for both edge through-cracks and semi-elliptical cracks. As expected, the normalised lifetime is equal to one for a relative stress gradient approaching zero, i.e. $(d\sigma/dx)/\sigma_{\max} = 0$. Furthermore, the normalised lifetimes increase as the stress gradient increases. By investigating the normalised lifetimes for the two initial crack depths, i.e. $a_\mathrm{i} = 0.015$mm and $a_\mathrm{i} = 0.15$mm, it is clear that the deep initial crack ($a_\mathrm{i} = 0.15$) yields a longer normalised life than the shallow crack ($a_\mathrm{i} = 0.015$). Furthermore, the normalised lifetimes for semi-elliptical cracks are generally shorter than for edge through-cracks.

Figure 5 shows the crack aspect ratio a/c against the crack depth, a, describing the evolution of a/c throughout the fatigue life. The crack aspect ratio is presented for two different stress gradients. The dashed lines represent the homogeneously stressed specimen which quickly settles at $a/c \approx 0.9$. For cracks growing in a gradient stress field, the crack aspect ratio decreases continuously, and it is seen that a/c decreases more rapidly for higher stress gradients.

Edge through-cracks generally yield more conservative results than semi-elliptical cracks. This can be explained by studying the a/c ratio throughout the fatigue life of semi-elliptical cracks. As can be seen from Figure 5, the a/c ratio decreases for semi-elliptical cracks in stress gradient fields, while a/c of a crack in a

homogeneous stress field is constant around 0.9. Due to the lower a/c ratio, the geometry factor $F_{A,0}$ becomes higher for a crack growing in a stress gradient field compared to a corresponding crack growing in a homogeneous stress field. This is not the case for edge through-cracks, where F_0 is equal to 1.122 in both cases. In terms of crack growth, this means that the growth rate of a crack in a stress gradient field normalised with respect to the growth rate of a crack of equal depth in a homogeneous stress field is larger for semi-elliptical cracks than for edge through-cracks. Thus, due to the higher relative growth rates, the normalised lifetimes of semi-elliptical cracks are shorter than those of edge through-cracks.

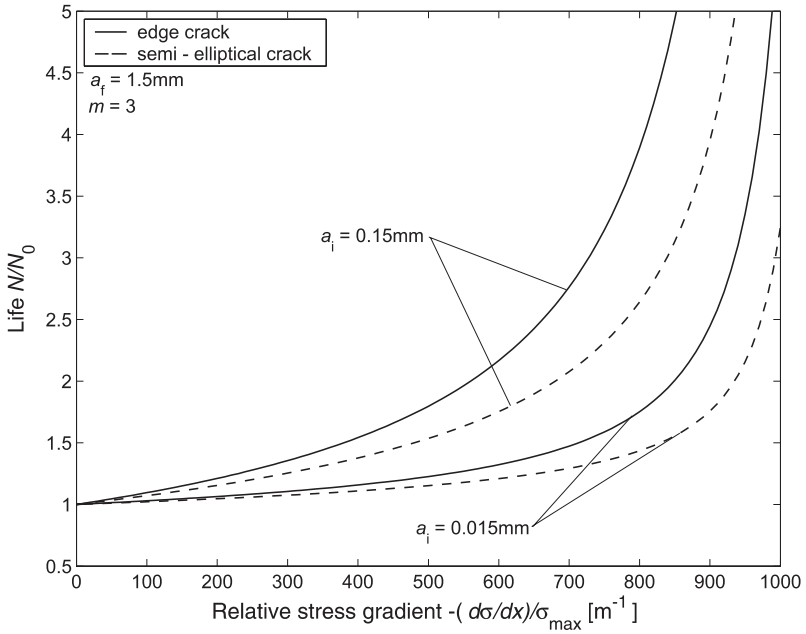

Figure 4: Normalised lifetimes as functions of the relative stress gradient for specimens with a linearly decreasing stress field.

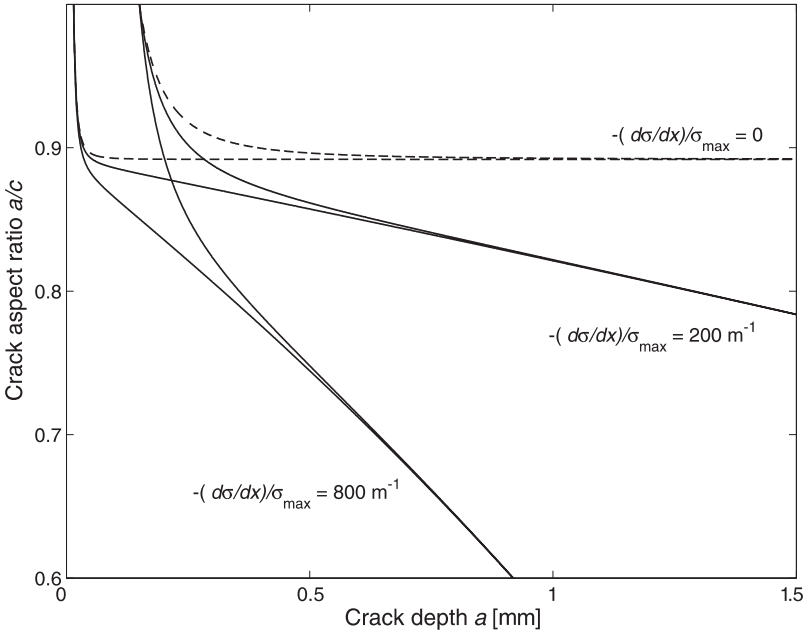

Figure 5: Development of the semi-elliptic crack aspect ratio from the initial to the final crack depth for specimens with a linearly decreasing stress field.

Normalised lifetimes for notched specimens

Similar analyses were performed on notched specimens with different notch curvatures $1/\rho$. The lifetimes were normalised with respect to the lifetime of a smooth homogeneously stressed body with $\sigma = K_t \sigma_\infty$. The normalised lifetimes are shown in Figure 6 as functions of the notch curvature. As expected, the normalised lifetimes approach unity as $1/\rho$ approaches zero. The general features observed in Figure 4 also apply to notched specimens. Thus, deeper initial crack depths result in longer normalised lives, and edge through-cracks yield longer normalised lives than semi-elliptical cracks.

Figure 7 shows the crack aspect ratio throughout the fatigue lifetime. *a/c* is presented for two different notch curvatures as solid lines, and the dashed lines represent the homogeneously stressed specimen. According to Thum et al. [8], the notch curvature is related to the relative stress gradient through

$$\frac{2}{\rho} = -\frac{1}{K_t \sigma_\infty} \frac{\mathrm{d}\sigma}{\mathrm{d}x}\bigg|_{x=0} . \tag{22}$$

Hence, the same characteristics as shown in Figure 5 can be seen for the current specimen, where an increased notch curvature, i.e. a higher relative stress gradient, causes the crack aspect ratio to decrease more rapidly. Contrary to the specimen with a linearly decreasing stress field, the stress in the notched specimen approaches the remote uniform stress σ_∞. Wormsen et al. [6] found that a crack growing from the root of a notch will behave as a crack in a homogeneously stressed body after it has grown out of the notch root stress field. Thus, after reaching a minimum, the *a*/*c* ratio will begin to increase and converge towards 0.9 as the crack grows out of the notch root stress field.

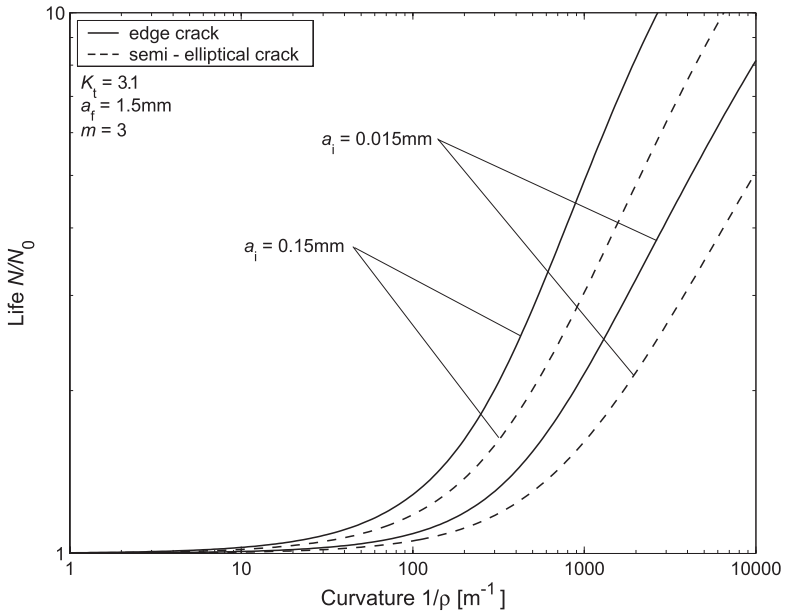

Figure 6: Normalised lifetimes as functions of notch curvature for specimens subjected to a uniform remote stress.

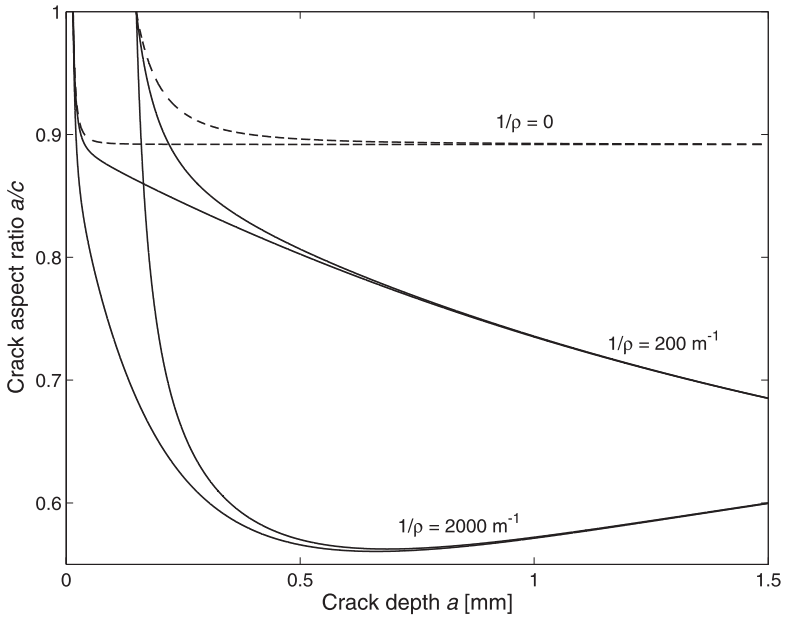

Figure 7: Development of the crack aspect ratio from the initial to the final crack depth for notched specimens subjected to a remote stress.

CONCLUSIONS

This paper treats the influence of a stress gradient of smooth and notched components on the fatigue life. Due to the difficulties related to crack growth analyses in real components, fatigue lives are often predicted by means of the maximum stress at the component surface. In many instances, this approach may yield satisfactory solutions, especially since life estimates will always be on the safe side. However, the maximum stress approach may sometimes lead to overconservative estimates. This paper has quantified the degree of conservatism and identified features influencing the normalised lifetime by performing crack growth analyses both on the real and the smooth specimens. Two cases were considered: a semi-infinite smooth specimen subjected to a linearly decreasing stress and a semi-infinite notched specimen subjected to a uniform remote stress. The degree of conservatism of the maximum stress approach was quantified by normalising the lifetime calculated for the actual specimen with respect to the lifetime of a smooth homogeneously stressed specimen subjected to the same maximum stress. The normalised lifetimes were presented for various initial crack depths as a function of the relative stress gradient and notch curvature. Generally, there are two main features influencing the degree of conservatism: (*i*) the initial crack depth, a_i, and (*ii*) the stress field in the plane of the crack, quantified by the stress gradient or the notch curvature. Deep initial crack depths, a_i, and high relative stress gradients lead to overconservative estimates, especially for edge through-cracks. Using the maximum stress approach gives the best results for semi-elliptical cracks with shallow initial cracks a_i, where good lifetime estimates are achieved even for relatively high stress gradients.

ACKNOWLEDGEMENTS

The authors gratefully acknowledge the research support for this work provided by The Research Council of Norway and the industrial participants within the NorLight project.

REFERENCES

1. Benthem, J. P. and Koiter, W. T. (1973). In: *Mechanics of Fracture,* Volume 1, pp. 131-178. Nordhoff.
2. Newman Jr., J. C. and Raju, I. S. (1981). *Engineering Fracture Mechanics*, 15(1-2), pp. 185-192.
3. Tada, H., Paris, P. C. and Irwin, G. R. (2000). In: *The Stress Analysis of Cracks Handbook.* Professional Engineering Publishing (Limited), Bury St. Edmunds and London, 3rd edition
4. Jergéus, H. Å. (1978). *International Journal of Fracture*, 14, pp. R113-R116.
5. Härkegård. G. (1982). In: *Fatigue Thresholds: fundamentals and engineering applications,* Volume 2, pp. 1005-1118. Engineering Materials Advisory Services (Limited).
6. Wormsen, A., Fjeldstad, A. and Härkegård, G. (2005). The application of asymptotic solutions to a semi-elliptical crack at the root of a notch. Accepted for publication in *Engineering Fracture Mechanics*.
7. Paris, P. and Erdogan, F. (1963). ASME. *Journal of Basic Engineering*, 85(4), pp. 528-534.
8. Thum, A., Petersen, C. and Svenson, O. (1960). In: Verformung, Spannung und Kerbwirkung. Eine Einführung. VDI-VERLAG, Düsseldorf.

Paper 5

ARTICLE IN PRESS

Available online at www.sciencedirect.com
ScienceDirect

Engineering Fracture Mechanics xxx (2007) xxx–xxx

Engineering Fracture Mechanics

www.elsevier.com/locate/engfracmech

Approximate stress intensity factors for cracked V-notched specimens based on asymptotic solutions with application to T-joints

A. Fjeldstad *, A. Wormsen, G. Härkegård

Department of Engineering Design and Materials, Norwegian University of Science and Technology, Richard Birkelandsvei 2B, Trondheim NO-7491 , Norway

Received 7 September 2006; received in revised form 24 April 2007; accepted 26 April 2007

Abstract

This paper presents an approximate method based on asymptotic solutions for estimating the stress intensity factor K for semi-elliptic surface cracks at stress concentrations. The proposed equations make use of a reference solution to interpolate over the entire range from shallow to deep cracks. The reference solution is obtained by considering the current crack emanating from the associated specimen with a sharp notch. It is shown that the proposed formulae satisfy the shallow and deep crack asymptotes. The asymptotic solutions are applied to a T-joint with a fillet-weld-shaped transition. The accuracy of the predictions is assessed using numerical calculations.

Keywords: Stress intensity factor; Geometry factor; Asymptotic solution; Shallow crack; Deep crack; V-notch; T-joint

1. Introduction

A potential failure mode of welded components is fatigue crack propagation of shallow surface cracks from the weld toe. These cracks, which are roughly semi-elliptic, often grow in stress fields that decrease rapidly, i.e., the stress gradient is high. Hence, a crack growth analysis assuming a homogeneous stress field equal to the maximum stress acting at the surface may lead to overconservative predictions of the lifetime of the component [1]. Since crack growth predictions require the stress intensity factor K to be known, it is of great practical interest to establish simple formulae for estimating K for a semi-elliptical crack at the root of the weld toe.

* Corresponding author.
E-mail address: arne.fjeldstad@ntnu.no (A. Fjeldstad).

0013-7944/$ - see front matter © 2007 Elsevier Ltd. All rights reserved.
doi:10.1016/j.engfracmech.2007.04.028

Nomenclature

A	deepest point of crack front
a	crack depth
a^*	transition crack depth between shallow and deep crack asymptotes
C	intersection between crack front and free surface
c	half the surface crack length
d	notch depth
E	Young's modulus
E_2	complete elliptic integral of the second kind
$F(a/c)$	geometry factor for a surface crack
$F_0(a/c)$	geometry factor for a surface crack emanating from a smooth surface
$F_\infty(a/c)$	reference geometry factor for a sharply notched specimen
$F_P(a/c)$	geometry factor for a surface crack in a finite plate
FEA	finite element analysis
g	weight function
K	stress intensity factor $= F\sigma_\infty\sqrt{\pi a}$
K_t	stress concentration factor $= \sigma_{max}/\sigma_\infty$
k_0	parameter of the singular stress field
w_b	semi-width of brace
w_c	width of chord
$\Gamma(v)$	gamma function $= \int_0^\infty \exp(-t)t^{v-1}\,dt$
$\lambda - 1$	exponent of singular stress field
v	Poisson's ratio
ξ	dimensionless co-ordinate $= x/a$
ρ	notch root radius
σ_y	normal stress in y-direction
σ_{max}	maximum stress at crack initiation point
σ_∞	remote stress
ϕ	angle defining location at semi-elliptical crack front
ω	notch opening angle

While K estimation procedures are well established for cracks emanating from a smooth surface, the situation is much less satisfactory, when it comes to cracks at the root of a notch. Wormsen et al. [2] presented an approximate method based on asymptotic solutions for estimating the stress intensity factor K for a semi-elliptical crack at the root of a semi-circular notch. Based on numerical calculations and solutions found in the literature, the accuracy of the approximate method was found to be very good. In the present paper, the asymptotic method presented in [2] is extended to cover cracked V-notched specimens.

During the last few years, empirical stress intensity factors for more complex stress fields have been established. Bowness and Lee [3] presented equations for estimating K for semi-elliptical surface cracks in T-butt joints. The proposed solutions include parameters like crack depth and aspect ratio, attachment footprint and weld angle. Using the body force method [4], Pommier et al. [5] derived a set of emprical equations for estimating the stress intensity factor for a semi-elliptical surface crack located in a semi-infinite plate subjected to mode I loading. Their solution uses the stress field ahead of the crack-free notch as the boundary load on the crack surfaces. The 'notch stress intensity factor' was first introduced by Verreman and Nie [6,7] and further developed by Lazzarin et al. [8–12]. It represents the magnitude of the singular stress field ahead of a V-notch.

The objective of the current investigation is to present simplified solutions for the stress intensity factor K for cracked V-notched specimens. These formulae make use of a reference solution to interpolate over the entire range from shallow to deep cracks. This investigation is restricted to K at the deepest point of the semi-elliptical crack front.

Please cite this article in press as: Fjeldstad A et al., Approximate stress intensity factors for cracked ..., Eng Fract Mech (2007), doi:10.1016/j.engfracmech.2007.04.028

2. V-notches without cracks

The configuration considered is a V-notched plate as shown in Fig. 1. The V-notch is characterised by its depth d, its root radius ρ, its opening angle ω and its elastic stress concentration factor $K_t = \sigma_{max}/\sigma_\infty$. The V-notched plate is loaded by a remote stress σ_∞ perpendicular to the symmetry plane of the notch.

Based on the theory of linear elasticity, Williams [13] was able to show that the asymptotic normal stress in the y-direction, see Fig. 1a, is given by

$$\lim_{x\to 0}\sigma_y(x) = \frac{K}{\sqrt{2\pi x}}, \tag{1}$$

as $\rho/d \to 0$ and $\omega \to 0$.

Williams [13] further demonstrated that singularites less severe than $1/\sqrt{x}$ arise when the notch opens, i.e., $\omega > 0$. In this case, the near-stress-field depends on the notch opening angle ω and may be expressed as [14]

$$\lim_{x\to 0}\sigma_y(x) = \frac{\tilde{K}}{\sqrt{2\pi}x^{1-\lambda}}, \tag{2}$$

where $\tilde{K}$ denotes a generalised stress intensity factor. In the limit when $\omega \to 0$, Eq. (2) reduces to Eq. (1) and $\tilde{K}$ coincides with the standard stress intensity factor K. The eigenvalue λ_i, which determines the order of the stress singularity, is given by

$$\lambda_i \sin 2\alpha + \sin 2\lambda_i\alpha = 0, \quad i = 1, 2, \ldots, \tag{3}$$

where $\alpha = \pi$-$\omega/2$. As ω goes from 0 (cracked body) to π (smooth body), λ varies from 1/2 to 1.

Based on dimensional considerations, it should be possible to rewrite Eq. (2) as [7,15,16]

$$\lim_{x\to 0}\frac{\sigma_y(x)}{\sigma_\infty} = k_0\left(\frac{x}{d}\right)^{\lambda-1}, \tag{4}$$

where k_0 is a dimensionless parameter, which in the case of a semi-infinite cracked V-notched specimen depends only on the opening angle ω.

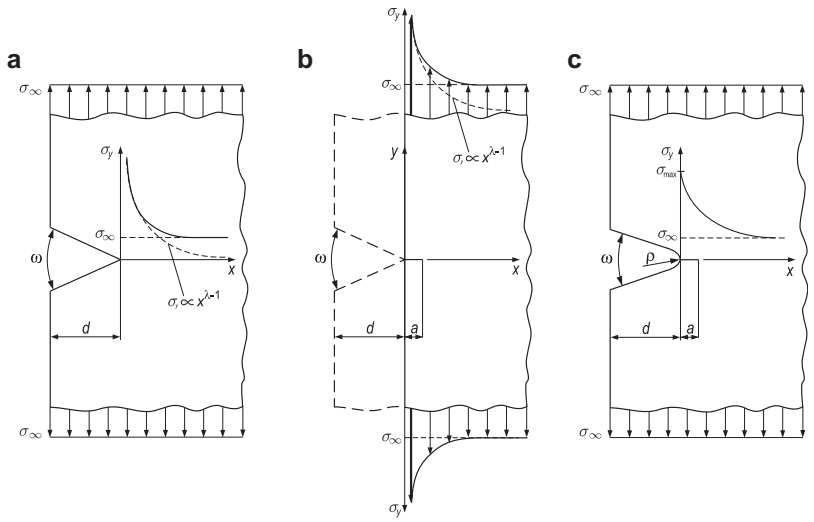

Fig. 1. Semi-infinite V-notched plate under remote uniform stress σ_∞; (a) sharp notch and stress field, (b) unnotched cracked plate subjected to the singular notch stress field $\sigma_y(x)$, (c) through-crack at the root of a blunt notch.

Please cite this article in press as: Fjeldstad A et al., Approximate stress intensity factors for cracked ..., Eng Fract Mech (2007), doi:10.1016/j.engfracmech.2007.04.028

In the following section, stress intensity factors are presented for arbitrarily shaped surface cracks at the root of a notch.

3. V-notches with cracks

As stated in the introduction, cracks frequently initiate at the root of a notch and propagate perpendicularly to the free surface under the influence of a fatigue loading. In order to carry out calculations of fatigue crack growth, it is necessary to know the stress intensity factors for such cracks.

For an arbitrary body with a surface crack of depth a under remote uniaxial tension σ_∞ perpendicular to the plane of the crack, K can be written as

$$K = F(\phi; a/c)\sigma_\infty\sqrt{\pi a}, \tag{5}$$

where $F(\phi;a/c)$ is a dimensionless function of the geometry of the body and the crack. ϕ is an angle defining the location at a semi-elliptical crack front, see Fig. 2. For a surface crack emanating from a smooth surface, i.e., $\omega = \pi$ and $d = 0$, $F(\phi;a/c) = F_0(\phi;a/c)$.

Solutions for a semi-elliptical surface crack in a finite plate under tension and bending have been presented by Newman and Raju [17]. For a semi-elliptic surface crack with aspect ratio a/c, cf. Fig. 2, the geometry factor of the deepest point of the crack front A$(a;0)$ can be estimated as

$$F_0(\phi = \pi/2; a/c) = F_{A,0} = \frac{1.13 - 0.09\frac{a}{c}}{E_2(a/c)}, \tag{6}$$

where the complete elliptic integral of the second kind, $E_2(a/c)$, can be approximated by

$$E_2(a/c) \approx \sqrt{1 + 1.464\left(\frac{a}{c}\right)^{1.65}}, \quad 0 \leqslant a/c \leqslant 1. \tag{7}$$

For an edge through-crack, i.e., $a/c = 0$, Eq. (6) reduces to $F_0 = F_{A,0} = 1.13$, in good agreement with the more precise solution $F_0 = 1.122$ [18]. It should be noted that $F_0 = 1.122$ is used in this paper.

In the following sections, ϕ is set to $\phi = \pi/2$, i.e., the deepest point of the crack front. The geometry factor for an arbitrary surface crack is in the following denoted by $F(a/c)$, while the geometry factors for an edge through-crack and a semi-elliptical crack are denoted by F and F_A, respectively.

3.1. Stress intensity factors for cracks in regular stress fields

For a shallow crack in the notch stress field, the stress intensity solution is asymptotically the same as for a surface crack in a smooth solid, except that the remote stress is being amplified by the stress concentration factor $K_t = \sigma_{max}/\sigma_\infty$, see Fig. 1c. Thus, as $a \to 0$,

$$K = F(a/c)\sigma_\infty\sqrt{\pi a} = F_0(a/c)K_t\sigma_\infty\sqrt{\pi a}. \tag{8}$$

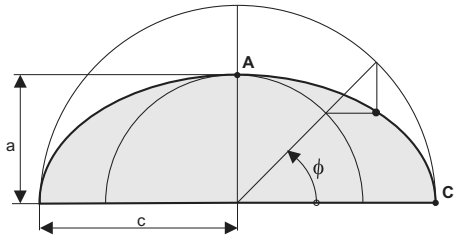

Fig. 2. Two-dimensional view of a semi-elliptical crack.

Please cite this article in press as: Fjeldstad A et al., Approximate stress intensity factors for cracked ..., Eng Fract Mech (2007), doi:10.1016/j.engfracmech.2007.04.028

Neuber [19] found that the stress concentration factor K_t for a semi-infinite V-notched plate under uniform tension is nearly independent of the opening angle ω in the range $0 \leqslant \omega < \pi/2$. This is in agreement of the observation by Nowell et al. [20] that a V-notch with $\omega < \pi/2$ may be regarded as a U-shaped notch with the same depth d and root radius ρ.

When the crack grows beyond the notch stress field, the remote stress field dominates the stress intensity factor, which may be estimated by

$$K = F_0(a/c)\sigma_\infty\sqrt{\pi(a+d)}. \tag{9}$$

Identification with Eq. (5) yields

$$F(a/c) = F_0(a/c)\sqrt{1+\frac{d}{a}}. \tag{10}$$

3.2. Stress intensity factors for cracks in singular stress fields

The overall geometry is now as shown in Fig. 1a, where the notch is considered sharp, i.e., $\rho/d \to 0$, and there is a crack of depth a emanating from the root of the notch. The geometry factor of the sharply V-notched specimen is denoted by F_∞.

Before introducing stress intensity factor solutions for cracks in singular stress fields, it would be convenient to present the weight function method used for deriving a closed form solution of K.

3.2.1. Weight function

When solutions for $F(a/c)$ are not available, the so called weight function may give the geometry factor for an arbitrary crack. A crack of depth a, whose surfaces are subjected to a pair of opposite point forces is considered. Once the stress in the plane of the subsequent crack and the appropriate weight function are known, determination of $F(a/c)$ is reduced to a simple integration procedure.

Consider now a crack of depth a located in a smooth plate subjected to the notch stress field $\sigma_y(x)$, cf. Fig. 1b. The geometry factor F_∞ can then be estimated according to

$$F_\infty(a/c) = \frac{1}{\pi}\int_0^1 \frac{\sigma_y(a\xi)}{\sigma_\infty} g(\xi, a/c)\,\mathrm{d}\xi, \tag{11}$$

where $g(\xi, a/c)$ is the weight function and $\xi = x/a$.

3.2.2. Weight function for edge through-cracks

For a shallow crack, $a/d \ll 1$, Eq. (11) is used as a starting-point. According to Hartranft and Shih [21], the weight function for a crack of depth a, whose surfaces are subjected to a pair of opposite point forces in a semi-infinite plate is given by

$$g(\xi) = \frac{2(1+f(\xi))}{\sqrt{1-\xi^2}}, \tag{12}$$

$$f(\xi) = (1-\xi^2)(0.2945 - 0.3912\xi^2 + 0.7685\xi^4 - 0.9942\xi^6 + 0.5094\xi^8). \tag{13}$$

As was concluded earlier, a sharply notched configuration gives rise to a stress singularity, cf. Eq. (4). This singular term dominates when $a/d \ll 1$, and thus, $\sigma_\infty k_0 (x/d)^{\lambda-1}$ is used as the stress acting on the crack surface. The geometry factor F_∞ is then obtained from Eq. (11) as

$$F_\infty = \frac{2}{\pi}k_0\int_0^1 \frac{1+f(\xi)}{\sqrt{1-\xi^2}}\left(\frac{a\xi}{d}\right)^{\lambda-1}\mathrm{d}\xi. \tag{14}$$

In order to obtain a closed form expression for F_∞, Eq. (14) can be rewritten as

$$F_\infty = \frac{2}{\pi}k_0\tilde{g}_0\int_0^1 \frac{1}{\sqrt{1-\xi^2}}\left(\frac{a\xi}{d}\right)^{\lambda-1}\mathrm{d}\xi, \tag{15}$$

Please cite this article in press as: Fjeldstad A et al., Approximate stress intensity factors for cracked ..., Eng Fract Mech (2007), doi:10.1016/j.engfracmech.2007.04.028

where the factor $1 + f(\xi)$ has been replaced by the constant value $\tilde{g}_0$. The value of $\tilde{g}_0$ will obviously depend on the stress distribution σ_y, which, in the case of a singular stress field, depends on the notch opening angle ω. The constant $\tilde{g}_0$ can be expressed as

$$\tilde{g}_0 = F_0 g_0 = 1.122 g_0. \tag{16}$$

From Table 1 can be seen that g_0 is only weakly dependent on ω, with a maximum difference of less than 5%.

Solving the integral in Eq. (15) and introducing Eq. (16) give

$$F_\infty = F_0 g_0 k_0 l_0 \left(\frac{a}{d}\right)^{\lambda-1}, \tag{17}$$

where

$$l_0 = \frac{1}{\sqrt{\pi}} \frac{\Gamma(\lambda/2)}{\Gamma(\lambda/2 + 1/2)}, \tag{18}$$

and $\Gamma(\cdot)$ denotes the gamma function. Eq. (17) can now be rewritten as

$$F_\infty = F_0 g_0 k_0 l_0 \left(\frac{a}{d}\right)^{\lambda-1} = F_0 F' \left(\frac{a}{d}\right)^{\lambda-1}, \tag{19}$$

where F' is given by

$$F' = g_0 k_0 l_0. \tag{20}$$

3.2.3. Weight function for semi-elliptical cracks

According to Shen and Glinka [23], the weight function for the deepest point of a semi-elliptical surface crack is given by

$$g(\xi) = \frac{2(1 + f(\xi, a/c))}{\sqrt{2(1-\xi)}}, \tag{21}$$

where $f(\xi, a/c)$ can be found in Ref. [23]. By introducing Eq. (21) into Eq. (11), the reference geometry factor, $F_{A,\infty}$, for a semi-elliptical crack located in a singular stress field can be calculated as

$$F_{A,\infty} = \frac{2}{\pi} k_0 \int_0^1 \frac{1 + f(\xi, a/c)}{\sqrt{2(1-\xi)}} \left(\frac{a\xi}{d}\right)^{\lambda-1} d\xi. \tag{22}$$

As in the previous subsection, the expression given in Eq. (22) can be rewritten in order to simplify the integration procedure.

$$F_{A,\infty} = \frac{2}{\pi} k_0 \tilde{g}_{A,0} \int_0^1 \frac{1}{\sqrt{2(1-\xi)}} \left(\frac{a\xi}{d}\right)^{\lambda-1} d\xi, \tag{23}$$

Table 1
Values of λ, g_0, k_0, l_0, F' and F'/k_0 for a V-shaped through-cracked notch with $\rho/d = 0$ and $a/d \to 0$

	Notch opening angle ω										
	0°	20°	40°	60°	80°	90°	100°	120°	140°	160°	180°
λ	0.5	0.501	0.504	0.512	0.530	0.544	0.563	0.616	0.697	0.819	1
g_0	1.048	1.048	1.047	1.046	1.044	1.042	1.040	1.034	1.025	1.014	1
k_0	0.572	0.578	0.586	0.611	0.660	0.670	0.744	0.863	1.018	1.148	1
l_0	1.669	1.666	1.659	1.639	1.595	1.563	1.522	1.421	1.295	1.151	1
F'	1	1.009	1.020	1.047	1.098	1.133	1.176	1.268	1.351	1.340	1
F'/k_0	1.749	1.744	1.740	1.714	1.665	1.629	1.582	1.469	1.328	1.167	1

The parameters k_0 and F' are from Ref. [22].

Please cite this article in press as: Fjeldstad A et al., Approximate stress intensity factors for cracked ..., Eng Fract Mech (2007), doi:10.1016/j.engfracmech.2007.04.028

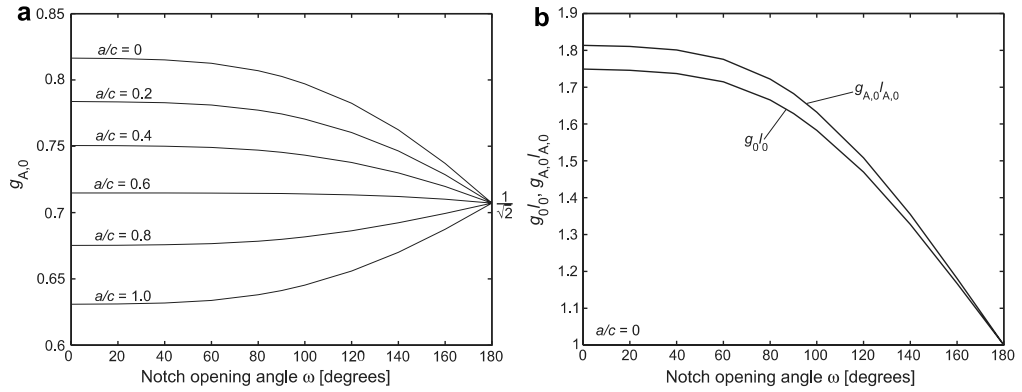

Fig. 3. (a) $g_{A,0}$ as a function of the notch opening angle ω for different values of a/c, (b) g_0l_0 and $g_{A,0}l_{A,0}$ for $a/c = 0$ plotted against the notch opening angle, ω.

where the factor $1 + f(\xi, a/c)$ is replaced by the constant value $\tilde{g}_{A,0}$, which depends on both the opening angle ω and the aspect ratio a/c. $\tilde{g}_{A,0}$ can further be expressed as

$$\tilde{g}_{A,0} = F_{A,0}g_{A,0}. \tag{24}$$

Fig. 3a shows $g_{A,0}$ against ω for different values of a/c.

Solving the integral in Eq. (23) and introducing Eq. (24) give

$$F_{A,\infty} = F_{A,0}g_{A,0}k_0l_{A,0}\left(\frac{a}{d}\right)^{\lambda-1}, \tag{25}$$

where

$$l_{A,0} = \sqrt{\frac{2}{\pi}}\frac{\Gamma(\lambda)}{\Gamma(\lambda+1/2)}. \tag{26}$$

Finally, $F_{A,\infty}$ can be presented on the same form as Eq. (19):

$$F_{A,\infty} = F_{A,0}g_{A,0}k_0l_{A,0}\left(\frac{a}{d}\right)^{\lambda-1} = F_{A,0}F'_A\left(\frac{a}{d}\right)^{\lambda-1}. \tag{27}$$

Fig. 3b shows $g_{A,0}l_{A,0}$ and g_0l_0 versus the opening angle ω. The product $g_{A,0}l_{A,0}$ is obtained using the aspect ratio $a/c = 0$. From the figure it can be seen that the weight function solution for semi-elliptic cracks presented by Shen and Glinka [23] is in good agreement with the edge through-crack solution by Hartranft and Shih [21], with a maximum difference of less than 4%.

4. Geometry factors

4.1. Reference geometry factor $F_\infty(a/c)$

In the present Section, simple expressions for the geometry factors of through-cracks and semi-elliptical cracks emanating from the root of a notch are presented. These expressions have been based on the reference geometry factor $F_\infty(a/c)$ for a sharply cracked V-notched specimen.

In Fig. 4, the geometry factor $F_\infty(a/c)$ has been drawn as a dashed curve. For a shallow crack, i.e., $a/d \to 0$, the singular notch stress field tends to dominate as expressed by Eq. (27). Hence, $F_\infty(a/c)$ asymptotically tends to infinity. As the normalised crack depth a/d increases, $F_\infty(a/c)$ continuously decreases. For sufficiently deep cracks, $F_\infty(a/c)$ asymptotically approaches the geometry factor $F_0(a/c)$ for the current surface crack emanating from a smooth surface.

Please cite this article in press as: Fjeldstad A et al., Approximate stress intensity factors for cracked ..., Eng Fract Mech (2007), doi:10.1016/j.engfracmech.2007.04.028

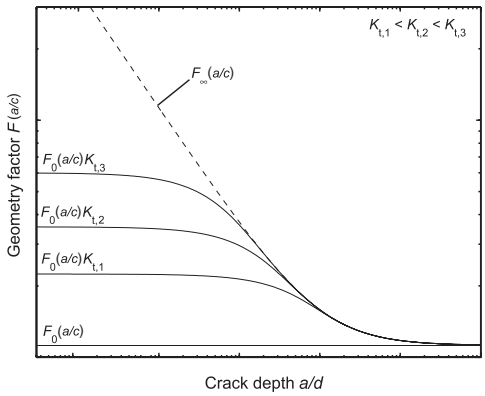

Fig. 4. Principle graphs of geometry factors against the normalised crack depth a/d.

4.2. Geometry factors for cracks in regular stress fields

Geometry factors, $F(a/c)$, have been plotted against the normalised crack depth a/d in Fig. 4 for three notched plates. For shallow cracks, the geometry factor assumes the constant value $F_0(a/c)K_t$. As a increases, $F(a/c)$ continuously decreases and asymptotically approaches $F_\infty(a/c)$. As the crack grows beyond the notch root stress field, the remote stress becomes dominating and both approach the constant value $F_0(a/c)$.

4.3. Normalised geometry factors

Normalising the shallow crack geometry factor solution obtained from Eq. (8) with respect to the geometry factor, $F_\infty(a/c)$, for a surface crack emanating from the root of a sharp notch, i.e., $\rho/d \to 0$, cf. Eq. (27), yields

$$\frac{F(a/c)}{F_\infty(a/c)} = \frac{K_t}{F'(a/c)}\left(\frac{a}{d}\right)^{1-\lambda}. \tag{28}$$

As the crack grows deeper, the above $F_\infty(a/c)$ becomes less sensitive to the singular stress field. Hence, the above fraction asymptotically approaches

$$\frac{F(a/c)}{F_\infty(a/c)} = 1, \tag{29}$$

as shown in Fig. 5a for the notched plate in Fig. 1c. In addition, normalising the crack depth a with respect to a transition crack depth a^* yields a single curve, as shown in Fig. 5b. Wormsen et al. [2] introduced an equation for the normalised geometry factor F/F_∞, which asymptotically agrees with the near and remote field estimates. They suggested that the normalised geometry factor could be written as

$$\frac{F(a/c)}{F_\infty(a/c)} = \left[1 - \exp\left(-\frac{a}{a^*}\right)\right]^{1-\lambda}, \tag{30}$$

where a^* is defined as the crack depth at which the shallow and deep crack asymptotes given by Eqs. (28) and (29), intersect. Hence, a^* is determined by

$$a^* = d\left(\frac{F'(a/c)}{K_t}\right)^{\frac{1}{1-\lambda}}. \tag{31}$$

Please cite this article in press as: Fjeldstad A et al., Approximate stress intensity factors for cracked ..., Eng Fract Mech (2007), doi:10.1016/j.engfracmech.2007.04.028

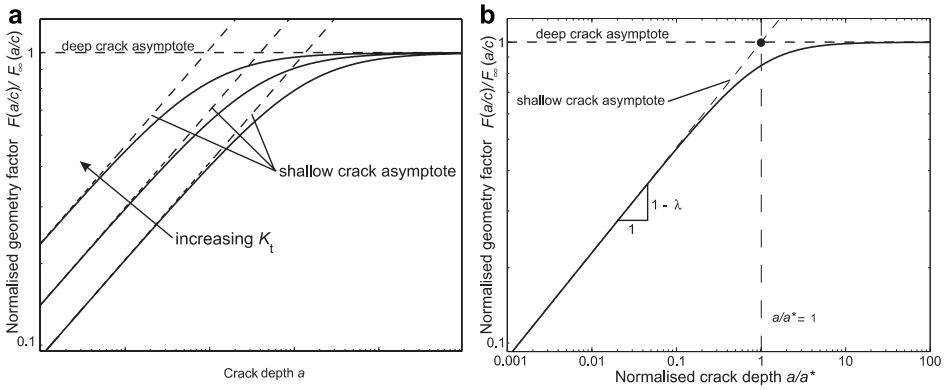

Fig. 5. Principle graphs of normalised geometry factors against (a) the crack depth a, (b) the normalised crack depth a/a^*.

For a notch with $\omega < \pi/2$ and $\rho \ll d$, the stress concentration factor is approximately given by

$$K_t \approx 2\sqrt{\frac{d}{\rho}} \tag{32}$$

With $F' = 1$, see Table 1, the transition crack depth a^* for an edge through-crack becomes

$$a^* \approx \frac{\rho}{4}. \tag{33}$$

An alternative equation that satisfies the shallow and deep crack asymptotes is given by

$$\frac{F(a/c)}{F_\infty(a/c)} = \left[1 + \left(\frac{a^*}{a}\right)^\beta\right]^{\frac{\lambda-1}{\beta}}, \tag{34}$$

where a^* is given by Eq. (31). It has been found that Eq. (34) gives $F(a/c)$ values in somewhat better agreement with numerical values over a wider range of notch opening angles ω and ρ/d values than Eq. (30), provided that the parameter β is chosen properly. With $\beta = 1.35$, Eqs. (30) and (34) differ by less than 3.5%.

5. T-joint configuration

The expressions for the semi-infinite V-notched specimen can be used as a basis for establishing approximate closed form solutions for the geometry factor $F(a/c)$ for finite width T-joints (see Fig. 6). The notch geometry for the T-joints is very similar to the V-notch geometry, both characterised by an opening angle ω and a notch root radius ρ. For both cases, the shallow crack asymptote is given by Eq. (8). However, for the stress raisers shown in Fig. 6, there is no notch depth d that will 'add' to the crack depth, when the crack becomes deeper. Therefore, the deep crack asymptote of the stress intensity factor is given by

$$K = F_0\left(\frac{a}{c}\right)\sigma_\infty\sqrt{\pi a}, \quad a \gg \rho. \tag{35}$$

5.1. Geometry

The accuracy of the formulae presented in Section 4.3 will now be assessed by numerical analyses of a T-joint with a fillet-weld-shaped transition as shown in Fig. 6. The T-joint has a chord width w_c and a brace semi-width $w_b = 3/4w_c$. Its stress concentration factors have been summarised in Table 2. Both edge through-cracked and semi-elliptically cracked specimens will be considered.

The T-joint has a weld-shaped transition as shown in Fig. 6. The transition can be described by a straight line creating a 135° angle with the longitudinal direction of the chord. A circular arc of radius ρ connects the

Please cite this article in press as: Fjeldstad A et al., Approximate stress intensity factors for cracked ..., Eng Fract Mech (2007), doi:10.1016/j.engfracmech.2007.04.028

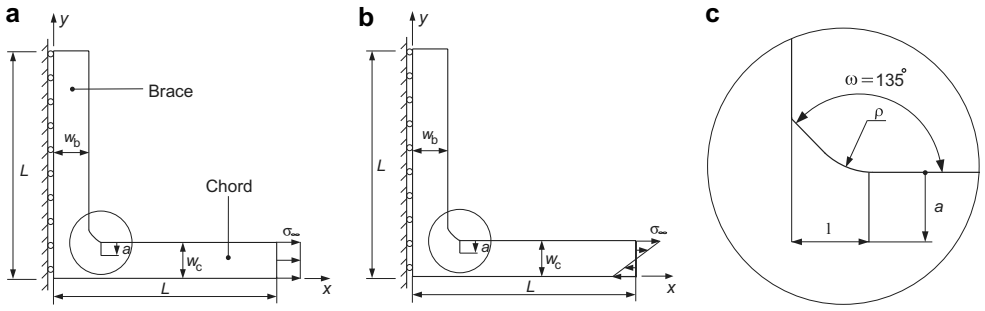

Fig. 6. Boundary conditions applied to the cracked specimens: (a) chord subjected to homogeneous stress, (b) chord subjected to pure bending and, (c) close-up of the notch geometry.

Table 2
Summary of FEA based stress concentration factors for the investigated T-joint

Specimen number	Normalised notch radius ρ/w	Stress concentration factor K_t
1. Fig. 6a	0.0125	2.86
	0.025	2.32
	0.0625	1.84
2. Fig. 6b	0.0125	3.20
	0.025	2.56
	0.0625	1.98

weld and the chord as shown in Fig. 6c. The weld leg length is set to $l = 0.2w_c$. The weld geometry parameters ρ, ω and l are defined according to Tveiten et al. [24]. A surface crack of depth a emanates from the point, where the chord enters the weld toe. The cracked T-joint was subjected to two different loading conditions, namely tension and bending, as shown in Fig. 6a and b, respectively. Symmetry about the vertical centre-line, i.e., $x = 0$, makes it sufficient to model only one half of the T-joint.

6. Geometry factors for T-joint configurations

6.1. Edge through-cracks

In Section 3, simple expressions for the geometry factor, F, for cracks emanating from the root of a V-notch were introduced, which asymptotically agree with the shallow and deep crack asymptotes. These expressions were based on the reference solution F_∞, for a sharply notched specimen, i.e., $\rho/w \to 0$. Next, the expressions for the V-notched plate will be used as a basis for estimating the geometry factor F of a cracked T-joint.

For the V-notched plate in Fig. 1, the geometry factor was given as a function of a/d. However, a characteristic notch depth, d, cannot be defined for a T-joint. Instead, it is suggested that the width, w, of the cracked part of the T-joint to be used as the characteristic length parameter. The geometry factor of the cracked T-joint can then be obtained from Eq. (34), with the transition crack depth given by

$$a^* = w\left(\frac{F'}{K_t}\right)^{\frac{1}{1-\lambda}}. \tag{36}$$

The effect of finite width is taken into account by means of the reference geometry factor F_∞. Hence, for deep cracks, F_∞ asymptotically approaches the geometry factor for the current edge through-crack emanating from the smooth surface of a plate of finite width w. For a single-edge-cracked plate of width w under uniform tension, the geometry factor is given in [18].

Please cite this article in press as: Fjeldstad A et al., Approximate stress intensity factors for cracked ..., Eng Fract Mech (2007), doi:10.1016/j.engfracmech.2007.04.028

6.2. Semi-elliptical cracks

For the semi-elliptically cracked T-joints, the geometry factor F_A for the deepest point at the crack front, A(a;0), can be estimated by means of Eq. (27), see Fig. 2. As for the edge through-cracked specimens, the effect of finite width is taken into account by means of the reference geometry factor $F_{A,\infty}$. Hence, for deep surface cracks, $F_{A,\infty}$ asymptotically approaches the geometry factor for a surface crack in a finite plate of width w. Solutions for surface cracks in a finite plate under tension and bending have been presented by Newman and Raju [17], see Section 3.

The weight-function can be used to compute the reference geometry factor, F_∞ for a through-crack of arbitrary depth. For a semi-elliptical crack, the weight-function is expected to yield accurate results as long as the crack depth is small compared with the notch radius. When the crack grows and become comparable with the root radius, the use of Eq. (6) is questionable for arbitrary notch angles since the used weight-function, see Eq. (21), is strictly speaking only valid for smooth plates. As a consequence, the accuracy of the K approximation in the intermediate regime can be expected to be higher for through-cracks than for semi-elliptical cracks. To increase the accuracy of $F_{A,\infty}$ one could use finite element results instead of the weight-function method.

7. Numerical analysis

The observation that the geometry factor $F(a/c)$ for various specimens can be estimated by means of Eq. (34), if the geometry factor $F_\infty(a/c)$ is known, is an important aspect of the use of crack mechanics in design. It is therefore of great interest to study the influence on $F(a/c)/F_\infty(a/c)$ of parameters such as crack depth a, aspect ratio a/c, T-joint geometry, and applied loading (actual force or bending moment). The cracked specimens considered are shown in Fig. 6. For each specimen, the geometry factor was evaluated for three ρ/w ratios, cf. Table 2. In the following Subsections, the accuracy of Eq. (34) is assessed by using $\beta = 1.35$.

7.1. Evaluation procedures

Linear elastic plane strain analyses of the edge through-cracked specimens were performed using the finite element program ABAQUS [25]. Eight-noded isoparametric second order plane strain elements with reduced integration were used. Poisson's ratio was chosen to be $\nu = 0.3$ and small displacement theory was assumed throughout. The geometry factors, F_A, for the semi-elliptically cracked specimens were obtained using a set of empirical equations presented by Pommier et al. [5].

$F(a/c)$ is for both edge through-cracks and semi-elliptical cracks normalised by means of the reference solution $F_\infty(a/c)$. Appendix A describes in detail how $F_\infty(a/c)$ can be obtained.

7.2. Geometry factors

7.2.1. Edge through-cracks

The cracked configurations are shown in Fig. 6. Representative finite element solutions are those of the T-joint with a weld-shaped transition under uniform tension, i.e., the specimen shown in Fig. 6a. Finite element geometry factors, F, have been plotted against the normalised crack depth a/w in Fig. 7a. For shallow cracks, say $a/w < 0.001$, the notch stress field dominates and the geometry factor assumes the constant value F_0K_t, while F_∞ asymptotically tends to infinity. As the crack depth increases, F continuously decreases and asymptotically approaches F_∞. As the crack grows beyond the notch stress field, the remote stress becomes dominating and F and F_∞ asymptotically approach the geometry factor for the current surface crack emanating from a smooth surface in a finite plate.

In Fig. 7b, the finite element F values have been normalised with respect to F_∞. As can be seen, F/F_∞ approaches the deep crack asymptote in a similar fashion for all ρ/w ratios. In fact, by normalising the crack depth a with respect to the transition crack depth a^*, F/F_∞ reduces to a single curve as shown in Fig. 8a. The expression for the solid curve is given by Eq. (34). As can be seen from Fig. 8a, Eq. (34) is in excellent agreement with the finite element results. As shown in Fig. 8b, this is also true for the specimen in Fig. 6b.

Please cite this article in press as: Fjeldstad A et al., Approximate stress intensity factors for cracked ..., Eng Fract Mech (2007), doi:10.1016/j.engfracmech.2007.04.028

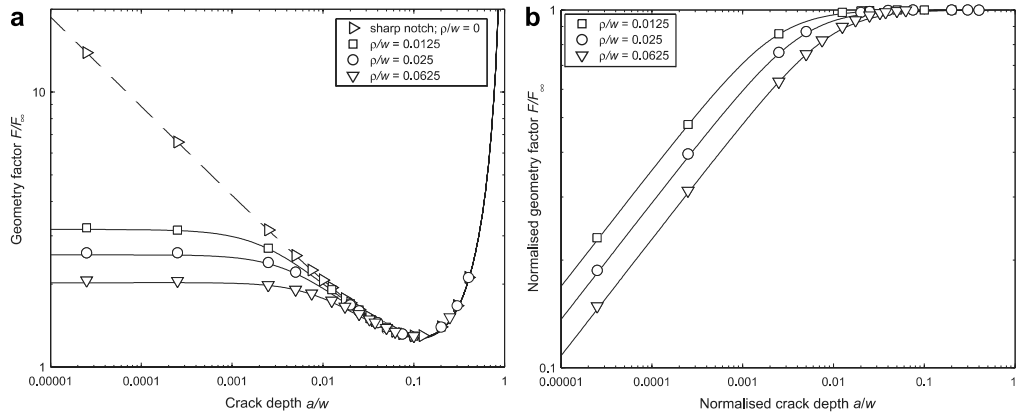

Fig. 7. Geometry factors due to FEA for specimen in Fig. 6a with a through-crack emanating from the chord transition: (a) F and F_∞ against a/w, (b) F/F_∞ against a/w.

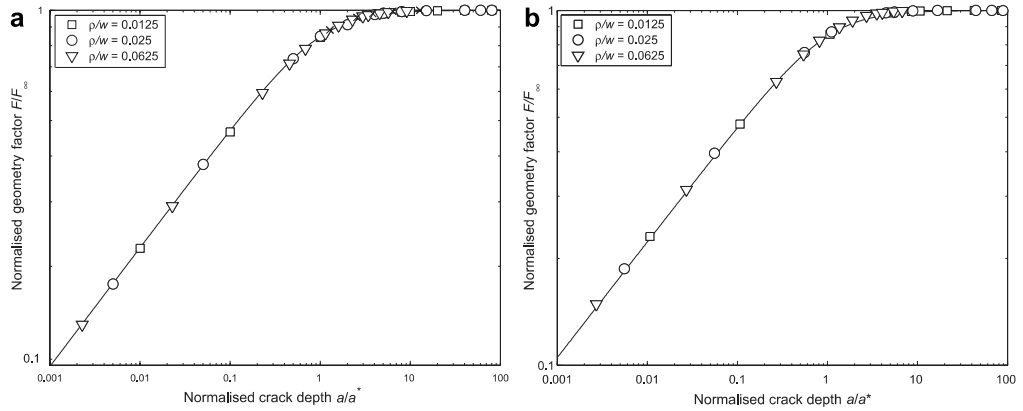

Fig. 8. F/F_∞ finite element results as a function of the normalised crack depth a/a^* for the edge through-cracked (a) specimen in Fig. 6a, (b) specimen in Fig. 6b.

7.2.2. Semi-elliptical cracks

In the previous Subsection, finite element results of F/F_∞ for edge through-cracked specimens were presented. This subsection presents results of $F_A/F_{A,\infty}$, when the crack is semi-elliptic, cf. Fig. 2.

Numerical results in Fig. 9a are for the specimen in Fig 6a with an aspect ratio $a/c = 0.5$ and three (cf. Table 2) different relative notch root radii, ρ/w. Initially, the geometry factor F_A for the deepest point A$(a;0)$ is equal to $F_{A,0}K_t$. For the specimen with a sharp notch, i.e., $\rho/w \to 0$, the geometry factor $F_{A,\infty}$ tends to infinity as $a/w \to 0$, cf. Eq. (27) with d replaced by w. The geometry factor $F_{A,\infty}$ is shown as a dashed line in Fig. 9a. When a/w increases, F_A and $F_{A,\infty}$ continuously decrease.

In Fig. 9b, the geometry factors, F_A, for the specimens with a finite notch root radius, i.e., $\rho/w > 0$, are normalised with respect to the associated factors for a specimen with a sharp notch. Results from analyses carried out on semi-elliptical cracks with aspect ratios $a/c = 0.2$ and 1 are also included. As can be seen, the ratio $F_A/F_{A,\infty}$ asymptotically approaches the deep crack asymptote in a similar fashion for all ρ/w ratios. Hence,

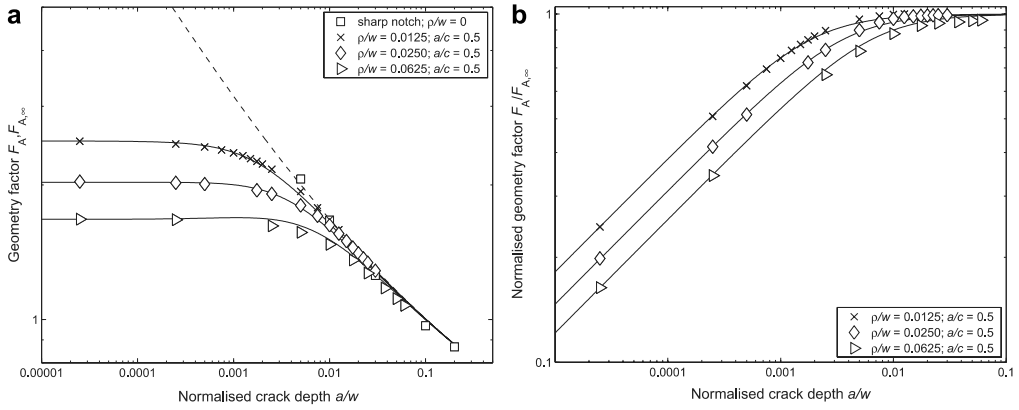

Fig. 9. Geometry factors for the crack front A(a;0) (Fig. 2) for specimen in Fig. 6a: (a) F_A and $F_{A,\infty}$ against a/w, (b) $F_A/F_{A,\infty}$ against a/w.

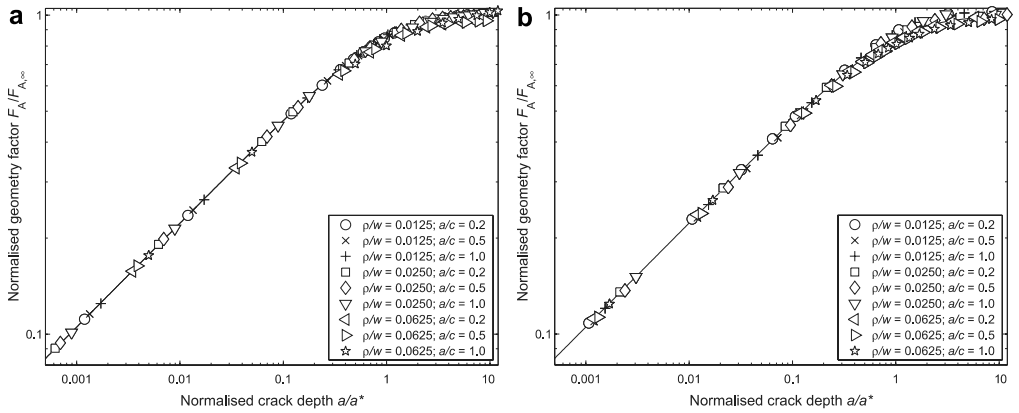

Fig. 10. $F_A/F_{A,\infty}$ results as a function of the normalised crack depth a/a^* for the semi-elliptically cracked (a) specimen in Fig. 6a, (b) specimen in Fig. 6b.

by normalising the crack depth a with respect to the transition crack depth a^*, $F_A/F_{A,\infty}$ reduces to a single curve as shown in Fig. 10a. The expression for the solid curve is given by Eq. (34). As also can be seen from Fig. 10b, Eq. (34) is in excellent agreement with the numerical results.

8. Conclusions

Notched specimens with through-cracks or semi-elliptical cracks emanating from the root of the notch have been investigated. Simplified formulae for obtaining the stress intensity factor K have been presented. The proposed equations for estimating K make use of a reference solution to interpolate over the entire range from shallow to deep cracks. The reference solution is obtained by considering the current crack emanating from the corresponding specimen with a sharp notch. The formulae satisfy the shallow and deep crack asymptotes.

An important aspect of the work has been to apply the solutions to a T-joint configurations. The aim was to calculate K as a function of the normalised crack depth a/w. These results were used to obtain values of the geometry factors $F(a/c)$ and $F_\infty(a/c)$. Once $F_\infty(a/c)$ has been determined, the geometry factor, $F(a/c)$, for spec-

Please cite this article in press as: Fjeldstad A et al., Approximate stress intensity factors for cracked ..., Eng Fract Mech (2007), doi:10.1016/j.engfracmech.2007.04.028

imens with a finite notch root radius, i.e., $\rho/w > 0$, can be estimated using simplified interpolation functions (see Section 4). Moreover, the proposed method and numerical calculations, covering different geometries and applied loading conditions, showed excellent agreement both for edge through-cracks and semi-elliptical cracks.

The procedure for the approximate determination of K should be a useful tool for the life assessment of cracked V-notched specimens and T-joints subject to fatigue loading.

Acknowledgements

The authors gratefully acknowledge the research support for this work provided by The Research Council of Norway and the industrial participants within the NorLight project, and by GE Energy (Norway) AS. The authors also wish to thank Dr. Hans-Jörg Huth for permission to use a fatigue crack growth code with stress intensity factors based on Pommier et al.

Appendix A

Presented in this appendix is a set of formulae for establishing the reference geometry factor $F_\infty(a/c)$. In this work, $F_\infty(a/c)$ is expressed by

$$F_\infty\left(\frac{a}{c},\frac{a}{w}\right) = \left[F'\left(\frac{a}{c}\right)\cdot\left(\frac{a}{w}\right)^{\lambda-1} + f\left(\frac{a}{c},\frac{a}{w}\right)\right]F_P\left(\frac{a}{c},\frac{a}{w}\right), \tag{37}$$

where $F_P(a/c)$ is the geometry factor for the current surface crack emanating from a smooth surface. Fig. 11 shows the geometry factor for a smooth plate, $F_P(a/c)$, along with the reference solution $F_\infty(a/c)$ for a sharp notch ($\rho = 0$) and the geometry factor $F(a/c)$ for a notched specimen with $\rho/w > 0$. The geometry factor for a notched specimen asymptotically approaches $F_P(a/c)$, when the crack has grown beyond the notch root stress field. $F_P(a/c)$ is used in Eq. (37) for describing the deep crack behaviour, since $F_\infty(a/c)/F_P(a/c) = 1$ when $a/w \to 1$. Hence, for deep cracks the following condition applies:

$$\lim_{a/w\to 1} F'\left(\frac{a}{c}\right)\cdot\left(\frac{a}{w}\right)^{\lambda-1} + f\left(\frac{a}{w}\right) = 1. \tag{38}$$

In Eqs. (37) and (38), $F'(a/c)\cdot(a/w)^{\lambda-1}$ accounts for the behaviour of shallow cracks located in singular stress fields, while $f(a/w)$ describes the transition between shallow and deep crack behaviour.

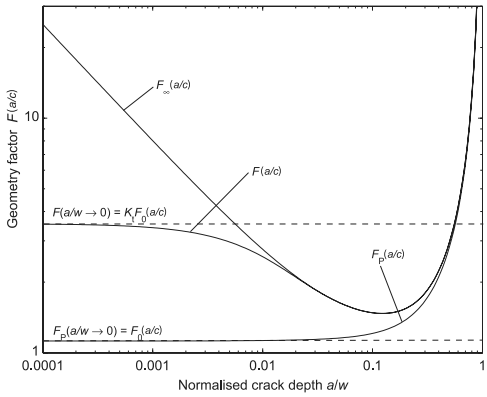

Fig. 11. Principle graphs of the geometry factors for a smooth plate, F_P, sharp-notched plate ($\rho = 0$), F_∞, and a notched plate with a finite notch radius ($\rho/w > 0$), F.

Please cite this article in press as: Fjeldstad A et al., Approximate stress intensity factors for cracked ..., Eng Fract Mech (2007), doi:10.1016/j.engfracmech.2007.04.028

Table 3
Summary of curve fit parameters for F_∞(a/c)

Cracked configuration	a/c	$F'(a/c)$	Regression parameters				$a/w \leqslant$
			b_0	b_1	b_2	b_3	
Fig. 6a[a]	0	0.392	−0.1580	0.4690	0	0	0.9
Fig. 6a[b]	0.2	0.383	−0.4614	0.0356	0.0594	0.0410	0.2
	0.5	0.369	−0.3729	0.0906	0.0560	0.0326	0.2
	1.0	0.340	0.0988	1.4277	1.0177	0.2249	0.2
Fig. 6b[a]	0	0.451	−0.1510	0.8310	0.1590	0.0264	0.9
Fig. 6b[b]	0.2	0.441	−0.4107	0.5193	0.5529	0.1691	0.2
	0.5	0.424	−0.5348	0.1251	0.2237	0.0850	0.2
	1.0	0.391	−1.0548	−0.6227	−0.0543	0.0533	0.2

Here, $\lambda = 0.674$ ($\omega = 135°$) for the configurations considered.
[a] Edge through-crack.
[b] Semi-elliptical crack.

For shallow cracks, $f(a/w)$ approaches zero and $F_P(a/c)$ assumes the constant value $F_0(a/c)$. Hence, Eq. (37) is in total agreement with Eq. (19). Rearranging Eq. (37) gives

$$f\left(\frac{a}{c},\frac{a}{w}\right) = \frac{F_\infty(a/c)}{F_P(a/c)} - F'\left(\frac{a}{c}\right)\cdot\left(\frac{a}{w}\right)^{\lambda-1}. \tag{39}$$

Thus, $f(a/w)$ is bounded between 0 and $1 - F'(a/c)$. Based on numerical results, it is found that $f(a/w)$ can be well approximated by

$$f\left(\frac{a}{w}\right) = 10^{\eta(a/w)}, \tag{40}$$

where the exponent $\eta(a/w)$ is given by the polynomial

$$\eta\left(\frac{a}{w}\right) = b_0 + \sum_{i=1}^{3} b_i\left[\log_{10}\left(\frac{a}{w}\right)\right]^i. \tag{41}$$

The parameters b_i ($i = 0,\ldots,3$) of all specimens considered have been collected in Table 3. The associated values of the factor $F'(a/c)$ of Eq. (39) have also been listed in Table 3. For the through-cracked specimens the parameters have been found by means of the finite element method. The parameters for semi-elliptical cracked specimens have been obtained from a set of empirical equations presented by Bowness and Lee [3].

References

[1] Fjeldstad A, Härkegård G, Wormsen A. The influence of a stress gradient on the growth of a fatigue crack. In: Johnson WS et al., editors. Proceedings of the international fatigue congress 2006, Atlanta, Georgia, USA. Elsevier; 2006.
[2] Wormsen A, Fjeldstad A, Härkegård G. The application of asymptotic solutions to a semi-elliptical crack at the root of a notch. Engng Fract Mech 2006;73(13):1899–912.
[3] Bowness D, Lee MMK. Prediction of weld toe magnification factors for semi-elliptical cracks in T-butt joints. Int J Fatigue 2000;22(5):369–87.
[4] Murakami Y. Analysis of stress intensity factors of mode I, II and III for inclined surface cracks of arbitrary shape. Engng Fract Mech 1985;22(1):101–4.
[5] Pommier S, Sakae C, Murakami Y. An empirical stress intensity factor set of equations for a semi-elliptical crack in a semi-infinite body subjected to a polynomial stress distribution. Int J Fatigue 1999;21(3):243–51.
[6] Nie B, Verreman Y. Rationalization of short crack propagation life at V-notches with the notch stress intensity factor. In: Baïlon JP, Dickson JI, editors. Proceedings of FATIGUE 93. vol. III, 1993. p. 1657–62.
[7] Verreman Y, Nie B. Early development of fatigue cracking at manual fillet welds. Fatigue Fract Engng Mater Struct 1996;19(6):669–81.
[8] Lazzarin P, Tovo R. A unified approach to the evaluation of linear elastic stress fields in the neighborhood of cracks and notches. Int J Fract 1996;78(1):3–19.
[9] Lazzarin P, Tovo R. Notch stress intensity factor approach to the stress analysis of welds. Fatigue Fract Engng Mater Struct 1998;21(9):1089–103.

Please cite this article in press as: Fjeldstad A et al., Approximate stress intensity factors for cracked ..., Eng Fract Mech (2007), doi:10.1016/j.engfracmech.2007.04.028

[10] Lazzarin P, Zambardi R. A finite-volume-energy based approach to predict the static and fatigue behaviour of components with sharp V-shaped notches. Int J Fract 2001;112(3):275–98.
[11] Lazzarin P, Livieri P. Notch stress intensity factors and fatigue strength of aluminium and steel welded joints. Int J Fatigue 2001;23(3):225–32.
[12] Lazzarin P, Lassen T, Livieri P. A notch stress intensity approach to fatigue life predictions of welded joints with different local toe geometry. Fatigue Fract Engng Mater Struct 2003;26(1):49–58.
[13] Williams ML. Stress singularities resulting from various boundary conditions in angular corners of plates in extension. J Appl Mech 1952;24:109–14.
[14] Atzori B, Lazzarin P, Tovo R. Stress distributions for V-shaped notches under tensile and bending loads. Fatigue Fract Engng Mater Struct 1997;20(8):1083–92.
[15] Verreman Y, Baïlon J-P. Fatigue of V-notched members: short crack behaviour and endurance limit. Engng Fract Mech 1987;28(5–6):773–83.
[16] Rooke DP, Baratta FI, Cartwright DJ. Simple methods of determining stress intensity factors. Engng Fract Mech 1981;14(2):397–426.
[17] Newman Jr JC, Raju IS. An empirical stress-intensity factor equation for the surface crack. Engng Fract Mech 1981;15(1–2):185–92.
[18] Tada H, Paris PC, Irwin GR. The stress analysis of cracks handbook. 3rd ed. Bury St. Edmunds and London: Professional Engineering Publishing Limited; 2000.
[19] Neuber H. Kerbspannungslehre. 2nd ed. Berlin: Springer-Verlag; 1958.
[20] Nowell D, Dini D, Duó P. Stress analysis of V-notches with and without cracks, with application to foreign object damage. J Strain Anal Engng Des 2003;38(5):429–41.
[21] Hartranft RJ, Sih GC. Alternating method applied to edge and surface crack problems. Methods of analysis and solutions of crack problems. Mechanics of fracture. Leyden: Nordhoff; 1973 [chapter 4].
[22] Hasebe N, Iida J. A crack originating from a triangular notch on a rim of a semi-infinite plate. Engng Fract Mech 1978;10(4):773–82.
[23] Shen G, Glinka G. Weight functions for a surface semi-elliptical crack in a finite thickness plate. Theor Appl Fract Mech 1991;15(3):247–55.
[24] Tveiten BW, Fjeldstad A, Härkegård G, Myhr OR, Bjørneklett B. Fatigue life enhancement of aluminium joints through mechanical and thermal prestressing. Int J Fatigue 2006;28(12):1667–76.
[25] Abaqus/Standard, User's manual, version 6.4. Hibbit, Karlsson and Sorensen, Pawtucket, Rhode Island, 2003.

Please cite this article in press as: Fjeldstad A et al., Approximate stress intensity factors for cracked ..., Eng Fract Mech (2007), doi:10.1016/j.engfracmech.2007.04.028

Paper 6

A post-processor for fatigue crack growth analysis based on a finite element stress field

A. Wormsen*, A. Fjeldstad and G. Härkegård
Norwegian University of Science and Technology, Trondheim, Norway.

Abstract

In this paper the algorithm needed for performing a crack growth analysis of a three-dimensional component by post-processing results from a standard finite element stress analysis is given. Weight functions are used for calculating the stress intensity factor for an embedded crack and a surface crack. Defects are generated in several nominally equal components, and crack growth calculations are carried out by using a short crack model to determine the probability of component fatigue failure. The algorithm has been implemented in a finite-element post-processor.

Keywords: Finite element analysis, fatigue crack growth, weight function, defect size distribution, probability of component fatigue failure.

NOTATION

A	defect size (random variable)
A_{crack}	defect area
a	defect size
a'	intrinsic crack length
a_0	scale parameter in the extreme value distribution
a_0^*	characteristic largest defect size
a_{crit}	critical defect size
a_{f}	final defect size
a_{i}	initial defect size
a_{th}	peak over threshold defect size
C	coefficient in crack growth law
c	half the surface crack length
F	geometry factor
FEA	finite element analysis
$G(a)$	generalised extreme value distribution
g	weight function
$H(a)$	generalised Pareto distribution
$\|\mathbf{J}\|$	Jacobian determinant
K	stress intensity factor
K_{Ic}	fracture toughness
K_{t}	stress concentration factor $= \sigma_{\max}/S_{\text{net}}$
ΔK_{th}	threshold stress intensity factor range
L	distance from a given point to the free surface
m	exponent in crack growth law
n	number of cycles
$\mathbf{N}$	element shape functions
N_{els}	number of elements
N_{Gauss}	number of Gauss points in one of the coordinate directions
N_{nodes}	number of nodes
$N_{\text{nodes,el}}$	number of nodes per element
$\mathbf{n}_1$	eigenvector associated with the maximum principal stress
$\mathbf{n}_{\text{f}}$	element face normal
P_{s}	probability of survival
R	stress ratio $= \sigma_{\min}/\sigma_{\max}$
$\mathbf{R}$	orthogonal rotation matrix
$\mathbf{S}$	translation vector
S_{net}	net-section stress
$\mathbf{T}$	transformation matrix
V	volume
ΔV	element volume
W_i	weight factor of the i^{th} Gauss point
x, y, z	global coordinate system
x', y', z'	transformed coordinate system
z_1	number of critical defects per unit volume
$\Delta\sigma$	stress range $= \sigma_{\max} - \sigma_{\min}$
σ_{a}	(equivalent) stress amplitude
σ_{A}	fatigue limit
σ_{m}	(equivalent) mean stress
$\sigma_{\max}$	maximum stress
$\sigma_{\min}$	minimum stress
σ_{n}	stress normal to the crack plane
σ_{ij}	operating stress tensor
σ_{ij}^0	residual stress tensor
ξ, η, ζ	non-dimensional parent element coordinates
ξ'	shape parameter in the extreme value distribution

*Corresponding author: Department of Engineering Design and Materials, Norwegian University of Science and Technology, Richard Birkelandsvei 2B, Trondheim, NO-7491 , Norway; email: anders.wormsen@ntnu.no

1 Introduction

At a time when the industry is continuously challenged to come up with better and less costly products, and this in ever shorter cycles, all product development processes must be improved, including fatigue design. In order to comply with this development, it is the authors' conviction that standard fatigue analysis tools should reflect that fatigue is caused by the (random) growth of fatigue cracks from randomly distributed defects. Unfortunately, this is bound to make the fatigue design process much more complex. Hence, a robust fatigue assessment tool, directly applicable to the results from a standard finite element stress analysis, would be of great importance in the process of developing optimised, safe and reliable structural components.

As shown in Table 1, there is a variety of approaches to the fatigue analysis of a mechanical component, all basically related to fatigue crack propagation. The initiation based approaches use conventional $S-N$-data as a starting point, and the fatigue life, N, is usually defined as the number of load cycles required for a macroscopic crack to develop. The propagation based approaches consider the actual growth of a crack from an initial (defect) size a_{i} to a final size a_{f}.

Standard methods for fatigue life predictions are deterministic by nature, i.e., material properties including defect size are considered as predetermined quantities. Two of the most widespread deterministic fatigue assessment methods are:

- '*Local stress approach*' – Life prediction based on the equivalence between the most highly stressed point of a component and a standard smooth fatigue specimen under the same stress.

- '*Single defect approach*' – Life prediction based on the growth of a single 'worst-case' crack-like defect at the location of maximum stress.

The probabilistic approaches, on the other hand, assume material properties to be randomly distributed:

- '*Weakest-link approach*' – Assumes the probability of survival of a component to be the product of the probabilities of survival of the (small) elements into which the component has been divided for purposes of analysis. The probability of survival of an element is a function of the stress cycle, the characteristic fatigue strength and the size of the element.

- '*Random defect approach*' – The model is based on a finite element stress analysis and assumptions on the defect distribution as well as a theory for the growth of short cracks. Each finite element is associated with one or more defects by 'drawing' from a Poisson distribution. The initial posistion of a defect is obtained from a uniform distribution while its size is obtained from an extreme value distribution. The defects are considered to be crack-like, and the number of cycles required for each defect to become critical is determined. By carrying out a large number of such simulations, the fatigue life distribution of the component is obtained.

When a commerically available finite element code such as ABAQUS is used for performing a crack growth analysis, the crack is explicitly modelled as an integrated part of the component. For each crack growth increment, the mesh surrounding the crack has to be remeshed. Re-meshing techniques applied to crack growth problems have been treated in several papers, e.g. [**1**–**3**]. Examples of codes that have implemented re-meshing techniques for handling crack growth analysis of 3D components are FRANC3D [**4**], BEASY [**5**] (both use the boundary element method) and ADAPCRACK3D [**6,7**] (uses the finite element method). In order to reduce the time required for performing a crack growth analysis, the component geometry is often simplified so that a standard handbook solution can be used for performing a fatigue life prediction. Such handbook solutions are available in the programs NASGRO [**8**] and AFGROW [**9**]. Another approach is to perform the crack growth analysis by assuming a homogeneous stress field based on the maximum stress acting on the component surface. This maximum stress approach yields acceptable results provided that the stress decreases slowly, i.e., the stress gradient is low, and when the geometrical simplification can be justified. An alternative is to use results from a standard finite element stress analysis and account for a crack by using weight functions [**10, 11**]. This approach has been implemented in the stand-alone finite-element post-processor P•FAT. By 'drawing' the number, size and position of crack-like defects from distribution functions and repating this process for a large number of nominally equal components ('Monte Carlo' simulation), the fatigue life distribution of the component could be obtained. With this, one has a post-processing tool that can estimate the probability of component failure by means of fatigue crack growth calculations. The application of this feature should be of considerable interest in assessing the influence of defects on the reliability of cast components.

The finite-element post-processor also supports the local stress approach and the weakest-link approach [**12**–**14**]. The post-processor can perform fatigue crack growth calculations of embedded cracks and surface cracks, see Fig. 1. The code strictly handles only homogeneous mechanical properties. Piecewise homogeneous 'quality zones' may be taken into account in the process of generating defects, i.e., number, position and size. In addition, the proposed method is presently restricted to proportional loading.

Table 1: Different approaches to fatigue analysis, all related to fatigue crack growth.

Approaches to fatigue analysis	Deterministic	Probabilistic
Initiation based	Local Stress	Weakest Link
Propagation based	Single Defect	Random Defect

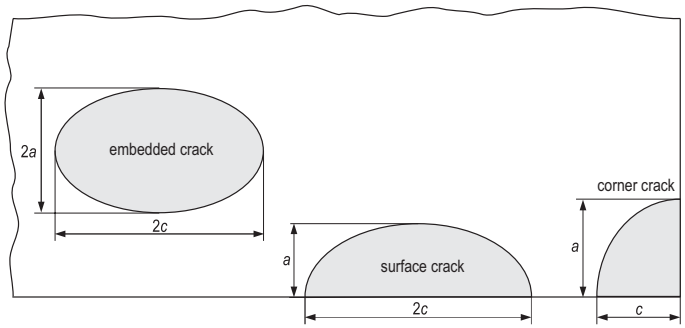

Figure 1: Crack configurations implemented in the finite-element post-processor.

The paper is organised as follows. In Section 2, the principal features of the finite-element post-processor are given. Section 3 addresses the basic numerical codes needed, and in Section 4 it is shown how crack-like defects are propagated. Section 5 describes how defects are generated, and in Section 6 a flow-chart of the random defect module is given. Finally, some conclusions are drawn in Section 7.

2 Principal features of P•FAT

P•FAT is designed as a stand-alone finite-element post-processor with the component geometry and stresses given by a standard finite element program. Data needed for the computation are nodal coordinates, element topology and stresses. In addition to operating stresses, process-related residual stresses can be taken into account. Such residual stresses may be imported directly from, e.g., casting or welding simulations. The surface elements are found automatically and are used for defining the geometry of the component.

In the propagation based approaches, the initial crack-like defect is regarded as an embedded crack, or as a surface crack, depending on the location of the crack front relative to the free surface. A crack is treated as a corner crack, if it starts from or propagates into a right-angled corner.

Failure of a component occurs, when the crack has reached a predefined size, or the stress intensity factor K has reached the fracture toughness K_{Ic}. When a surface crack breaks the opposing free surface, it has to be treated as a through-crack. This may be a most relevant situation, e.g., for a crack growing through a thin plate. On the other hand, for initial defects that are much smaller than the thickness of the plate, a through-crack is only present during a small fraction of the component life. Thus, instead of explicitly modelling the through-crack, crack growth is terminated as soon as the surface crack breaks the opposing free surface.

P•FAT is compatible with standard finite element codes such as ABAQUS, ANSYS and NASTRAN. It is written in standard FORTRAN and can be operated under Windows and UNIX/LINUX.

3 Post-processing of finite element stress analysis

3.1 Multiaxial stress criterion

The fatigue crack growth is assumed to be controlled by the normal stress cycle on the plane perpendicular to the direction of the maximum principal stress at the crack origin. Thus, the stress amplitude, σ_{a}, at an arbitrary point on the crack plane is calculated according to

$$\sigma_{\mathrm{a}} = \sigma_{\mathrm{n,a}} = n_{1i}\sigma_{ij,\mathrm{a}}n_{1j},\ i,j = 1,2,3, \qquad (1)$$

and the mean stress, σ_{m}, by

$$\sigma_{\mathrm{m}} = \sigma_{\mathrm{n,m}} = n_{1i}(\sigma_{ij,\mathrm{m}} + \sigma^{0}_{ij})n_{1j}. \qquad (2)$$

$\mathbf{n}_1$ is the unit eigenvector of the maximum principal operating stress, and σ^0_{ij} denotes the residual stress tensor.

Generally, the direction of maximum principal stress in the uncracked component changes as the crack grows on a specific plane. In the present work, the change of the crack growth direction is neglected. Generally, this can be justified as long as the crack is small compared with the dimension of the component, i.e., for a large fraction of the fatigue life.

3.2 Numerical formulation

Consider now a defect located in an arbitrary elastic body subject to the combined operating and residual stress field $\sigma_{ij}(\mathbf{x})$. The origin of the crack-like defect is given by the reference point $\mathbf{x}_0 = [x_0, y_0, z_0]^{\mathrm{T}}$. A local coordinate system, $\mathbf{x}'$, is attached to the crack origin, $\mathbf{x}_0$, as shown in Fig. 2. The local coordinate system is defined by means of the transformation matrix

$$\mathbf{T} = [\mathbf{R}\ \mathbf{S}] = \begin{bmatrix} R_{11} & R_{12} & R_{13} & x_0 \\ R_{21} & R_{22} & R_{23} & y_0 \\ R_{31} & R_{32} & R_{33} & z_0 \end{bmatrix}, \qquad (3)$$

where $\mathbf{R}$ is a 3×3 orthogonal matrix, known as the rotation matrix, defining the orientation of the local coordinate system. $\mathbf{S}$ is a 3×1 translation vector defining the origin of the coordinate system. Vectors given in the local coordinate system are marked with a prime ($'$). The rotation matrix is given by the vectors $\mathbf{n}_2$, $\mathbf{n}_3$, and $\mathbf{n}_1$, respectively, as

$$\mathbf{R} = [\mathbf{n}_2\ \mathbf{n}_3\ \mathbf{n}_1], \qquad (4)$$

where $\mathbf{n}_1$ is perpendicular to the crack surface and is equal to the eigenvector associated with the maximum principal stress. The $\mathbf{n}_3$ vector is determined as the vector that gives the shortest length, L, between a free surface point and the crack origin, see Fig. 2. $\mathbf{n}_2$ is perpendicular to $\mathbf{n}_3$ and $\mathbf{n}_1$. Since $\mathbf{R}$ is an orthogonal matrix, i.e., $\mathbf{R^{-1}} = \mathbf{R}^{\mathrm{T}}$, the transformation from global to local coordinates, is given by

$$\mathbf{x}' = \mathbf{R}^{\mathrm{T}}\mathbf{x} - \mathbf{R}^{\mathrm{T}}\mathbf{S}. \qquad (5)$$

To obtain the stress intensity factor, K, the crack surface is automatically meshed with plane isoparametric elements in the post-processor. The stress amplitude normal to the crack plane, σ_{a}, can be found when the corresponding parent global element coordinates, $\boldsymbol{\xi} = [\xi, \eta, \zeta]^{\mathrm{T}}$, and the element number in the un-cracked component is known. The latter is found by first performing a transformation from $\boldsymbol{\xi}'$ to $\mathbf{x}'$. $\boldsymbol{\xi}'$ is the parent element coordinates for the crack elements. With an isoparametric description of the crack geometry, the transformation is given by

$$\mathbf{x}' = \mathbf{N}(\boldsymbol{\xi}')\mathbf{x}'_{\mathrm{nodes}}, \qquad (6)$$

where $\mathbf{N}$ is the element shape function matrix and $\mathbf{x}'_{\mathrm{nodes}}$ is the local coordinates of the nodes in the crack element mesh. The corresponding global point $\mathbf{x}$ is found according to

$$\mathbf{x} = \mathbf{R}\mathbf{x}' + \mathbf{S}. \qquad (7)$$

The point $\mathbf{x}$ is within an element if the following condition is satisfied for all element faces

$$\mathbf{n}_{\mathrm{f}} \cdot \mathbf{v} \geq 0,\ \mathbf{v} = \mathbf{x}_{\mathrm{s}} - \mathbf{x}, \qquad (8)$$

where $\mathbf{n}_{\mathrm{f}}$ denotes the surface normal at the point $\mathbf{x}_{\mathrm{s}}$, see Fig. 3.

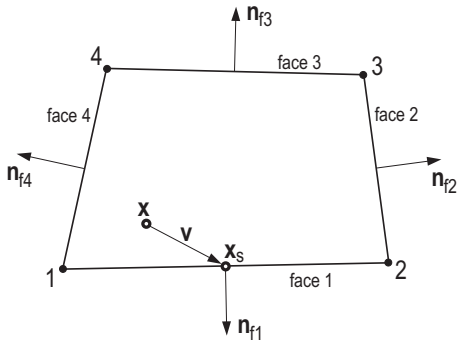

Figure 3: A point $\mathbf{x}$ within an element and definition of the element face normal $\mathbf{n}_{\mathrm{f}}$ (a plane four-noded element is used for illustration).

The parent global element coordinates, $\boldsymbol{\xi}$, are obtained by using a Newton-Kantorovich iteration algorithm. This algorithm computes a solution of

$$\mathbf{f}(\boldsymbol{\xi}) = \mathbf{x} - \mathbf{N}\mathbf{x}_{\mathrm{nodes}} = \mathbf{0}, \qquad (9)$$

given an initial approximation $\boldsymbol{\xi}^{(0)}$ (starting value of the iteration). It is appropriate to use $\boldsymbol{\xi}^{(0)} = \mathbf{0}$ as a starting value, i.e., the center of the element. For the initial guess, one has the Taylor series with remainder in the form

$$\mathbf{f}(\boldsymbol{\xi}) = \mathbf{f}(\boldsymbol{\xi}^{(0)}) + \mathbf{f}'(\boldsymbol{\xi}^{(0)})(\boldsymbol{\xi} - \boldsymbol{\xi}^{(0)}) + \mathbf{R}(\boldsymbol{\xi}). \qquad (10)$$

If one omits the remainder term $\mathbf{R}(\boldsymbol{\xi})$, then

$$\mathbf{f}(\boldsymbol{\xi}^{(0)}) + \mathbf{f}'(\boldsymbol{\xi}^{(0)})(\boldsymbol{\xi} - \boldsymbol{\xi}^{(0)}) = \mathbf{0}. \qquad (11)$$

Hence, one could form the iterative sequence of approximations as

$$\boldsymbol{\xi}^{(k+1)} = \boldsymbol{\xi}^{(k)} - \mathbf{f}'^{(k)}(\boldsymbol{\xi}^{(k)})^{-1}\mathbf{f}(\boldsymbol{\xi}^{(k)}),\ k = 0, 1, \ldots, \qquad (12)$$

where

$$f'_{ij} = -\left(\frac{\partial \mathbf{N}}{\partial \boldsymbol{\xi}_j}\right)\mathbf{x}_{\mathrm{nodes},i},\ i, j = 1, 2, 3. \qquad (13)$$

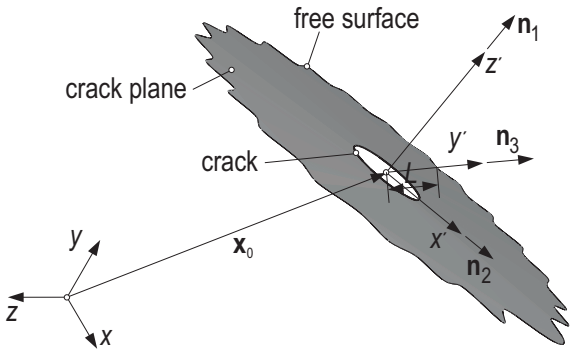

Figure 2: Definition of the crack plane and the local coordinate system $\mathbf{x}'$.

The iteration is continued until the condition

$$|\boldsymbol{\xi}^{(k+1)} - \boldsymbol{\xi}^{(k)}| \leq \epsilon, \tag{14}$$

is satisfied with the desired accuracy ϵ.

The stress amplitude normal to the crack plane, σ_{a}, at a given position $\mathbf{x}$, can then be found as **[15]**

$$\sigma_{\mathrm{a}} = \sum_{i=1}^{N_{\mathrm{nodes,el}}} N_i(\boldsymbol{\xi})\sigma_{\mathrm{a}i}, \tag{15}$$

where the index i ranges over the number of nodes in the element and N_i is the i^{th} element of the element shape function.

Since the influence of a free surface is included in the calculation of the stress intensity factor K, the surface elements of the component must be identified. A free element surface is characterised by a unique combination of face nodes.

When the component surface is identified the distance, L, from the point $\mathbf{x}$ to the free surface in a direction $\mathbf{e}$ (unit vector) can be calculated, cf. Fig. 4. However, before L can be found the element surface which $\mathbf{e}$ passes through must be identified. The vector $\mathbf{e}$ passes through a free element surface, if and only if,

$$\mathbf{n}_{\mathrm{sf}} \cdot \mathbf{e} \leq 0, \tag{16}$$

for all spanned faces, see Fig. 4. Here, $\mathbf{n}_{\mathrm{sf}}$ is the spanned face normal as shown in Fig. 4. The distance, L, between $\mathbf{x}$ and an unknown point $\mathbf{x}_{\mathrm{s}}$ [see Fig. 4] located on the element surface is found according to

$$L = \frac{(\mathbf{x}_{\mathrm{node}} - \mathbf{x}) \cdot \mathbf{n}_{\mathrm{f}}}{\mathbf{e} \cdot \mathbf{n}_{\mathrm{f}}} = \frac{|\mathbf{x}_{\mathrm{node}} - \mathbf{x}| \cos\alpha}{\cos\theta}. \tag{17}$$

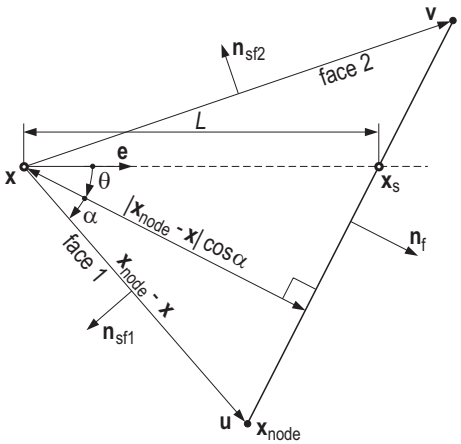

Figure 4: Graphical illustration of the distance L between the point $\mathbf{x}$ and a free element face with face normal $\mathbf{n}_{\mathrm{f}}$.

4 Crack growth approach

In the propagation based modules, the fatigue life is obtained by summing up the number of cycles necessary to propagate an initial crack-like defect to a user defined

critical state. For the fatigue life to be properly calculated, the crack growth law should take the behaviour of short cracks into account [**16, 17**]. In the next Subsection, the crack growth law is presented, followed by a short description of the crack growth increment procedure. Finally, it is shown how the stress intensity factor, K, is calculated using the stress field from the un-cracked component.

4.1 Crack growth law

El Haddad et al. [**18**] defined the 'effective' crack length as the sum of the actual crack length and an intrinsic crack length. By using this effective crack length in conjunction with the fatigue crack growth law by Klesnil and Lukáš [**19**], Fjeldstad et al. [**20**] derived the following equation for the growth rate of short fatigue cracks:

$$\frac{\mathrm{d}a}{\mathrm{d}n} = C\Delta K_{\mathrm{th}}^{m}\left[\left\{\left(\frac{\Delta\sigma}{\Delta\sigma_{\mathrm{A}}}\right)^{2}+\left(\frac{\Delta K}{\Delta K_{\mathrm{th}}}\right)^{2}\right\}^{\frac{m}{2}}-1\right]. \tag{18}$$

In equation (18), $\Delta\sigma_{\mathrm{A}}$ is the fatigue limit of a smooth, polished fatigue specimen without (major) defects, $\Delta\sigma$ is the stress range normal to the crack plane and ΔK_{th} is the threshold stress intensity range.

The constant C of the crack growth law, the fatigue limit and the threshold stress intensity range can all be transformed to the present R-ratio by using Walker's equation [**21**] as shown in [**22**]. The exponent m of the crack growth law generally varies only weakly with R [**22**] and can be assumed to be constant.

4.2 Determination of crack growth increments

By rearranging equation (18), the fatigue life, n, is obtained by means of numerical integration with an adaptive crack increment control. The maximum allowable crack increment is controlled in such a way that the aspect ratio a/c cannot change more than, say, 2% for each incremental step. The increment is denoted by $\delta(\mathrm{A})$ and represents the growth of the point A on the crack front (see Figs. 5(a) and 8(b)). By using $\delta(\mathrm{A})$ as a starting point, the incremental growth, $\delta(\mathrm{P})$, for an arbirary point P along the crack front is estimated according to

$$\delta(\mathrm{P}) = \delta(\mathrm{A})\left(\frac{\Delta K(\mathrm{P})}{\Delta K(\mathrm{A})}\right)^{m}. \tag{19}$$

4.3 Stress intensity factor

The prediction of crack behaviour has always been a challenge for researchers, and crack propagation represents a real concern among engineers. In linear elastic crack mechanics, the stress intensity factor, K, is the main parameter to seek. In this Subsection, a method for numerical determination of stress intensity factors in three-dimensional geometries will be given and verified. The method is based on the theory of weight functions, which computes the required stress intensity factor based on the stress field of the crack-free component. The use of weight functions in crack mechanics was first proposed by Bueckner [**10**] and subsequently generalised by Rice [**11**]. The reader is referred to the above references for a detailed discussion on the theoretical aspects of the method.

Consider now a two-dimensional crack located in an arbitrary elastic body subjected to the combined operating and residual stress field $\sigma_{ij}(\mathbf{x})$. The crack is assumed to grow in a direction perpendicular to the direction of the maximum principal stress determined at the crack origin $\mathbf{x}_0$, cf. Fig. 2. A local coordinate system $\mathbf{x}'$ is introduced at $\mathbf{x}_0$, see Fig. 2. The transformation from global to local coordinates is given by equation (5). The weight function, $g(x', y'; \mathrm{P})$, is defined as the stress intensity factor value at the crack front point P, when a pair of symmetrical unit opening forces are applied at an arbitrary point P′ on the crack surface, cf. Fig. 5(a). In the case of a distributed symmetrical loading on the crack surface, the stress intensity factor K is obtained by integrating the product of the weight function $g(x', y'; \mathrm{P})$ and the stress distribution of the crack free solid $\sigma_{\mathrm{a}}(x', y')$ over the crack surface area A_{crack}:

$$K(\mathrm{P}) = \int_{A_{\mathrm{crack}}} \sigma_{\mathrm{a}}(x', y')g(x', y'; \mathrm{P})\,\mathrm{d}A_{\mathrm{crack}}. \tag{20}$$

The relationship between the weight function and the displacement field is given in [**11**].

The integral in equation (20) can be solved numerically for instance by Gauss-Legendre quadrature. This procedure subdivides the crack surface into N_{els} plane elements with N_{nodes} nodes. By virtue of the property of definite integrals, the stress intensity factor is obtained by performing a summation over all elements on the crack surface:

$$K \approx \sum_{k=1}^{N_{\mathrm{els}}}\Big(\sum_{i=1}^{N_{\mathrm{Gauss}}}\sum_{j=1}^{N_{\mathrm{Gauss}}}\sigma_{\mathrm{a}}(\xi_i', \eta_j')g(\xi_i', \eta_j'; P')\times |\mathbf{J}(\xi_i', \eta_{\mathbf{j}}')|\, W_i\, W_j\Big). \tag{21}$$

Here, $|\mathbf{J}|$ is the determinant of the Jacobian maxtrix and (ξ', η') the corresponding non-dimensional parent crack element coordinates at the Gauss points. W_i is the weight factor of the i^{th} Gauss point and N_{Gauss} is the number of Gauss points in each coordinate direction.

4.3.1 *Embedded crack*

For an infinite body with an embedded crack under distributed loading perpendicular to the plane of the crack,

the weight function is given by **[23]**

$$g(x', y'; P') = \frac{\sqrt{2s}}{\pi^{3/2}\rho^2}\sqrt{1 - \frac{s}{8\rho_1} - \frac{s}{8\rho_2} - \frac{s}{8\rho_3} - \frac{s}{8\rho_4}}, \tag{22}$$

where s is the shortest distance between the point P′ and the crack front, and ρ is the distance between P and P′, see Fig. 5(a). ρ_1 to ρ_4 are parameters depending on the shape of the crack **[23]**.

To obtain the stress intensity factor, the crack surface is meshed with plane elements as shown in Fig. 5(b). K is calculated numerically by using equation (21). The mesh density and size are adjusted according to the local value of the weight function. Since the weight function becomes singular when P′ approaches P, a fine mesh is used around P. Fig. 5(b) illustrates a typical finite element mesh used. In order to obtain a proper description of the growth of an embedded crack, K is calculated at four locations, i.e., points A, B, C and D [see Fig. 5(a)], at the crack front.

The K solution proposed by Wang et al. **[23]** holds for an embedded elliptical crack located in an infinite body. In order to take into account the free surface effect on K, an empirical 'stress intensity magnification factor' proposed by Fett and Mattheck **[24]** is used. The magnification factor is multiplied with the weight function based K solution. The stress intensity magnification factor depends on the distance, L, from the crack center to the free surface and the aspect ratio a/c, cf. Fig. 6.

In Fig. 6(a), geometry factors F [see equation (24)] at four locations on the crack front of an embedded crack have been plotted against the aspect ratio, a/c. The crack is located in an infinite body and the crack surface is subjected to the stress field

$$\sigma_{\mathrm{a}}(y') = \sigma_0 \left(\frac{y'}{a}\right)^i. \tag{23}$$

The geometry factor F is defined as

$$F = \frac{K}{\sigma_0\sqrt{\pi a}}. \tag{24}$$

The solid and dotted lines are obtained by using the weight function given in equation (22). Along with these solutions, analytical results presented by Green and Sneddon **[25]** ($i = 0$) and Shah and Kobayashi **[26]**($i = 1, 2$) are shown as single points. As can be seen, the weight function based F values are in good overall agreement with the analytical predictions, with a maximum deviation of less than 4%. Fig. 6(b) shows the geometry factor at the same four locations, but now plotted against a/L. The weight function based F values, shown as solid lines, are obtained for a crack with aspect ratio $a/c = 0.5$ and subjected to a uniform stress field, i.e., $i = 0$. Results presented by Noguchi et al. **[27]** are shown as squares. For $a/L = 0$, the geometry factor solution corresponds to an embedded crack located in an infinite body. As a/L increases, the influence of the free surface leads to higher F values. The weight function based F values are in good agreement with the results presented by Noguchi et al., with a maximum deviation of less than 4% when $a/L \leq 0.9$.

When the embedded elliptical crack shown in Fig. 7 reaches the free surface, there follows a relatively rapid crack extension through the cusp-shaped ligaments on each side of the point of break-through **[28]**. After this transitory phase, the depth of the surface crack $\approx 2a$, and the curvature at the deepest point of the crack is nearly the same as that of the embedded crack. If the shape of the surface crack is to remain semi-elliptic, its semi-width $\approx \sqrt{2}c$, i.e., it is about 40% wider than the crack before break-through. However, in order to compensate for the 'missing' cycles of the transitory phase, the 'effective' semi-elliptic surface crack is assumed to be somewhat smaller and to have the same area as the embedded crack, as shown in Fig. 7.

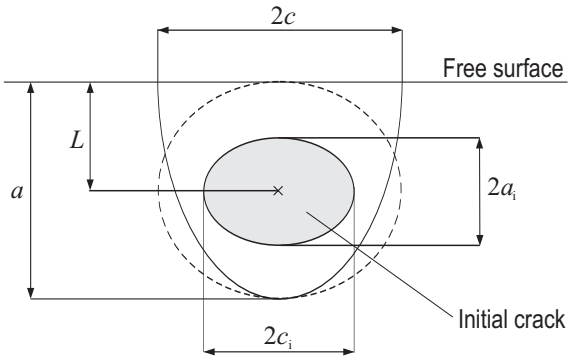

Figure 7: Sketch of a near surface crack and how it is assumed to unfold to a surface crack.

4.3.2 *Surface crack*

For a semi-elliptical surface crack growing in an arbitrary component, the crack will in many cases propagate along an uneven surface. Hence, the local coordinate system of the crack must be updated for each crack growth increment. The initial coordinate system is denoted by $\mathbf{x}'_{\mathrm{s}}$, see Fig. 8(a). The semi-elliptical crack is growing perpendicularly to the maximum principal stress. The updated coordinate system is denoted by $\mathbf{x}''_{\mathrm{s}}$, as shown in Fig. 8(a). The updated coordinate system is determined by the two points where the crack front and the free surface intersect. The updated coordinate system is rotated until the x''_{s}-axis is parallel with the line between the two surface points, see Fig. 8(a). These are found by stepwise moving along the crack front until the points are found to be outside the

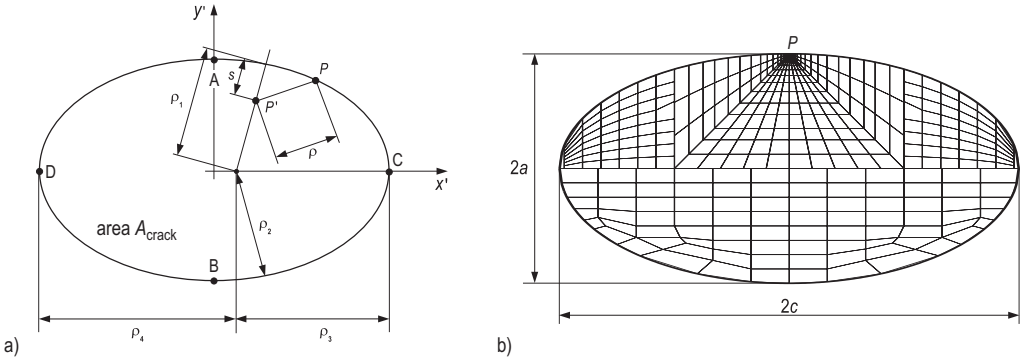

Figure 5: (a) Schematic drawing of an embedded elliptical crack and definition of parameters for obtaining the stress intensity factor. (b) Typical finite element mesh used for an embedded elliptical crack.

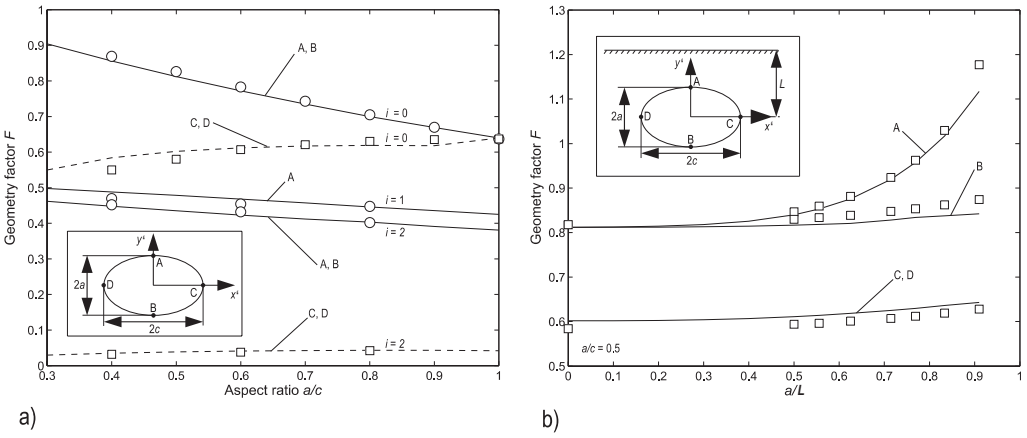

Figure 6: Geometry factors for an embedded crack (a) in an infinite body and (b) in a semi-infinite body. In (b) the aspect ratio $a/c = 0.5$.

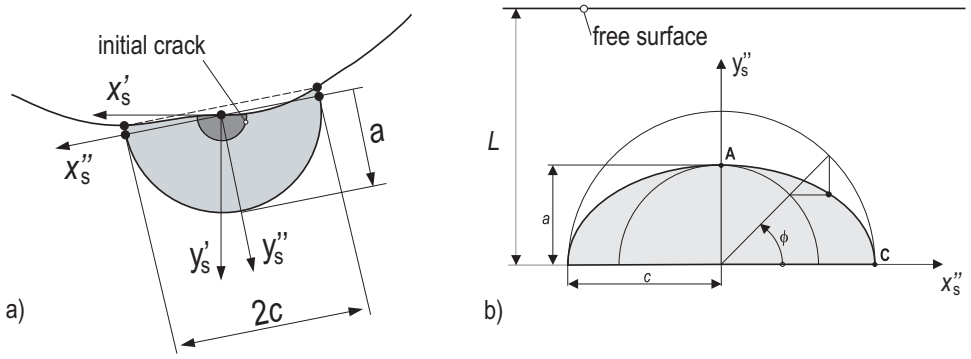

Figure 8: (a) Definition of the crack coordinate system and (b) a two dimensional view of a semi-elliptical crack.

component geometry, followed by an iterative process in order to determine the points more accurately.

For an arbitrary body with a semi-elliptic surface crack of depth a and aspect ratio a/c (cf. Fig. 8(b)) under a loading, σ_{a}, perpendicular to the crack surface, the weight function at the deepest point of the crack front $\mathrm{A}(a;0)$ is given by

$$g_{\mathrm{A}}(y_{\mathrm{s}}'';a/c) = \frac{2\,(1+f_{\mathrm{A}}(y_{\mathrm{s}}'',a/c,a/L))}{\sqrt{2\pi(a-y_{\mathrm{s}}'')}}. \qquad (25)$$

The function $f_{\mathrm{A}}(y_{\mathrm{s}}'',a/c,a/L)$ is given in [**29**]. Similarly, at the intersection between the crack front and the free surface, $\mathrm{C}(0;c)$, the weight function is given by [**29**]

$$g_{\mathrm{C}}(y_{\mathrm{s}}'';a/c) = \frac{2\,(1+f_{\mathrm{C}}(y_{\mathrm{s}}'',a/c,a/L))}{\sqrt{\pi y_{\mathrm{s}}''}}. \qquad (26)$$

The above weight function for the surface point C was established by Shen and Glinka [**29**] from a near surface point by means of the finite element method. The reason for this is that the stress singularity at the surface point is different from $1/\sqrt{r}$ and that the conventional stress intensity factor, therefore, does not apply at C. There is, however, only a small region in the vicinity of C, where the stress singularity is different from $1/\sqrt{r}$.

As can be seen from equations (25) and (26), the underlying weight function only considers the stress gradient in the depth direction of the crack. To obtain the stress intensity factor, K, the line from the crack origin to the deepest point of the crack is meshed with two noded line elements. The element length is progressively decreased towards the point where the weight function becomes singular. The numerical integration is performed according to equation (21).

Fig. 9(a) shows the geometry factor F_{A} for the deepest point, $\mathrm{A}(a;0)$ (cf. Fig. 8(b)), versus a/L when the crack surface is subjected to four different stress fields, see equation (23). The solid lines are obtained by using the weight function of equation (25). Along with weight function based F_{A} values, finite element results presented by Nilsson [**30**] are shown. As can be seen, the weight function based F_{A} values are in good overall agreement with the results presented by Nilsson, with a maximum difference of less than 4%. In Fig. 9(b), the corresponding geometry factors, F_{C}, for the crack surface point $\mathrm{C}(0;c)$ are shown. Also for the crack surface point, the agreement is found to be good.

5 Defect generation

Scatter plays an eminent role in the prediction of the fatigue life of a component. There are several possible sources for the scatter. It may be due to the random character of the loading. It may also be due to inaccuracies in how the loading is applied. Deviations from the nominal dimensions of the component cause scatter in the stresses. Lacking repeatability in the manufacturing conditions leads to variability of chemical composition, microstructure and mechanical properties. This includes fatigue limit and the crack growth rate of the material. Last, but not least, metal alloys contain metallurgical defects such as non-metallic inclusions and pores. Fatigue cracks are prone to initiate and grow from such defects. The present Section presents a methodology for generating the number, position and size of defects within a component.

5.1 Number and position of defects

There are two different approaches based on the statistics of extremes for estimating the size of the largest defect in a large volume of material. The first approach, called the *block maximum* method, uses the generalised extreme value distribution [**31**]. In this method, a polished cross-section is divided into k equally sized areas of size A_0 that are inspected for defects using optical microscopy [**32**]. Hence, the observation set consists of k measurements of maximum defect sizes, $a_{\mathrm{max1}},\ldots,a_{\mathrm{max}}$. The corresponding sizes in a volume V_0 can be estimated by using a stereological approximation as shown in [**33, 34**]. The expected number of defects per unit volume of the material is denoted by z_0. In the second approach, all defects with sizes above a certain (high) threshold, a_{th}, are considered. The differences between the defect sizes and the threshold, i.e., $a_i - a_{\mathrm{th}}$, are fitted to a generalised Pareto distribution [**31**]. This approach is therefore often called the *peak over threshold* method. The expected number of defects with sizes greater than a_{th} is denoted by $z_0(a_{\mathrm{th}})$.

The number of defects in a finite element of volume ΔV is obtained by 'drawing' from a Poisson distribution, i.e.,

$$\Pr(I=i) = \frac{[z_0\Delta V]^i}{i!}\exp[-z_0\Delta V],\ i\in\{0,1,2,\ldots\} \qquad (27)$$

where, I is the random number of defects. The element volume is calculated as

$$\Delta V = \sum_{i=1}^{N_{\mathrm{Gauss}}}\sum_{j=1}^{N_{\mathrm{Gauss}}}\sum_{k=1}^{N_{\mathrm{Gauss}}} |\mathbf{J}(\xi_i,\eta_j,\zeta_k)|\,W_i\,W_j\,W_k. \qquad (28)$$

It should be noted that the intrinsic property of a Poisson process is that the occurrence of a defect at a location $\mathbf{x}\in V$ neither encourages, nor inhibits, the occurrence of other defects in a neighborhood of $\mathbf{x}$, or in any other location, and that defects in separate volumes are mutually independent [**34**]. This assumption requires that the number of potentially life-controlling defects is small, a situation that occurs for stress cycles close to the fatigue limit (in the HCF regime) and for components with a low density of 'large' metallurgical defects.

When assigning the defect location, the parent element domain $\boldsymbol{\xi}$ is used. The location of a defect within

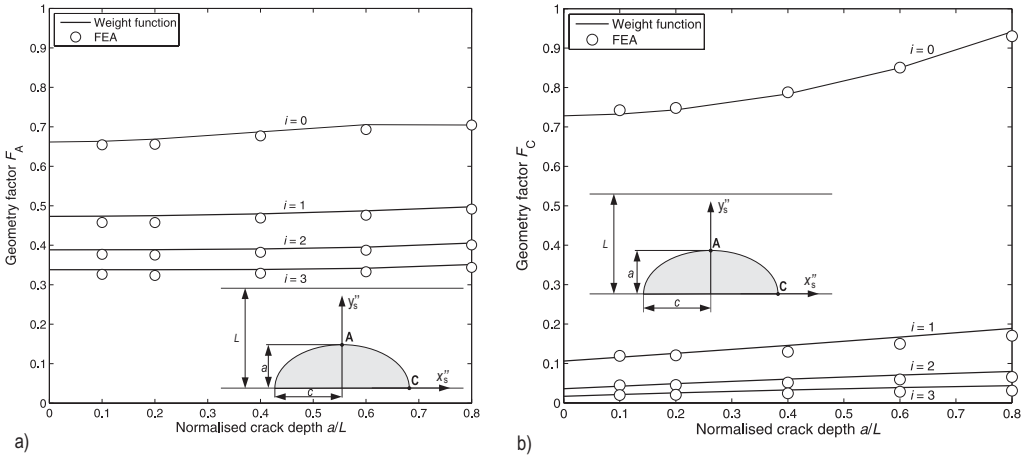

Figure 9: Geometry factors (a) F_{A} for the deepest point $\mathrm{A}(a;0)$ and (b) F_{C} for the surface point $\mathrm{C}(0;c)$ of a semi-elliptical crack with aspect ratio $a/c = 1$.

an element is obtained according to

$$\begin{bmatrix} \xi \\ \eta \\ \zeta \end{bmatrix} = 2 \begin{bmatrix} U_1(0,1) \\ U_2(0,1) \\ U_3(0,1) \end{bmatrix} - 1, \tag{29}$$

where U is a uniform random number between 0 and 1. Fig. 10 shows the position of randomly generated defects within a cube of volume 1000 mm^3.

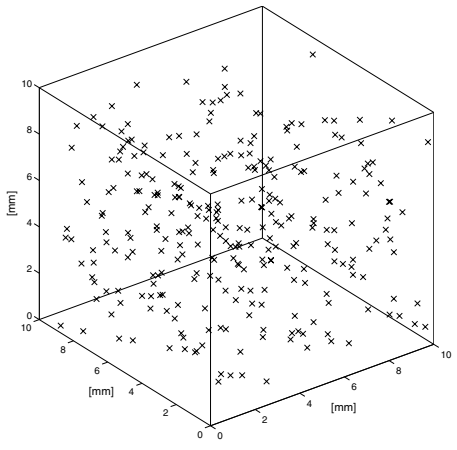

Figure 10: Example of generated number and position of defects within a 1000 mm^3 cube.

5.2 Defect size distributions

According to the generalised extreme value (GEV) distribution the probability that a defect of size $A_{\max} \leq a_{\max}$ is located within an element of volume ΔV is given by

$$\begin{aligned} G(a_{\max}) &= \Pr[A_{\max} \leq a_{\max}] \\ &= \exp\left\{ -\left[1 + \xi'\left(\frac{a_{\max} - a_0^*}{a_0}\right)\right]^{-1/\xi'} \frac{\Delta V}{V_0} \right\}, \end{aligned} \tag{30}$$

where $a_0 > 0$ denotes the scale parameter, a_0^* the location parameter and ξ' the shape parameter. The probability that a defect of size $A_{\max} \leq a_0^*$ is located within the control region V_0 equals $\exp(-1) \approx 36.8\%$. The location parameter, a_0^*, is therefore often called the characteristic largest defect size in volume V_0 **[34]**. The GEV distribution combines the Gumbel (Type I, $\xi' = 0$), Fréchet (Type II, $\xi' > 0$) and the reversed Weibull (Type III, $\xi' < 0$) distributions into a single distribution.

The Gumbel, Fréchet and reversed Weibull distributions have distinctly different forms of tail behaviour. When $\xi' < 0$, i.e., for the reversed Weibull distribution, the upper limit $a_{\max+} = a_0^* - a_0/\xi'$. Thus, the probability of finding defects $\geq a_{\max+}$ is zero. The Gumbel ($\xi' = 0$) and Fréchet ($\xi' > 0$) distributions have no upper limit.

When the peak over threshold method is used, all defects larger than a sufficiently high threshold a_{th} are measured either from a single inspection region or from k sub-regions. The observation set then consists of i measurements, $a_1, \ldots, a_i$. A generalised Pareto distri-

bution with distribution function **[31]**

$$H(a) = \Pr[A \leq a | A > a_{\text{th}}] = 1 - \left[1 + \xi' \left(\frac{a - a_{\text{th}}}{\tilde{a}_0}\right)\right]^{-1/\xi'}, \tag{31}$$

is fitted to the values $a_i - a_{\text{th}}$. The scale parameter $\tilde{a}_o$ is given by

$$\tilde{a}_0 = a_0 + \xi'(a_{\text{th}} - a_0^*), \tag{32}$$

where a_0, a_0^* and ξ' are equal to those in equation (30). The range of $a - a_{\text{th}}$ is $0 < a - a_{\text{th}} < \infty$ if $\xi' \geq 0$ and $0 < a - a_{\text{th}} < -\tilde{a}_0/\xi'$ if $\xi' < 0$. The generalised Pareto distribution was applied to defects in clean steels for the first time in **[35, 36]**.

The generated sample of defect sizes is converted into crack dimensions by first assuming that all generated defects are embedded circular cracks of radius c. If the drawn defect cuts the free surface of the component, the 'effective' surface crack is assumed to be semi-elliptic of width $2c$ and a depth a equal to the depth below the surface of the drawn defect.

5.3 Defect criterion and probability of fatigue failure

The Kitagawa-Takahashi diagram **[37]** clearly shows that the fatigue strength decrease with increasing crack size. In addition, there exists a critical crack size, a_{crit}, below which cracks are non-damaging. In the present work, the Kitagawa-Takahashi diagram **[37]** is used for finding out whether a crack is potentially damaging or not.

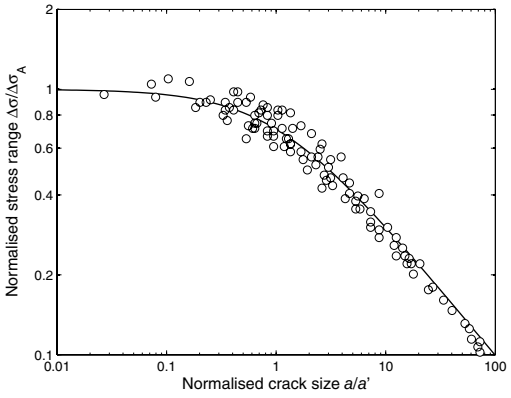

Figure 11: Kitagawa-Takahasi diagram with experimental data for both ferrous and nonferrous alloys gathered by Tanaka et al. **[38]** and Hertzberg **[39]**.

Consider now a small, homogeneously stressed volume element ΔV subjected to an equivalent stress amplitude σ_{a}. The smallest crack initiating failure in ΔV is denoted by a_{crit} and can be estimated according to **[37]**

$$a_{\text{crit}} = a' \left[\left(\frac{\Delta\sigma_{\text{A}}}{\Delta\sigma}\right)^2 - 1\right], \tag{33}$$

where the 'intrinsic' crack length is given by

$$a' = \left(\frac{\Delta K_{\text{th}} \Delta\sigma}{\Delta K \Delta\sigma_{\text{A}}}\right)^2 a. \tag{34}$$

Cracks with sizes less than a_{crit} are removed from the component. The expected number of remaning cracks per unit volume is denoted by z_1. The critical crack density, z_1, is defined as the expected number of cracks per unit volume of the material that yields a fatigue strength (random variable) $\sigma_{\text{A}} \leq \sigma_{\text{a}}$.

6 Flow-chart of the random defect module

In this Section a flow-chart of the random defect module is presented. The flow-chart is shown in Fig. 12. The flow-chart can be divided into three main parts: (i) input, (ii) defect generation and (iii) crack growth.

In the input part of the flow-chart, data needed for the computation are given. In the defect generation part, the number, size and position of the defects are generated. The number of critical defects, z_1, are subsequently determined by using a Kitagawa-Takahashi diagram, see Subsection 5.3.

In the crack growth part, all generated defects are initially embedded circular cracks of radius c. For defects cutting the free surface of the component, the 'effective' surface crack is assumed to be semi-elliptic of length $2c$ and a depth a, equal to the depth below the surface of the drawn defect. The location of the crack front relative to the free surface is determined for each crack growth increment. This enables one to determine when an embedded crack starts to grow as a surface crack and when a surface crack breaks the opposing free surface. Failure of a component occurs, when the crack has reached a predefined size a_{f}, or the stress intensity factor K has reached the fracture toughness K_{Ic}. The fatigue life of a single component is determined as the smallest computed life for all crack-like defects.

7 Conclusions

P•FAT is designed as a stand-alone finite-element post-processor with the component geometry and stresses given by a standard finite element program. Data needed for the computation are nodal coordinates, element topology and stresses. The surface elements are found automatically and are used for defining the geometry of the component.

The life-controlling defect is determined by means of the stress field and the initial crack growth rate. The

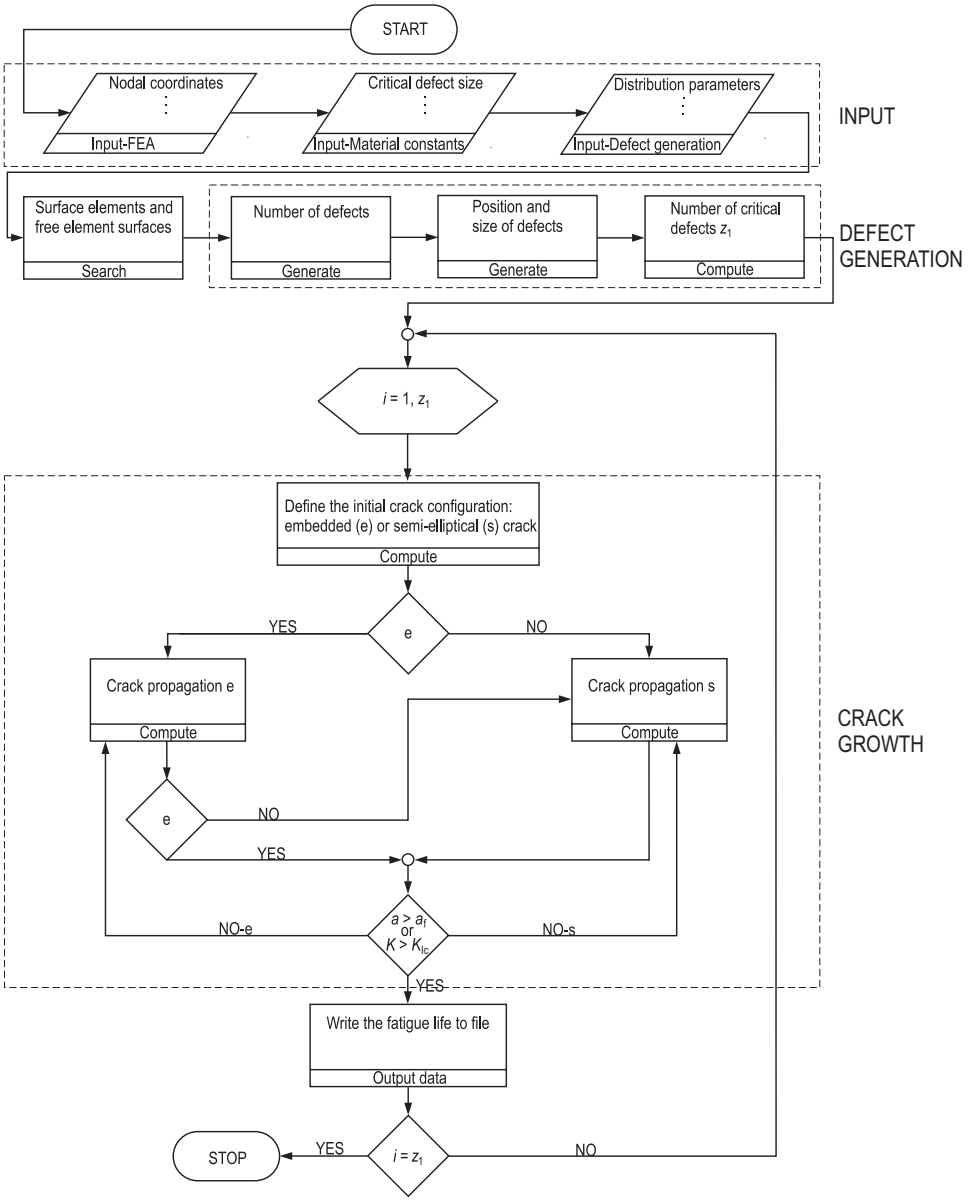

Figure 12: Flow-chart of the procedure for calculating the fatigue life of a single component.

number of defects in each finite element is obtained by 'drawing' from a Poisson distribution. The location of each defect in an element is found by drawing from a uniform distribution. The defect size is obtained by drawing from an extreme value distribution.

The life-controlling defect is then regarded as an embedded crack or as a surface crack. Fatigue life prediction is carried out using a short crack growth model. The defects are considered to be crack-like and to grow on the plane of maximum principal stress. Weight functions, together with the stress field of the crack-free component, are used to compute the required stress intensity factors. The crack surface is automatically meshed with plane elements with subsequent numerical integration (Gauss quadrature) for determining the stress intensity factor at several locations at the crack front. For each incremental step, this process repeats itself: the crack surface is re-meshed, and updated stress intensity factors for the current crack are obtained. The program also updates the location of the crack front relative to the free surfaces. Hence, if the crack grows through the component surface, the crack is regarded as a surface crack.

By repeating this process for a large number of nominally equal components (Monte Carlo simulation), the fatigue life distribution of the component is obtained. Thus, the designer will be able to estimate the probability of component fatigue failure.

Acknowledgments

The authors gratefully acknowledge the research support for this work provided by GE Energy (Norway) AS, the Research Council of Norway and the industrial participants within the NorLight project. The authors would like to express their gratitude to K. Holthe, O. I. Sivertsen, E. Berg and B. Skallerud for assistance and helpful discussions during the work presented herein.

References

[1] **Trädegård, A.**, **Nilsson, F.**, and **Östlund, S.** FEM-remeshing technique applied to crack growth problems. *Computer Methods in Applied Mechanics and Engineering*, 160(1-2):115–131, 1998.

[2] **Bouchard, P. O.**, **Bay, F.**, **Chastel, Y.**, and **Tovena, I.** Crack propagation modelling using an advanced remeshing technique. *Computer Methods in Applied Mechanics and Engineering*, 189(3):723–742, 2000.

[3] **Bouchard, P. O.**, **Bay, F.**, and **Chastel, Y.** Numerical modelling of crack propagation: automatic remeshing and comparison of different criteria. *Computer Methods in Applied Mechanics and Engineering*, 192(35-36):3887–3908, 2003.

[4] Cornell Fracture Group. *FRANC3D 2.6. Concepts and user guide*. Cornell University, Ithaca, New York, 2003.

[5] *BEASY User Guide, Computational Mechanics BEASY Ltd., 2001*, (Ashurst Lodge, Ashurst, Southampton, Hampshire, SO40 7AA, UK).

[6] **Schöllmann, M.**, **Fulland, M.**, and **Richard, H. A.** Development of a new software for adaptive crack growth simulations in 3D structures. *Engineering Fracture Mechanics*, 70(2):249–263, 2003.

[7] **Fulland, M.** and **Richard, H. A.** Application of the FE-method to the simulation of fatigue crack growth in real structures. *Steel Research*, 74(9):584–590, 2003.

[8] *NASA: Fatigue Crack Growth Computer Program 'NASGRO', version 3.0, 2000*, (Reference Manual, JSC-22267B, Engineering Directorate, National Aeronautics and Space Administration, Lyndon B. Johnson Space Center, Houston).

[9] *AFGROW Users Guide And Technical Manual. Air Vehicles Directorate, Air Force Laboratory, Wright-Patterson Air Force Base, Ohio.*

[10] **Bueckner, H. F.** A novel principle for the computation of stress intensity factors. *Z. Angewandte Math. Mech.*, 50:529–546, 1970.

[11] **Rice, J. R.** Some remarks on elastic crack-tip stress fields. *International Journal of Solids and Structures*, 8(6):751–758, 1972.

[12] **Wormsen, A.**, **Sjödin, B.**, **Härkegård, G.**, and **Fjeldstad, A.** Non-local stress approach for fatigue assessment based on weakest-link theory and statistics of extremes. Accepted for publication in Fatigue & Fracture of Engineering Materials & Structures, August 2007.

[13] **Wormsen, A.**, **Härkegård, G.**, and **Huth, H. J.** Probabilistic fatigue assessment of a hydroturbine blade model. In W. S. Johnson et al., editor, *Proceedings of the International Fatigue Congress 2006*, Atlanta, Georgia, USA, May 2006. Elsevier.

[14] **Wormsen, A.** and **Härkegård, G.** Weibull fatigue analysis of notched components under constant and variable amplitude loading. In W. S. Johnson et al., editor, *Proceedings of the International Fatigue Congress 2006*, Atlanta, Georgia, USA, May 2006. Elsevier.

[15] **Cook, R. D.**, **Malkus, D. S.**, **Plesha, M. E.**, and **Witt, R. J.** *Concepts and applications of finite element analysis*. John Wiley and Sons, Inc., 4th edition, 2002.

[16] **Miller, K. J.** The behaviour of short fatigue cracks and their initiation. Part 1 – A review of two recent books. *Fatigue of Engineering Materials*, 10(2):75–91, 1987.

[17] **Miller, K. J.** The behaviour of short fatigue cracks and their initiation. Part 2 – A general summary. *Fatigue of Engineering Materials*, 10(2):93–113, 1987.

[18] **El Haddad, M. H.**, **Smith, K. N.**, and **Topper, T. H.** Fatigue crack propagation of short cracks. *Journal of Engineering Materials Technology*, 101(1):42–46, 1979.

[19] **Klesnil, M** and **Lukáš, P.** Influence of strength and stress history on growth and stabilisation of fatigue cracks. *Engineering Fracture Mechanics*, 4(1):77–92, 1972.

[20] **Fjeldstad, A.**, **Wormsen, A.**, and **Härkegård, G.** Simulation of fatigue crack growth in components with random defects. *Engineering Fracture Mechanics*, doi:10.1016/j.engfracmech.2007.04.006, 2007.

[21] **Walker, K.** The effect of stress ratio during crack propagation and fatigue for 2024-T3 and 7075-T6 aluminum. In *Effects of Environment and Complex Load History on Fatigue Life*, pages 1–14. ASTM STP 462, Philadelphia, 1970.

[22] **Mann, T.** *Fatigue assessment methods for welded structures and their application to an aluminium T-joint*. PhD thesis, Norwegian University of Science and Technology, Trondheim, Norway, 2006.

[23] **Wang, X.**, **Lambert, S. B.**, and **Glinka, G.** Weight functions for embedded elliptical cracks. *Engineering Fracture Mechanics*, 59(3):381–392, 1998.

[24] **Fett, T.** and **Mattheck**. Stress intensity factors of embedded elliptical cracks for weight function applications. *International Journal of Fracture*, 40(1):R13–R18, 1989.

[25] **Green, A. E.** and **Sneddon, I. N.** The distribution of stress in the neighborhood of a flat elliptical crack in an elastic body. Cambridge Philosophical Society, 1950.

[26] **Shah, R. C.** and **Kobayashi, A. S.** Stress intensity factor for an elliptical crack under arbitrary normal loading. *Engineering Fracture Mechanics*, 3(1):71–93, 1971.

[27] **Noguchi, H.**, **Smith, R. A.**, **Carruthers, J. J.**, and **Gilchrist, M. D.** Stress intensity factors of embedded elliptical cracks and an assessment of the ASME XI defect recharacterisation criteria. *International Journal of Pressure Vessels & Piping*, 70(1):69–76, 1997.

[28] **Dai, D. N.**, **Nowell, D.**, and **Hills, D. A.** Eigenstrain methods in 3-D crack problems; an alternative integration procedure. *Journal of Mechanics and Physics of Solids and Structures*, 41(6):1003–1017, 1993.

[29] **Shen, G.** and **Glinka, G.** Weight functions for a semi-elliptical crack in a finite thickness plate. *Theoretical and Applied Fracture Mechanics*, 15(3):247–255, 1991.

[30] **Nilsson, L.** Stress intensity factors for semi-elliptical surface cracks in plates subjected to a complex stress field. SAQ/FoU-Report 98/10, SAQ KONTROLL AB, Stockholm, Sweden, 1998.

[31] **Coles, S.** *An introduction to statistical modeling of extreme values*. Springer series in statistics, London, 3rd edition, 2001.

[32] **Atkinson, H. V.** and **Shi, G.** Characterization of inclusions in clean steels: a review including the statistics of extreme methods. *Progress in Materials Science*, 48:457–520, 2003.

[33] **Anderson, C. W.** and **Coles, S. G.** The largest inclusions in a piece of steel. *Extremes*, 5:237–252, 2002.

[34] **Anderson, C. W.**, **de Maré, J.**, and **Rootzén, H.** Methods for estimating the sizes of large inclusions in clean steels. *Acta Materialia*, 53(8):2295–2304, 2005.

[35] **Shi, G.**, **Atkinson, H. V.**, **Sellars, C. M.**, and **Anderson, C. W.** Application of the generalized Pareto distribution to the estimation of the size of the maximum inclusion in clean steels. *Acta Materialia*, 47(5):1455–1468, 1999.

[36] **Shi, G.**, **Atkinson, H. V.**, **Sellars, C. M.**, and **Anderson, C. W.** Comparison of extreme value statistics methods for predicting maximum inclusion size in clean steel. *Ironmaking and Steelmaking*, 26(4):239–246, 1999.

[37] **Kitagawa, H.** and **Takahashi, S.** Applicability of fracture mechanics to very small cracks or the cracks in the early stage. In *Proceedings of the Second International Conference on the Mechanical Behavior of Materials*, pages 627–631, Boston, Ma., 1976.

[38] **Tanaka, K.**, **Nakai, Y.**, and **Yamashita, M.** Fatigue growth threshold of small cracks. *International Journal of Fracture*, 17(5):519–533, 1981.

[39] **Hertzberg, R. W.** *Deformation and Fracture Mechanics of Engineering Materials.* John Wiley & Sons, Inc., 4th edition, 1996.

Paper 7

ARTICLE IN PRESS

Available online at www.sciencedirect.com
ScienceDirect

Engineering Fracture Mechanics xxx (2007) xxx–xxx

Engineering Fracture Mechanics

www.elsevier.com/locate/engfracmech

Simulation of fatigue crack growth in components with random defects

A. Fjeldstad *, A. Wormsen, G. Härkegård

Norwegian University of Science and Technology, Richard Birkelandsvei 2B, NO-7491 Trondheim, Norway

Received 18 December 2006; received in revised form 22 March 2007; accepted 3 April 2007

Abstract

The paper presents a probabilistic method for the simulation of fatigue crack growth from crack-like defects in the combined operating and residual stress fields of an arbitrary component. The component geometry and stress distribution are taken from a standard finite element stress analysis. Number, size and location of crack-like defects are 'drawn' from probability distributions. The presented fatigue assessment methodology has been implemented in a newly developed finite-element post-processor, P • FAT, and is useful for the reliability assessment of fatigue critical components. General features of the finite element post-processor have been presented. Important features, such as (i) the determination of the life-controlling defect, (ii) growth of short and long cracks, (iii) fatigue strength and fatigue life distribution and (iv) probability of component fatigue failure, have been treated and discussed. Short and long crack growth measurements have been presented and used for verification of the crack growth model presented.

Keywords: Fatigue; Crack growth; Short crack; Probability of failure; Defect size distribution; Finite-element post-processor

1. Introduction

In terms of fatigue design, it is of ultimate importance that computer simulations undergoes the same improvements regarding accuracy and speed as all the other steps in a product development process. It is the authors' conviction that a standard fatigue analysis tool should reflect that fatigue is a probabilistic phenomenon caused by the (random) growth of small fatigue cracks from randomly distributed defects. Unfortunately, this is bound to make the fatigue design process much more complex. Hence, a robust fatigue assessment tool, directly applicable to the results from a standard finite element stress analysis, would be of great importance in the process of developing optimised, safe and reliable structural components.

* Corresponding author. Present address: Department of Engineering Design and Materials, Norwegian University of Science and Technology, Richard Birkelandsvei 2B, NO-7491 Trondheim, Norway.
E-mail address: Arne.Fjeldstad@ntnu.no (A. Fjeldstad).

0013-7944/$ - see front matter © 2007 Elsevier Ltd. All rights reserved.
doi:10.1016/j.engfracmech.2007.04.006

Nomenclature

A	defect size (random variable)
a	defect size
a'	intrinsic crack length
a_0	scale parameter in the extreme value distribution
a_0^*	characteristic largest defect size
a_{crit}	critical defect size
a_{th}	peak over threshold defect size
c	half the surface crack length
C	coefficient in crack growth law
d	notch depth
F	geometry factor
$G(a)$	generalised extreme value distribution
$H(a)$	generalised Pareto distribution
ΔK	stress intensity range
ΔK^*	stress intensity range associated with $R = 0$
ΔK_{eq}	equivalent stress intensity range
K_{Ic}	mode I fracture toughness
K_{t}	stress concentration factor $= \sigma_{\max}/S$
ΔK_{th}	threshold stress intensity range
m	exponent in crack growth law
N	fatigue life (random variable)
n	number of cycles
$\mathbf{n}_1$	unit eigenvector of the maximum principal stress
P_{f}	probability of failure
P_{s}	probability of survival $= 1 - P_{\text{f}}$
R	stress ratio
S	remote stress
S_{net}	net-section stress
t	thickness of plane specimen
V	volume
V_0	reference volume
w	width of plane specimen
z_1	critical defect density
γ	Walker exponent
ξ'	shape parameter in the extreme value distribution
ρ	notch radius
σ_1	maximum principal stress
σ_{a}	stress amplitude $= \Delta\sigma/2$
σ_{m}	mean stress
σ_{A}	fatigue strength (random variable)
σ_{A0}^*	characteristic fatigue strength
σ_{ij}	operating stress tensor
σ_{ij}^0	residual stress tensor

To comply with thise needs, a probabilistic fatigue assessment tool has been developed that is capable of predicting the fatigue life of a component. The prediction is based on the fatigue properties of the material and their scatter, and on the operating stresses from a finite element analysis of the component. The post-

Please cite this article in press as: Fjeldstad A et al., Simulation of fatigue crack growth in components with ..., Eng Fract Mech (2007), doi:10.1016/j.engfracmech.2007.04.006

processing of the stresses includes residual stresses, which may be imported directly from casting or welding simulations.

Scatter plays an eminent role in the prediction of the fatigue life of a component. There are several possible sources for the scatter. It may be due to the random character of the loading. It may also be due to inaccuracies in how the loading is applied. Deviations from the nominal dimensions of the component cause scatter in the stresses. Lacking repeatability in the manufacturing conditions leads to variability of chemical composition, microstructure and mechanical properties. This includes fatigue limit and the crack growth rate of the material. Last, but not least, metal alloys contain metallurgical defects such as non-metallic inclusions and pores. Fatigue cracks are prone to initiate and grow from such defects. The present work describes a methodology for simulating the scatter of the fatigue life based on the statistical distributions of defect density and defect size. Material parameters of the crack growth law may also be treated as random variables [1].

2. Finite-element post-processor

P • FAT is designed as a stand-alone, finite-element post-processor with the component geometry and stresses given by a standard finite element program. Data needed for the computation are nodal coordinates, element topology and stresses. It has been developed to perform predictions of crack growth in arbitrary three-dimensional components. It supports the simulation of both a single crack-like defect that can be inserted into the component at a desired location (*single defect module*) and randomly inserted crack-like defects (*random defect module*). The finite element post-processor uses a short crack model to determine the crack growth rate, see Section 3.1. The reader is referred to Ref. [1] for the numerical aspects of the crack-growth modules.

The number of defects in each finite element is obtained by 'drawing' from a Poisson distribution. The location of each defect in an element is obtained from a uniform distribution, and the defect size is obtained by 'drawing' from an extreme value distribution. The defects are considered to be crack-like, and the number of cycles required for a given defect to become critical is determined.

The crack-like defects are assumed to grow on the plane of maximum principal stress. Weight-functions [2], together with the stress field of the crack-free component, are used to compute the required stress intensity factors. Generally, the direction of maximum principal stress in the uncracked component changes as the crack grows on a specific plane. In the present work, the change of the crack growth direction is neglected. Generally, this is a good approximation as long as the crack is small compared with the dimensions of the component, i.e., for a large fraction of the fatigue life.

The crack surface is automatically meshed with plane elements. Subsequently, numerical integration (Gauss quadrature) is performed for determining the stress intensity factor at several locations at the crack front. For each incremental step, this process repeats itself: the crack surface is re-meshed, and updated stress intensity factors for the current crack are obtained. The program also updates the location of the crack front relative to the free surfaces. Hence, if the crack grows through the component surface, the crack is regarded as a surface crack or a corner crack, see Fig. 1. Failure of a component occurs when the crack has reached a predefined size, or if the stress intensity factor K has reached the fracture toughness K_{Ic}.

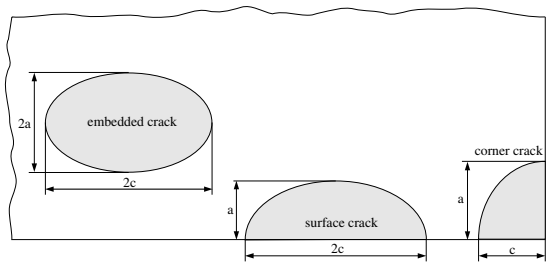

Fig. 1. Crack configurations implemented in the finite-element post-processor.

Please cite this article in press as: Fjeldstad A et al., Simulation of fatigue crack growth in components with ..., Eng Fract Mech (2007), doi:10.1016/j.engfracmech.2007.04.006

In the present investigation, the interaction between single cracks and the subsequent joining of these and the formation of a new, larger crack have been neglected. Thus, only one single, dominating crack is considered at a time. This assumption requires that the number of potentially life-controlling defects is small, a situation that occurs for stress cycles close to the fatigue limit (in the HCF regime) and for components with a low density of 'large' metallurgical defects. Future fatigue testing and simulation of components with known defect distributions should give a better understanding of the influence on fatigue life of the interaction between cracks.

By repeating the foregoing analysis for a large number of nominally equal components (Monte Carlo simulation), the fatigue life distribution of the component is obtained. Thus, the designer will be able to find the probability of fatigue failure.

The main steps for obtaining the fatigue life distribution of a component can be summarised as follows:

1. Develop a 3D FE model and perform a stress analysis of a component using a standard finite element program, such as ABAQUS, ANSYS, or NASTRAN.
2. The number, size and location of crack-like defects in each finite element are 'drawn' from probability distributions.
3. Calculate the maximum principal stress for all defects.
4. Perform fatigue crack growth calculations.
5. Repeat steps 2–4 for a large number of nominally equal components to obtain the fatigue life distribution of the component.

3. Crack growth law

The stress field ahead of a crack in a linear elastic body can be characterised by means of the stress intensity factor K. This is a function of the geometry of the component and the crack [cf. Fig. 1] as well as the stress field. For simple geometries, K can be obtained from handbook solutions [3] or asymptotic solutions [4,5]. For more complex geometries, the stress intensity factor can be obtained by using weight functions together with the stress field of the crack-free component. Weight factor solutions for an embedded crack [6], a surface crack [7] and a corner crack [8], as shown in Fig. 1, have been implemented. The current crack configuration is automatically identified. The initial crack is assumed to grow on the plane of maximum principal stress [1].

The stress amplitude, σ_a, at an arbitrary point on the crack plane, is given by

$$\sigma_a = n_{1i}\sigma_{ij,a}n_{1j}, \quad i,j = 1,2,3. \tag{1}$$

and the mean stress, σ_m, by

$$\sigma_m = n_{1i}(\sigma_{ij,m} + \sigma^0_{ij})n_{1j}. \tag{2}$$

$\mathbf{n}_1$ is the unit eigenvector of the maximum principal stress, and σ^0_{ij} denotes the residual stress tensor.

The use of stress intensity factors was extended to fatigue problems by Paris and Erdogan [9], who suggested a power-law relationship between the crack growth rate da/dn and the stress intensity range ΔK, viz.,

$$\frac{da}{dn} = C\Delta K^m, \tag{3}$$

where C and m are material parameters. Klesnil and Lukáš [10] extended Paris' law into the near threshold region by including the threshold stress intensity range, ΔK_{th}:

$$\frac{da}{dn} = C(\Delta K^m - \Delta K^m_{th}). \tag{4}$$

3.1. An equivalent stress intensity range for short cracks

The fatigue tests by Kitagawa and Takahashi [11] clearly show that the fatigue limit of a cracked solid can be determined by means of the threshold of the stress intensity range for long cracks only. For short cracks,

Please cite this article in press as: Fjeldstad A et al., Simulation of fatigue crack growth in components with ..., Eng Fract Mech (2007), doi:10.1016/j.engfracmech.2007.04.006

however, the fatigue limit asymptotically approaches the ordinary fatigue limit as determined by means of a smooth specimen. Both the long and the short crack fatigue limits are satisfied by an equation initially given by El Haddad et al. [12] for $F = 1$, and generalised by Härkegård [13] to an arbitrary geometry factor, F, viz.

$$\Delta\sigma = \frac{\Delta K_{\mathrm{th}}}{F\sqrt{\pi(a+a')}} = \frac{\Delta\sigma_{\mathrm{A}}}{\sqrt{1+a/a'}}. \tag{5}$$

The characteristic crack length, a', which signifies the transition between short cracks, $a < a'$, and long cracks, $a > a'$, is defined by

$$a' = \frac{1}{\pi}\left(\frac{\Delta K_{\mathrm{th}}}{F\Delta\sigma_{\mathrm{A}}}\right)^2. \tag{6}$$

By replacing the geometry factor F, a' can be written as

$$a' = \left(\frac{\Delta K_{\mathrm{th}}\Delta\sigma}{\Delta K\Delta\sigma_{\mathrm{A}}}\right)^2 a. \tag{7}$$

One may interpret a' as an 'intrinsic' crack length, which should be added to the length of the real crack to yield an 'effective' crack length. Fig. 2a shows a Kitagawa–Takahashi diagram with experimental data for both ferrous and nonferrous alloys gathered by Tanaka et al. [14] and Hertzberg [15]. When crack growth behaviour is controlled by linear elastic fracture mechanics, i.e., $a \gg a'$, $\Delta\sigma$ varies as $1/\sqrt{a}$. At the other extreme where $a \ll a'$, the fatigue limit asymptotically approaches the fatigue limit, $\Delta\sigma_{\mathrm{A}}$, of a smooth, polished fatigue specimen without major defects.

Rewriting Eq. (5) in terms of the stress intensity range yields

$$\Delta K = \frac{\Delta K_{\mathrm{th}}}{\sqrt{1+a'/a}}. \tag{8}$$

In Fig. 2b, Eq. (8) is shown as a solid line together with the data presented in [14,15]. For long cracks, ΔK asymptotically approaches the stress intensity range ΔK_{th}. For short cracks, however, the stress intensity range required for a crack to grow varies as $\sqrt{a}$.

The preceding equations explicitly depend on the intrinsic crack length, a', which, in its turn, depends on the geometry factor, F. The latter will not be constant, if the crack shape changes [16], or the finite dimensions of the solid must be considered. This inconvenience can be avoided by eliminating the crack length, a, between Eqs. (5) and (8). Thus, one obtains

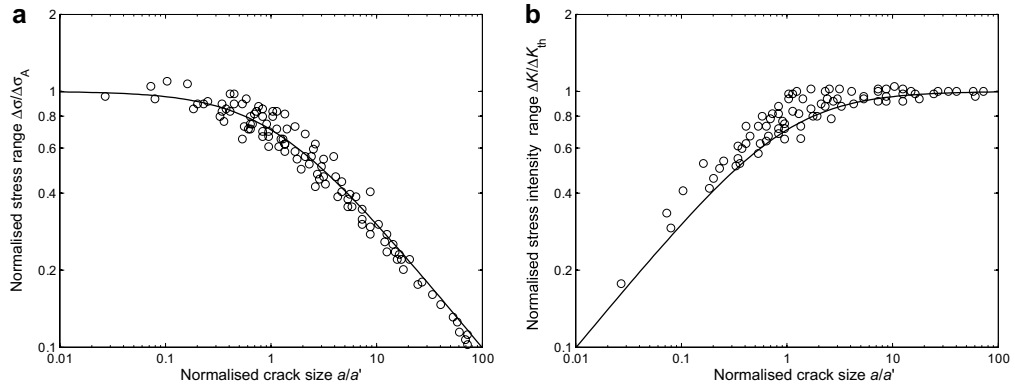

Fig. 2. Normalised threshold behaviour versus normalised crack size. (a) Normalised stress range and (b) normalised stress intensity range. Data points have been gathered by Tanaka et al. [14] and Hertzberg [15].

Please cite this article in press as: Fjeldstad A et al., Simulation of fatigue crack growth in components with ..., Eng Fract Mech (2007), doi:10.1016/j.engfracmech.2007.04.006

$$\left(\frac{\Delta K}{\Delta K_{\mathrm{th}}}\right)^2 + \left(\frac{\Delta\sigma}{\Delta\sigma_{\mathrm{A}}}\right)^2 = 1. \tag{9}$$

This equation was originally used by Härkegård et al. [17] to correlate the stress range, $\Delta\sigma$, and the stress intensity range, ΔK, below which short cracks did not propagate in two ferritic steels. In Fig. 3, the data points of Fig. 2 have been replotted in a diagram with $\Delta\sigma/\Delta\sigma_{\mathrm{A}}$ as the abscissa and $\Delta K/\Delta K_{\mathrm{th}}$ as the ordinate. The seemingly large scatter in Fig. 3 compared with that in Fig. 2a and b can be explained by the change to linear scales from logarithmic scales.

If Eq. (9) is rewritten as

$$\Delta K\left[1 + \left(\frac{\Delta K_{\mathrm{th}}}{\Delta K}\right)^2\left(\frac{\Delta\sigma}{\Delta\sigma_{\mathrm{A}}}\right)^2\right]^{1/2} = \Delta K_{\mathrm{th}}, \tag{10}$$

the left member may be interpreted as an equivalent stress intensity range for short and long cracks,

$$\Delta K_{\mathrm{eq}} = \Delta K\left[1 + \left(\frac{\Delta K_{\mathrm{th}}}{\Delta K}\right)^2\left(\frac{\Delta\sigma}{\Delta\sigma_{\mathrm{A}}}\right)^2\right]^{1/2}. \tag{11}$$

By introducing Eq. (7) into the above equation, ΔK_{eq} can be expressed as

$$\Delta K_{\mathrm{eq}} = \Delta K\sqrt{1 + \frac{a'}{a}}. \tag{12}$$

For $a \gg a'$, ΔK_{eq} asymptotically approaches the stress intensity range ΔK.

By introducing Eq. (11) into Eq. (4), the crack growth rate can be expressed as

$$\frac{\mathrm{d}a}{\mathrm{d}n} = C\Delta K_{\mathrm{th}}^m\left[\left\{\left(\frac{\Delta K}{\Delta K_{\mathrm{th}}}\right)^2 + \left(\frac{\Delta\bar{\sigma}}{\Delta\sigma_{\mathrm{A}}}\right)^2\right\}^{m/2} - 1\right]. \tag{13}$$

To determine the 'effective' stress range, $\Delta\bar{\sigma}$, for a surface crack at the root of a notch (Fig. 4, left), the same surface crack in a semi-infinite body is considered (Fig. 4, right). $\Delta\bar{\sigma}$ is now defined as the remote stress range that yields the same ΔK as for the crack at the root of a notch. Hence,

$$\Delta\bar{\sigma} = \frac{\Delta K}{F\sqrt{\pi a}}, \tag{14}$$

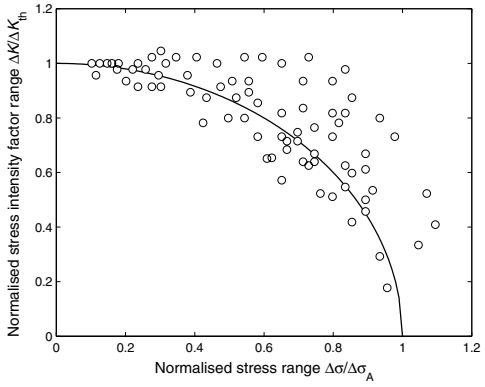

Fig. 3. Relation between the stress range and the stress intensity range required to propagate a crack. Data points have been gathered by Tanaka et al. [14] and Hertzberg [15].

Please cite this article in press as: Fjeldstad A et al., Simulation of fatigue crack growth in components with ..., Eng Fract Mech (2007), doi:10.1016/j.engfracmech.2007.04.006

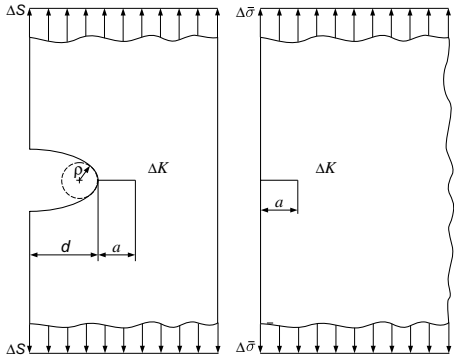

Fig. 4. Definition of the effective stress range $\Delta\bar{\sigma}$. The smooth edge-cracked plate has the same ΔK value as the notched plate when subjected to $\Delta\bar{\sigma}$.

where F is the geometry factor for the current crack in a semi-infinite plate. For an edge through-crack, $F = 1.122$ [3], and for an elliptic surface crack with aspect ratio $a/c = 1$, $F = 0.663$ [18] at the deepest point of the crack front.

For a long crack, i.e., $a \gg a'$, Eq. (13) reduces to the crack growth law proposed by Klesnil and Lukáš [10], see Eq. (4).

3.2. Influence of the load ratio

Several models that address the mean stress dependency of fatigue crack propagation have been presented in the literature. The different mean stress equations are either crack closure based or empirically based.

By plotting da/dn as a function of the equivalent zero-to-tension stress intensity range, and by suitable choice of the exponent γ

$$\Delta K^* = \frac{\Delta K}{(1-R)^{1-\gamma}}, \quad R = \frac{K_{\min}}{K_{\max}}, \tag{15}$$

Walker [19] found that he could make crack growth data for $R \neq 0$ fall into a narrow scatter-band corresponding to $R = 0$. At positive stress ratios, γ, usually takes values between 0.2 and 0.8, where $\gamma = 0.2$ gives a strong and $\gamma = 0.8$ a weak dependency on R. The constant C of the crack growth law, the stress range, the fatigue limit and the threshold stress intensity range can all be transformed to $R = 0$ by using Walker's equation as shown in [20,21]. The exponent m of the crack growth law generally varies only weakly with R [22] and is assumed to be constant in this work.

3.3. Crack growth measurements

Crack growth measurements obtained from the literature [23,24] have been reanalysed in order to verify the crack growth law given by Eq. (13). Both studies consider the growth of short cracks in the near-threshold regime.

Fig. 5 shows crack growth measurements carried out by Breat et al. [23] on A508 steel specimens. The objective of this investigation was to compare the crack growth behaviour of long cracks, initially 13–16 mm, with the behaviour of short cracks, initially 0.3–0.5 mm. The short crack measurements were performed on four point bending specimens. For long crack measurements, compact tension specimens were used. The crack propagation tests were carried out at $R = 0.1$. The specimens with long cracks were subjected to a nominal stress range well below that of specimens with short cracks. In both cases, the crack growth rates were measured

Please cite this article in press as: Fjeldstad A et al., Simulation of fatigue crack growth in components with ..., Eng Fract Mech (2007), doi:10.1016/j.engfracmech.2007.04.006

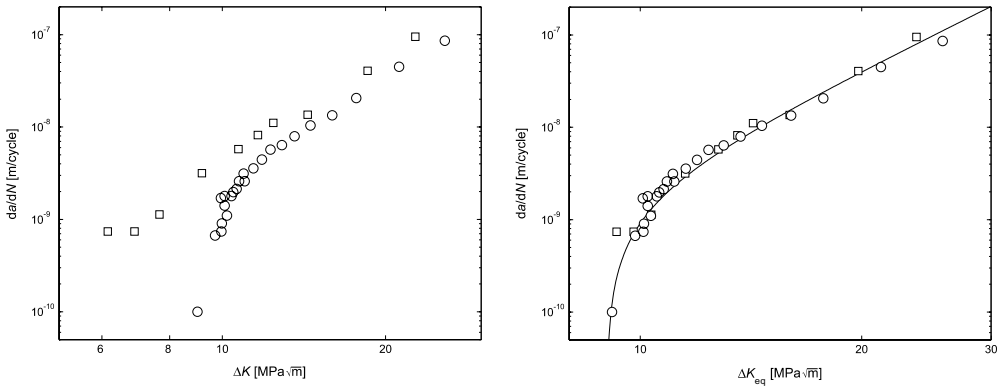

Fig. 5. Crack growth rates in A508 steel [23] as a function of (a) ΔK, and (b) ΔK_{eq}.

for increasing ΔK levels at a constant load level. Fig. 5a clearly shows that short cracks grow at a significantly higher rate than long cracks when rates are compared on the basis of ΔK. Tentative reasons for this state of affairs are:

- A short crack remains open during a larger part of the load cycle than a long crack [25].
- ΔK is no longer characterising the crack tip stress and strain field because the plastic zone is in the order of the crack length [26,27].

In Fig. 5b, the same data have been plotted against the equivalent stress intensity factor ΔK_{eq} [see Eq. (11)]. The short and long crack measurements collapse into one line, which is well described by the solid line, obtained from Eq. (4).

Fig. 6a shows crack growth data for the aluminium alloy 6082-T6. The crack growth measurements have been presented by Mann [24] and were carried out at a stress ratio of $R = 0.1$. According to Borrego et al. [28], the long crack stress intensity threshold of AA6082-T6 is given by $\Delta K_{th}(R = 0.1) = 2.08\ \mathrm{MPa}\sqrt{\mathrm{m}}$. The stress concentration factor at the starter notch was $K_t = 5.7$ [24]. Potential drop measurements were carried out to determine the crack depth, a. The stress intensity factor range, ΔK, was calculated by using an asymptotic

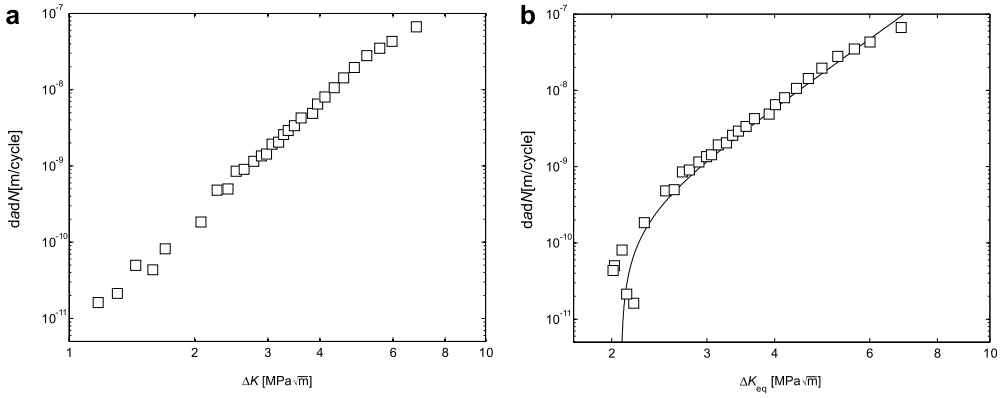

Fig. 6. Crack growth rates in AA6082-T6 [24] as a function of (a) ΔK and (b) ΔK_{eq}.

Please cite this article in press as: Fjeldstad A et al., Simulation of fatigue crack growth in components with ..., Eng Fract Mech (2007), doi:10.1016/j.engfracmech.2007.04.006

solution presented in [4]. The crack growth measurements of the aluminium alloy were carried out by increasing the applied load until a crack had been initiated. The initial crack depth was measured to be approximately 16 μm. Subsequently, the load was reduced stepwise until the crack had reached a depth of approximately 0.5 mm. The load was then kept constant. By applying ΔK_{eq} to the crack growth data in Fig. 6a, one obtains the plot shown in Fig. 6b. The (uncorrected) short crack growth data in the range $\Delta K = 1 - 2$ MPa$\sqrt{\text{m}}$ are seen to be shifted to $\Delta K_{eq} = 2.0 - 2.3$ MPa$\sqrt{\text{m}}$, which is in good agreement with the long crack stress intensity threshold due to Borrego et al. [28].

To judge from the preceding investigations, the crack growth law given by Eq. (13) is a robust and simple crack growth model.

4. Verification of fatigue life predictions

Wormsen et al. [1] showed that the K solutions [6,7] implemented in the finite-element post-processor are in good overall agreement with numerical calculations and solutions found in the literature [29,30]. Based on the conclusions drawn in [1], it is reasonable to assume that the finite-element post-processor yields accurate fatigue life predictions. However, fatigue life predictions may contain errors from other sources than the numerically calculated ΔK values, such as too large crack growth increments when a crack is growing (i) close to a free surface, or (ii) in a gradient stress field.

Life predictions reported in [31,32] have been reanalysed by using Paris' law, see Eq. (3). The mechanical properties presented in Table 1 will be used throughout this Section.

Dai et al. [31] simulated the growth of near-surface cracks located in a semi-infinite body subjected to a remote uniform stress range of $\Delta S = 500$ MPa. The embedded crack grows until it reaches the surface and continues its growth as a surface crack until the fracture toughness, K_{Ic}, is attained. The calculation of K is based on the eigenstrain procedure [33]. This allows the crack to evolve freely. Hence, the transition from an embedded crack to a surface crack may be modelled in detail. As described in [1], a simpler approach has been implemented in the finite-element post-processor. The crack unfolds to a surface crack, once the embedded crack has reached the surface, see Fig. 7. Presented in Table 2 are fatigue life predictions from Dai et al. [31] along with results from the finite-element post-processor. The predicted fatigue lives are consistently on the safe side of those reported in [31], with an observed maximum difference of less than 12%. The predicted number of cycles until breakthrough are in good overall agreement. Thus, the deviation between the

Table 1
Mechanical properties of the investigated steel

Fracture toughness	$K_{Ic} = 150$ MPa$\sqrt{\text{m}}$
Coefficient in Paris' law	$C = 1.0 \cdot 10^{-11}$ [MPa,m]
Exponent in Paris' law	$m = 3$

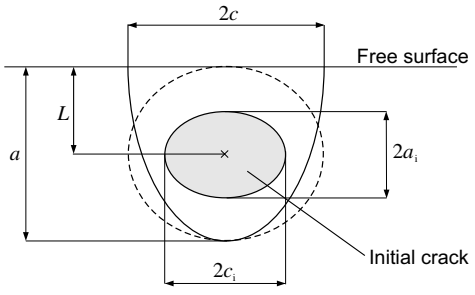

Fig. 7. Sketch of a near surface crack and how it unfolds to a surface crack.

Please cite this article in press as: Fjeldstad A et al., Simulation of fatigue crack growth in components with ..., Eng Fract Mech (2007), doi:10.1016/j.engfracmech.2007.04.006

Table 2
Fatigue life predictions presented by Dai et al. [31] and obtained by using P • FAT

Initial crack geometry [mm][a]			Cycles until breakthrough, n_1		Cycles after breakthrough, n_2		Total cycles until failure, $n_f = n_1 + n_2$	
a_i	c_i	L	Dai et al.	P • FAT	Dai et al.	P • FAT	Dai et al.	P • FAT
1	1	2	8867	8931	14034	11257	22901	20188
1	2	2	3801	4653	12363	11227	16164	15880
2	2	4	3283	3327	8136	6950	11419	10277

[a] See Fig. 7.

two lifetimes can be attributed to the surface crack growth. The difference in the predicted number of cycles after breakthrough is mainly due to the assumption that the embedded crack spontaneously unfolds to a surface crack, cf. Fig. 7.

Fjeldstad et al. [32] simulated the influence of a gradient stress field on the fatigue life using the asymptotic solution by Wormsen et al. [4]. A surface crack located at the root of a semi-circular edge notch ($d = \rho = 20$ mm) in a semi-infinite plate subjected to uniaxial tension $\Delta S = 100$ MPa perpendicular to the symmetry plane of the notch was considered. The cracked configuration is shown in Fig. 8a. The initial crack is characterised by its depth a_i and its surface length $2c_i$, cf. Fig. 8b. According to finite element analysis, the stress concentration factor $K_t = 3.1$ for the notched configuration. In Table 3, results obtained from the finite-element post-processor are presented along with results based on the work in [32]. Again, lifetime predictions from the finite-element post-processor are conservative, with a maximum difference of less than 20%. The difference in fatigue life is here mainly due to the different methods for obtaining ΔK. It is found that the crack aspect ratio a/c in the present analysis is generally beneath that of the analysis described in [32]. A smaller aspect ratio leads to a higher K, which results in a more rapid crack growth, and thus, a shorter fatigue life. Finding the cause of the slightly different behaviour is however outside the scope of this paper.

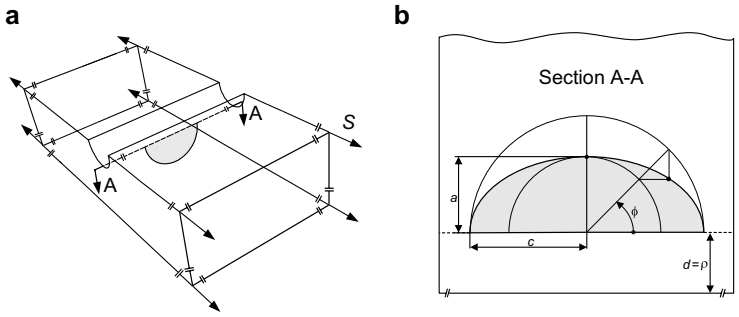

Fig. 8. Schematic drawings of a surface crack emanating from a notch with root radius $\rho = 20$ mm: (a) three-dimensional view and (b) two-dimensional view of the cracked section A–A.

Table 3
Fatigue life predictions of the component shown in Fig. 8 based on Fjeldstad et al. [32] and obtained by the finite-element post-processor

a_i [mm]	a_f [mm]	Fatigue life	
		Fjeldstad et al.	P • FAT
0.2	200	506780	412963
0.2	20	330260	295800
0.02	20	885150	854129

Here, $a_i/c_i = 1$ has been used.

Please cite this article in press as: Fjeldstad A et al., Simulation of fatigue crack growth in components with ..., Eng Fract Mech (2007), doi:10.1016/j.engfracmech.2007.04.006

5. Defects

The fatigue lifetime depends on material defects, e.g., porosity and non-metallic inclusions, which form as a natural part of the manufacturing processes. The volume fraction of inclusions depends directly on the oxygen and sulphur content of the steel.

Due to the small volume of steel that can be examined by conventional inspection methods, the number and size of defects in a large volume have to be estimated by statistical analysis. A description of the different inspection methods, such as non-destructive testing (e.g. ultrasonic, radiographic, eddy-current) and optical microscopy, are given in Ref. [34]. Ultrasonic inspection is nowadays used for the inspection of defects, whose size is greater than approximately 200 μm. The major advantage of this method is that a rather 'large' volume can be inspected. However, in most cases the initial defect size at the failure site is below the detection limit of the ultrasonic inspection method. By using techniques based on surface analysis and optical microscopy, one could detect defects as small as, typically 3 μm. The drawback of this method is that only a small area can be inspected, typically 1 mm^2–15 mm^2. To obtain a sufficient accuracy in the extrapolation from a small area to a large area, the number and size of defects should be counted and measured in several separate control regions.

In the following, methods for the prediction of the size of fatigue critical defects based on the statistics of extremes will be presented.

5.1. Defect distributions

The reliability and performance of metallic components are greatly affected by the size of defects contained in the most highly stressed volume. With improvements in steel-making, the amount and size of defects are being progressively reduced. The likely size of the largest defect within a cast of steel is an important indicator of the quality of the cast. It is of interest both to the manufacturer, for reasons of process control, and to the user, who may wish to use the information on defects to undertake defect-tolerant design and safety assessment of components. Because defects are small and are mostly inside the material, they are difficult to detect and measure. Observations using automated optical microscopy can, however, be made on polished plane regions (control areas), and the maximum defect size in a real component must be obtained by prediction based on some statistical analysis. There are two different approaches based on the statistics of extremes for estimating the sizes of large defects in a large volume from those of a small volume. The first approach, called the *block maximum* method, is based on the generalised extreme value distribution [35]. In this method, only the size of the largest defect in each of the k control areas is measured. The second approach is the *peak over threshold* method. Here, all defects with sizes above a certain high threshold are considered. The overshoot of the defect size above the threshold is fitted to a generalised Pareto distribution [35]. Both methods allow the data on defect sizes in the small control regions to be used for prediction of the maximum defect size in a large volume of steel. And they avoid difficulties in measuring small defects, particularly from a resolution point of view.

5.1.1. Block maximum method

For the block maximum method, the total inspection area is divided into k equally sized, polished control areas, each of size A_0. The three-dimensional size distribution of defects can be estimated from the two-dimensional size distribution by using a stereological approximation as shown in [36,37]. Hence, in the following a control region of volume V_0 is considered. For each of the k control regions, all the defects above the detection limit would need to be measured, to decide which is the largest, i.e., $a_{\max} = \max\{a_1, \ldots, a_i\}$. The result of the block maximum method is a set of k observations of maximum defect sizes, $a_{\max 1}, \ldots, a_{\max k}$. The generalised extreme value (GEV) distribution is fitted to these data. The GEV distribution for a controll region of volume, V_0, is given by

$$G(a_{\max}) = \Pr[A_{\max} \leqslant a_{\max}] = \exp\left\{-\left[1 + \xi'\left(\frac{a_{\max} - a_0^*}{a_0}\right)\right]^{-1/\xi'}\right\}, \tag{16}$$

Please cite this article in press as: Fjeldstad A et al., Simulation of fatigue crack growth in components with ..., Eng Fract Mech (2007), doi:10.1016/j.engfracmech.2007.04.006

where $a_0 > 0$ denotes the scale parameter, a_0^* the location parameter and ξ' the shape parameter. The location parameter, a_0^*, is the $\exp(-1) \approx 36.8\%$ quantile of the generalised extreme value distribution and is often called the characteristic largest defect size in volume V_0. The GEV distribution combines the Gumbel (Type I, $\xi' = 0$), Fréchet (Type II, $\xi' > 0$) and the reversed Weibull (Type III, $\xi' < 0$) distributions into a single distribution. The remarkable feature of the generalised extreme value distribution is that Eq. (16) is the only possible limit for the distribution of the maximum defect size [35].

The Gumbel, Fréchet and reversed Weibull, have distinctly different forms of tail behaviour. When $\xi' < 0$, i.e., for the reversed Weibull distribution, its upper end-point $a_{\max+} = a_0^* - a_0/\xi'$. Thus, the probability of finding defects $\geqslant a_{\max+}$ is zero. The Gumbel ($\xi' = 0$) and Fréchet ($\xi' > 0$) distributions are unlimited upwards.

Consider a homogeneously stressed volume, V_0, subjected to an (equivalent) stress amplitude σ_a. The smallest defect initiating failure in V_0 is denoted by a_{crit}. For long fatigue lives close to the fatigue limit, a_{crit} can be estimated by means of the Kitagawa-Takahashi model [11], cf. Eq. (5), as

$$a_{crit} = a' \left[\left(\frac{\sigma_A}{\sigma_a} \right)^2 - 1 \right], \tag{17}$$

where the intrinsic crack length, a', is given by Eq. (6). If the largest defect within V_0 exceeds a_{crit}, then V_0 will fail. This is the same as stating that the applied stress σ_a is above the fatigue limit (random variable), σ_A, for the volume element V_0. Hence,

$$\Pr[A_{max} \geqslant a_{crit}] = 1 - G(a_{crit}) = \Pr[\sigma_a \geqslant \sigma_A]. \tag{18}$$

In Fig. 9, a Kitagawa–Takahashi diagram is shown together with a probability density curve of the maximum defect size. The critical defect density, z_1, is defined as the expected number of defects per unit volume of the material that yields a fatigue limit (random variable) $\sigma_A \leqslant \sigma_a$. The shaded area in Fig. 9 is equal to the probability that at least one defect has a size greater than a_{crit}. The probability of failure under homogeneous stress is given by

$$P_{f,V_0} = \Pr[A_{max} \geqslant a_{crit}] = \Pr[\sigma_a \geqslant \sigma_A] = z_1 V_0. \tag{19}$$

From Fig. 9 it can be seen that the expected number of critical defects decreases with decreasing stress level. Clearly, this has a large effect on the probability of failure. A similar shift could arise from uncertainty in the Kitagawa–Takahashi model. Also a small reduction in maximum defect size by increasing the steel cleanliness,

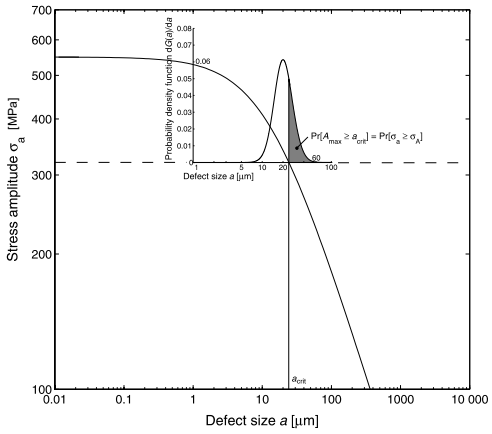

Fig. 9. Illustration of the block maximum method for estimating the fatigue failure probability of a homogeneously stressed volume due to the interaction between the defect size distribution and the applied loading.

Please cite this article in press as: Fjeldstad A et al., Simulation of fatigue crack growth in components with ..., Eng Fract Mech (2007), doi:10.1016/j.engfracmech.2007.04.006

which shifts the density curve to the left, has a similar, large effect. According to Eqs. (19) and (16), the probability of survival, $P_{s,V_0} = 1 - P_{f,V_0}$, is given by

$$P_{s,V_0} = 1 - z_1 V_0 = \Pr[A_{\max} \leqslant a_{\text{crit}}] = \exp\left\{-\left[1 + \xi'\left(\frac{a_{\text{crit}} - a_0^*}{a_0}\right)\right]^{-1/\xi'}\right\}. \tag{20}$$

For an arbitrary volume, V, under homogeneous stress, the probability of survival of the whole volume is equal to the product of the probabilities of survival of all the volume elements. Since, the number of volume elements is V/V_0, one obtains

$$P_{s,V} = P_{s,V_0}^{V/V_0} = \exp\left\{-\left[1 + \xi'\left(\frac{a_{\text{crit}} - a_0^*}{a_0}\right)\right]^{-1/\xi'} \frac{V}{V_0}\right\}. \tag{21}$$

Fig. 10 shows the probability of survival versus the applied stress assuming the maximum defect size to be Gumbel distributed. A homogeneously stressed bearing steel [38] with an intrinsic fatigue limit $\sigma_A = 550$ MPa and $a' = 9.5$ μm is considered. From the figure, it is seen that Eq. (21) takes the size of the specimen into account.

When the state of stress is inhomogeneous, it is appropriate to divide the component, whose overall volume is V, into a large number of small volume elements, ΔV_i, each with a nearly constant (equivalent) stress amplitude, σ_{ai}. Under inhomogeneous stress, a_{crit} will depend on the location $\mathbf{x} = [x, y, z]^{\mathrm{T}}$ of the volume element. Thus, the probability of survival of the i^{th} element is given by

$$P_{s,\Delta V_i} = \exp\left\{-\left[1 + \xi'\left(\frac{a_{\text{crit}}(\mathbf{x}) - a_0^*}{a_0}\right)\right]^{-1/\xi'} \frac{\Delta V_i}{V_0}\right\}. \tag{22}$$

Again, the probability of survival of the component equals the product of the probabilities of survival of all the volume elements, i.e.,

$$P_{s,V} = \exp\left\{-\sum_{i=1}^{V/\Delta V}\left[1 + \xi'\left(\frac{a_{\text{crit}}(\mathbf{x}) - a_0^*}{a_0}\right)\right]^{-1/\xi'} \frac{\Delta V_i}{V_0}\right\}. \tag{23}$$

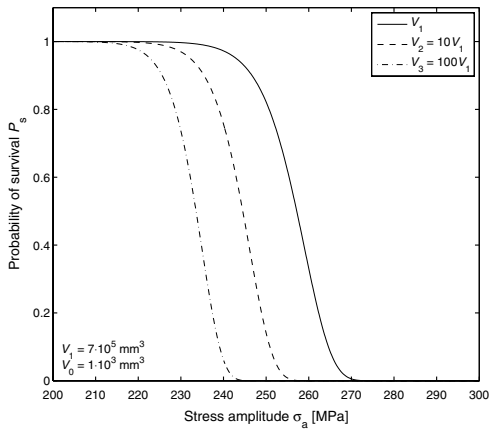

Fig. 10. Probability of survival for a smooth uniaxial loaded specimen versus the applied stress assuming the maximum defect size to be Gumbel distributed ($\xi' = 0$, $a_0^* = 20$ μm and $a_0 = 2$ μm).

Please cite this article in press as: Fjeldstad A et al., Simulation of fatigue crack growth in components with ..., Eng Fract Mech (2007), doi:10.1016/j.engfracmech.2007.04.006

As the volume of each individual element tends to zero, the overall probability of survival becomes

$$P_{s,V} = \exp\left\{-\int_V \left[1+\xi'\left(\frac{a_{crit}(\mathbf{x})-a_0^*}{a_0}\right)\right]^{-1/\xi'} \frac{dV}{V_0}\right\}. \tag{24}$$

This equation can either be solved by means of numerical integration or by 'drawing' defect sizes from the generalised extreme value distribution [see Eq. (16)].

5.1.2. Peak over threshold method

For the block maximum method, all the defects above the detection limit would need to be measured to decide which is the largest. The rest of the data are then discarded. This can be a wasteful process that sets aside valuable data. In contrast, for the peak over threshold method, *all* defects above a certain size are measured, giving more data to the parameter estimation of the defect size distribution. The peak over threshold method was applied to defects in clean steels for the first time by Shi et al. [39,40].

For the peak over threshold method, either a single inspection volume or k sub-volumes are chosen for counting and measuring defects larger than a sufficiently high threshold a_{th}. The result is a set of i observations, $a_1, \ldots, a_i$. The statistical analysis is made on the excesses of these sizes over the threshold, that is on the values $a_i - a_{th}$. A generalised Pareto distribution is given by [35]

$$H(a) = \Pr[A \leqslant a | A > a_{th}] = 1 - \left[1+\xi'\left(\frac{a-a_{th}}{\tilde{a}_0}\right)\right]^{-1/\xi'}, \tag{25}$$

is fitted to these excesses. The scale parameter $\tilde{a}_o$ is given by [35]

$$\tilde{a}_0 = a_0 + \xi'(a_{th} - a_0^*), \tag{26}$$

where a_0, a_0^* and ξ' coincide with the parameters of the associated generalised extreme value distribution for block maxima, see Eq. (16). The range of $a - a_{th}$ is $0 < a - a_{th} < \infty$ if $\xi' \geqslant 0$ and $0 < a - a_{th} < -\tilde{a}_0/\xi'$ if $\xi' < 0$. When $\xi' = 0$, the maximum defect size follows a Gumbel distribution [37]. For $\xi' > 0$, the maximum defect size follows a Fréchet distribution and for $\xi' < 0$, a reversed Weibull distribution [37].

The expected number of defects with sizes greater than a_{th} in the inspection volume V_0 is assumed to be Poisson distributed with mean $z_0(a_{th})V_0$, where $z_0(a_{th})$ is the expected number of defects of size greater than a_{th} per unit volume. The expected number of critical defects in V_0 is Poisson distributed with mean [37]

$$z_1 V_0 = z_0(a_{th}) V_0 \Pr[A \geqslant a_{crit} | A > a_{th}]. \tag{27}$$

The homogeneously stressed volume, V_0, will survive only if all defects have a size smaller than a_{crit}, i.e., $z_1 V_0 = 0$. Hence, from the Poisson distribution,

$$P_{s,V_0} = \Pr[A \leqslant a_{crit}] = \Pr[z_1 V_0 = 0] = \exp\{-z_0(a_{th}) V_0 \Pr[A \geqslant a_{crit} | A > a_{th}]\}, \tag{28}$$

and from Eq. (25), one obtains

$$P_{s,V_0} = \exp\left\{-z_0(a_{th}) V_0 \left[1+\xi'\left(\frac{a_{crit}-a_{th}}{\tilde{a}_0}\right)\right]^{-1/\xi'}\right\}. \tag{29}$$

If $z_0(a_{th}) = 1/V_0$ and $a_{th} = a_0^*$, the above equation becomes identical to Eq. (20). It is this fact that connects the peak over threshold method and the block maximum method.

6. A simplified procedure for determining the life-controlling defect

When performing a Monte Carlo simulation for obtaining the fatigue life distribution of a component, one must generally perform a crack growth analysis of all defects located in each one of the nominally equal components. Since a fatigue crack growth calculation is a computer intensive task, it would be of interest to see whether it is possible to directly identify the life-controlling defect from the stress field and the initial crack growth rate. If this is possible, one could greatly reduce the simulation time. A crude simplified defect selection procedure has been implemented in the finite-element post-processor. This procedure is presented below.

Please cite this article in press as: Fjeldstad A et al., Simulation of fatigue crack growth in components with ..., Eng Fract Mech (2007), doi:10.1016/j.engfracmech.2007.04.006

Non-propagating defects are removed from the component by means of the Kitagawa–Takahashi diagram [11]. The remaining defects are sorted based on their initial crack growth rate. In order to determine the life-controlling defect, the stress field in the proximity of the defect must be taken into account. This is done by using a crude correction of the initial crack growth rate with respect to the stress gradient acting on the crack surface. The method is described in Ref. [32]. Here, the fatigue life of cracked specimens subjected to a gradient stress field is compared with the fatigue life of cracked specimens subjected to a homogeneous stress field.

To see how well the defect selection procedure works, a double-edge-notched-tension plate subjected to a nominal stress range $\Delta S = 450$ MPa at $R = 0$ has been considered. The investigated configuration is shown in Figs. 11a and 12. The largest notch is semi-circular with a radius $\rho = 20$ mm and a stress concentration factor $K_t = 3.5$. The smallest notch is U-shaped with a radius $\rho = 2$ mm and depth $d = 7$ mm. The stress concentration factor for the U-shaped notch is $K_t = 4.8$. The notched configuration is an interesting example due to the two different notch geometries which both suit as potential locations for the life controlling defect. The material parameters used are given in Table 4.

Fig. 11a shows the locations of the potential life-controlling defects contained in one component. The number of critical defects is clearly highest in the proximity of the semi-circular notch, while only a few defects are located near the U-notch. This occurs since the semi-circular notch has a larger highly stressed volume than the U-notch. In order to validate the defect selection procedure, crack growth calculations have been performed for all the defects shown in Fig. 11a. Fig. 11b shows the a priori ranking of the fatigue critical defects due to the selection procedure against the a posteriori ranking obtained by means of crack growth calculations. The figure clearly shows that the defect selection procedure manages to identify the life controlling defect, i.e., the defect that gives the shortest life. However, one can not rule out the possibility that a somewhat less severe defect will be chosen occasionally.

Table 4
Material parameters for a high strength steel [38]

Coefficient in crack growth law	$C(R=0) = 2.08 \cdot 10^{-14}$ [MPa, m]
Exponent in crack growth law	$m = 4.8$
Threshold stress intensity factor range	$\Delta K_{th}(R=0) = 4.4$ MPa$\sqrt{\text{m}}$
Fatigue limit	$\sigma_A(R=0) = 550$ MPa

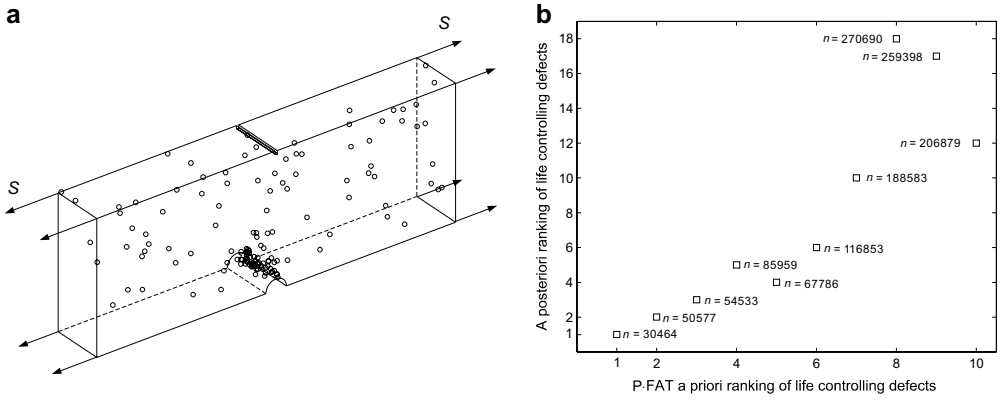

Fig. 11. (a) Potential life-controlling defects in one component, and (b) the a posteriori ranking of the life-controlling defects versus the a priori ranking from P • FAT.

Please cite this article in press as: Fjeldstad A et al., Simulation of fatigue crack growth in components with ..., Eng Fract Mech (2007), doi:10.1016/j.engfracmech.2007.04.006

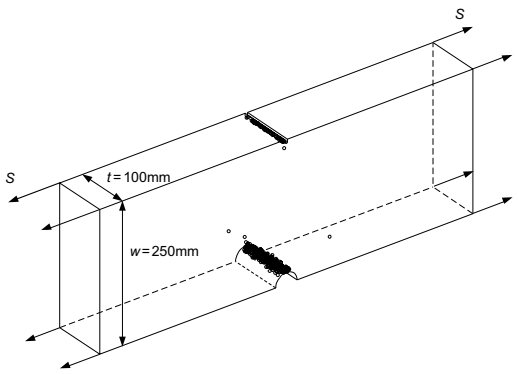

Fig. 12. Example of generated life-controlling defects of 500 components.

Fig. 12 shows the location of the life-controlling defect in 500 components. As can be seen, most of these defects are located in the highly stressed volume of the semi-circular notch, while only a few are located near the more highly stressed U-notch.

7. Simulations

7.1. Geometry

Two different configurations have been investigated: (a) a smooth tension plate and (b) a double-edge-notched tension plate. Both configurations have the volume $V = 6.9 \cdot 10^6\ \text{mm}^3$ and are subjected to the net-section stress amplitude, $S_{a,net} = 320$ MPa at $R = 0$. The specific numerical data employed in the present calculations are given in Table 4.

The first configuration is a smooth plate of width w, height h and thickness t, as shown in Fig. 13a. The double-edge-notched tension plate is shown in Fig. 13b. The notch is semicircular with radius $\rho = w/7$. According to FEA, the elastic stress concentration factor $K_t = \sigma_{1,max}/S = 3.1$ for the notched plate.

One thousand simulations have been carried out for each of the configurations under the assumption that the defect size is Gumbel or Fréchet distributed. The number of crack-like defects in each finite element is 'drawn' from a Poisson distribution. The initial defect locations are given by a uniform distribution [1].

7.2. Results

The different ways of modelling the defect size distributions are separately used to estimate the fatigue limit distribution and the fatigue life distribution of the two investigated configurations. In Table 5, the distribution parameters are presented along with mean and standard deviation values of the size of the life-controlling defect, fatigue limit and fatigue life. Beretta and Murakami [41] found that the distribution functions of inher-

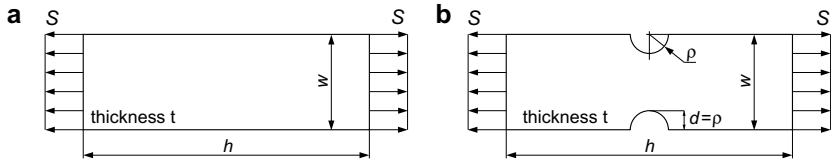

Fig. 13. Specimens considered. (a) A smooth tension plate and (b) a double-edge-notched tension plate.

Please cite this article in press as: Fjeldstad A et al., Simulation of fatigue crack growth in components with ..., Eng Fract Mech (2007), doi:10.1016/j.engfracmech.2007.04.006

Table 5
Mean values and standard deviations of the simulated life-controlling defect size, fatigue limit and fatigue life

Distribution	Parameters			Defect size [μm]		Fatigue limit [MPa]		Fatigue life [k cycles]	
$A_{max}\sim$	a_0^* [μm]	a_0 [μm]	ξ'	Smooth mean (std.[a])	Notched mean (std.[a])	Smooth mean (std.[a])	Notched mean (std.[a])	Smooth mean (std.[a])	Notched mean (std.[a])
Gumbel	20	2	0	38.9 (2.6)	23.0 (3.1)	244 (6.3)	148 (8.0)	110 (11)	4.9 (1.4)
Fréchet	20	0	11.4	46.2 (5.6)	23.2 (3.9)	228 (11)	148 (8.1)	86 (13)	4.9 (1.5)

[a] std: Standard deviation.

ent material inhomogeneities (graphite flakes or nodules, inclusions) have a shape ratio, a_0/a_0^*, typically less than 0.5. Under the assumption that the defect size is Gumbel distributed, a shape ratio $a_0/a_0^* = 0.1$ has been used in the simulations, cf. Table 5.

Size distributions for the life-controlling defects are shown in Fig. 14. Fig. 14a shows the defects size distribution under the assumption that the defect size follows a Gumbel distribution and Fig. 14b shows the associated plot when the defects are 'drawn' from a Fréchet distribution. The mean value and the standard deviation of the life-controlling defect size are given in Table 5. As can be seen, the life-controlling defect in the smooth plate is larger under a Fréchet assumption than under a Gumbel assumption. This occurs since the Fréchet distribution has a heavier upper tail than the Gumbel distribution. Furthermore, the size of the life-controlling defect is much smaller in the notched configuration compared to the smooth plate due to the smaller highly stressed volume. From Fig. 14 and Table 5, it can be seen that the type of the defect distribution has nearly no influence on the size of the life-controlling defect in the notched plate.

The size distributions of the life-controlling defect shown in Fig. 14 have been converted into fatigue limit distributions by using the Kitagawa–Takahashi diagram. The resulting fatigue limit data have been plotted in a Weibull probability chart in Fig. 15. The dashed lines are drawn by using a three-parameter Weibull distribution. The three-parameter (cumulative) Weibull distribution is given by

$$\Pr[\sigma_A \leqslant \sigma_a] = 1 - \exp\left[-\left(\frac{\sigma_a - \sigma_{A0}^*}{\sigma_0}\right)^{b_\sigma}\right], \tag{30}$$

where σ_0 denotes the scale parameter, σ_{A0}^* the location parameter and b_σ the shape parameter. The parameters are given in Table 6 and have been estimated using the maximum likelihood method [35]. Since the simulated data follow the dashed lines rather well, it can be accepted that the fatigue limit for both configurations and defect size distributions are well described by the Weibull distribution. From Fig. 15 and Table 5 it can be seen

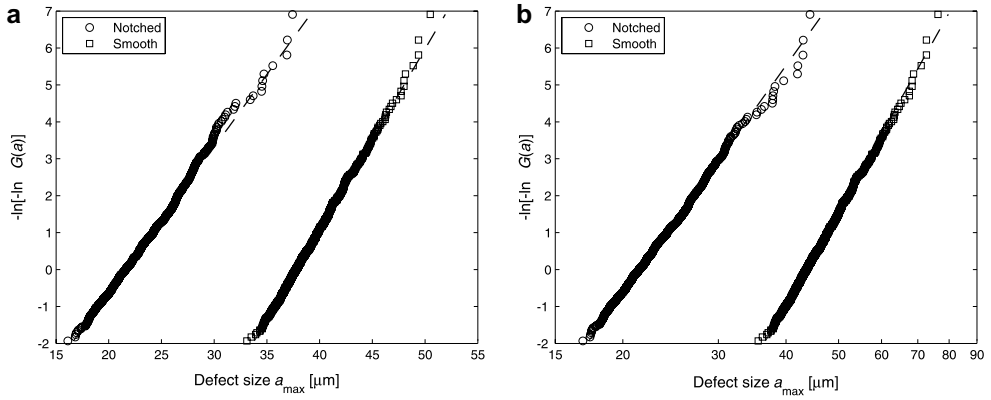

Fig. 14. Simulated life-controlling defect sizes in the two investigated configurations [see Fig. 13] under the assumption that the defect size follows (a) a Gumbel distribution and (b) a Fréchet distribution.

Please cite this article in press as: Fjeldstad A et al., Simulation of fatigue crack growth in components with ..., Eng Fract Mech (2007), doi:10.1016/j.engfracmech.2007.04.006

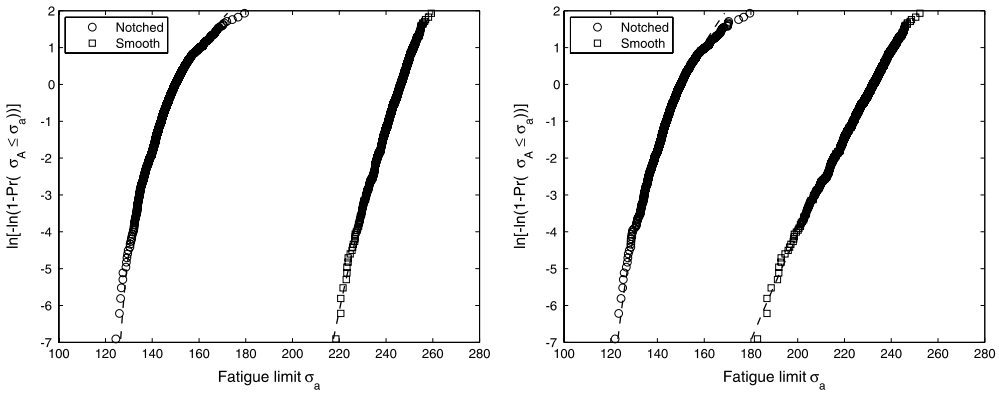

Fig. 15. Fatigue limit distribution for the two investigated configurations [see Fig. 13] under the assumption that the defect size follows (a) a Gumbel distribution and (b) a Fréchet distribution.

Table 6
Weibull distribution parameters of the simulated fatigue limit [Fig. 15] and fatigue life [Fig. 16]

Distribution $A_{max} \sim$		Parameters			Fatigue limit			Fatigue life		
		a_0^* [μm]	a_0 [μm]	ξ'	σ_{A0}^* [MPa]	σ_0 [MPa]	b_σ	n_0^*	n_0	b_n
Gumbel	Smooth	20	2	0	42	204	38.6	588330	551945	5.3
	Notched	20	2	0	123	27	3.3	10018	43429	2.9
Fréchet	Smooth	20	0	11.4	39	194	22.5	244470	664680	5.3
	Notched	20	0	11.4	120	31	3.7	10208	43539	2.8

that the fatigue limit distribution for the notched plate is nearly unaffected by the type of the defect size distribution, as could be expected from Fig. 14.

Fig. 16 shows the fatigue life distribution for the two investigated configurations for $S_{a,net} = 320$ MPa. The simulated data are again plotted in a Weibull probability chart. The dashed lines are drawn by using the three-parameter Weibull distribution:

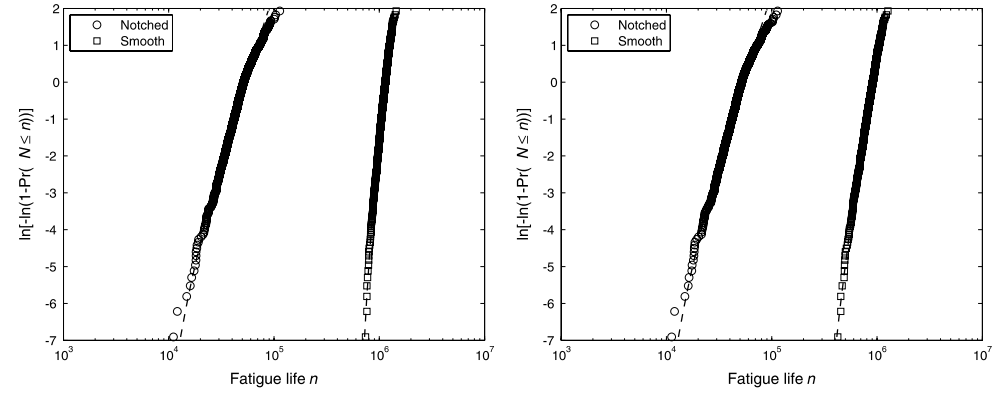

Fig. 16. Fatigue life distribution for the two investigated configurations [see Fig. 13] under the assumption that the defect size follows (a) a Gumbel distribution and (b) a Fréchet distribution.

Please cite this article in press as: Fjeldstad A et al., Simulation of fatigue crack growth in components with ..., Eng Fract Mech (2007), doi:10.1016/j.engfracmech.2007.04.006

$$\Pr[N \leqslant n] = 1 - \exp\left[-\left(\frac{n - n_0^*}{n_0}\right)^{b_n}\right]. \tag{31}$$

Here, n_0 denotes the scale parameter, n_0^* the location parameter and b_n the shape parameter. The parameters are given in Table 6. It can be seen from Fig. 16 that the simulated data are well described by the Weibull distribution. Fig. 16 and Table 6 show that the fatigue life for the notched plate is nearly unaffected by the choice of the defect size distribution.

8. Conclusions

The probability of component fatigue failure can be estimated from an extreme value distribution for large defects and the stress distribution within the component. The fatigue life distribution of a component is obtained by performing crack growth simulations for a large number of randomly distributed defects. The simulations are carried out by using a proposed short crack growth model. An analysis of short and long crack data demonstrated that the short crack model describes the crack growth data very well. Fatigue life predictions have been compared with predictions presented by Dai et al. [31] and Fjeldstad et al. [32]. The fatigue life predictions have been found to be in good agreement with the latter investigations. Further, it has been shown that the presented procedure takes into account the influence of the stress distribution as well as the size of a component on the probability of component fatigue failure. The method can also estimate the reduction in the probability of fatigue failure due to improvements in steel cleanliness and by careful component design.

Simulations of two configurations have been performed. Their fatigue limit and fatigue life distributions have separately been obtained, and found to be well described by a three-parameter Weibull distribution. For the notched configuration, it was found that the fatigue limit and fatigue life were nearly unaffected by the choice of the defect size distribution.

Acknowledgements

The authors gratefully acknowledge the research support for this work provided by The Research Council of Norway and the industrial participants within the NorLight project, and by GE Energy (Norway) AS.

References

[1] Wormsen A, Fjeldstad A, Härkegård G. 2006. A post-processor for fatigue crack growth analysis based a finite element stress field. Comput Method Appl Mech Engng., submitted for publication.
[2] Fett T, Munz D. Stress intensity factors and weight functions. International series on advances in fracture. Southampton: Computational Mechanics Publications; 1997.
[3] Tada H, Paris PC, Irwin GR. The stress analysis of cracks handbook. 3rd ed. Bury St. Edmunds and London: Professional Engineering Publishing Limited; 2000.
[4] Wormsen A, Fjeldstad A, Härkegård G. The application of asymptotic solutions to a semi-elliptical crack at the root of a notch. Engng Fract Mech 2006;73(13):1899–912.
[5] Fjeldstad A, Härkegård G, Wormsen A. Approximate stress intensity factors for cracked V-notched specimens based on asymptotic solutions with application to T-joints. Engng Fract Mech, accepted for publication.
[6] Wang X, Lambert SB, Glinka G. Approximate weight functions for embedded elliptical cracks. Engng Fract Mech 1998;59(3):381–92.
[7] Shen G, Glinka G. Weight functions for a surface semi-elliptical crack in a finite thickness plate. Theor Appl Fract Mec 1991;15(3):247–55.
[8] Zheng XJ, Glinka G, Dubey RN. Stress intensity factors and weight functions for a corner crack in a finite thickness plate. Engng Fract Mech 1996;54(1):49–61.
[9] Paris PC, Erdogan F. A critical analysis of crack propagation laws. J Basic Engng 1963;85:528–34.
[10] Klesnil M, Lukáš P. Influence of strength and stress history on growth and stabilisation of fatigue cracks. Engng Fract Mech 1972;4(1):77–92.
[11] Kitagawa H, Takahashi S. Applicability of fracture mechanics to very small cracks or the cracks in early stage. In: Proceedings of the second international conference on the mechanical behaviour of materials. Boston, Ma: 1976, p. 627–31.
[12] El Haddad MH, Topper TH, Smith KN. Prediction of non-propagating cracks. Engng Fract Mech 1979;11(3):573–84.

Please cite this article in press as: Fjeldstad A et al., Simulation of fatigue crack growth in components with ..., Eng Fract Mech (2007), doi:10.1016/j.engfracmech.2007.04.006

[13] Härkegård G. An effective stress intensity factor and the determination of the notched fatigue limit. In: Bäcklund J, Blom AF, Beevers CJ, editors. Fatigue thresholds: fundamentals and engineering applications, vol. 2. Engineering Materials Advisory Services Ltd.; 1982. p. 867–79.
[14] Tanaka K, Nakai Y, Yamashita M. Fatigue growth threshold of small cracks. Int J Fract 1981;17(5):519–33.
[15] Hertzberg RW. Deformation and fracture mechanics of engineering materials. 4th ed. John Wiley & Sons, Inc.; 1996.
[16] Green AE, Sneddon IN. The distribution of stress in the neighborhood of a flat elliptical crack in an elastic solid. Proc. Cambridge Phil. Soc. 1950:46.
[17] Härkegård G, Denk J, Stärk K. Growth of naturally initiated fatigue cracks in ferritic gas turbine rotor steels. Int J Fatigue 2005;27(6):715–26.
[18] Newman Jr JC, Raju IS. An empirical stress-intensity factor equation for the surface crack. Engng Fract Mech 1981;15(1–2):185–92.
[19] Walker K. The effect of stress ratio during crack propagation and fatigue for 2024-T3 and 7075-T6 aluminium. In: Effects of environment and complex load history on fatigue life, ASTM STP 462, Philadelphia, 1970, p. 1–14.
[20] Mann T, Tveiten BW, Härkegård G. Fatigue crack growth analysis of welded aluminium RHS T-joints with manipulated residual stress level. Fatigue Fract Engng Mater Struct 2006;29(2):113–22.
[21] Mann T. The influence of mean stress on fatigue crack propagation in aluminium alloys. Int J Fatigue 2007. doi:10.1016/j.ijfatigue.2006.11.010.
[22] Mann T. Fatigue assessments methods for welded structures and their application to an aluminium T-joint. PhD thesis, NTNU, Trondheim, Norway, 2006.
[23] Breat JL, Murdy F, Pineau A. Short crack propagation and closure effects in A508 steel. Fatigue Engng Mater Struct 1983;6(4):349–58.
[24] Mann T, Härkegård G, Stärk K. Short fatigue crack growth in aluminium alloy 6082-T6. Int J Fatigue 2007. doi:10.1016/j.ijfatigue.2007.01.00.
[25] Suresh S. Fatigue of materials. 2nd ed. Cambridge University Press; 1998.
[26] Miller KJ. The behaviour of short fatigue cracks and their initiation. Part I – A review of two recent books. Fatigue Engng Mater 1987;10(1):75–91.
[27] Miller KJ. The behaviour of short fatigue cracks and their initiation. Part II – A general summary. Fatigue Engng Mater 1987;10(2):93–113.
[28] Borrego LP, Ferreira JM, Costa JM. Fatigue crack growth and crack closure in an AlMgSi alloy. Fatigue Fract Engng Mater Struct 2001;24(4):255–65.
[29] Shah RC, Kobayashi AS. Stress intensity factor for an elliptical crack under arbitrary normal loading. Engng Fract Mech 1971;3(1):71–93.
[30] Nilsson L. Stress intensity factors for semi-elliptical surface cracks in plates subjected to a complex stress field. Technical Report 1401-5331, SAQ Kontroll AB, Stockholm, Sweden, 1998.
[31] Dai DN, Hills DA, Härkegård G, Pross J. Simulation of the growth of near-surface defects. Engng Fract Mech 1998;59(4):415–24.
[32] Fjeldstad A, Härkegård G, Wormsen A. The influence of a stress gradient on the growth of a fatigue crack. In: Johnson WS et al., editors. Proceedings of the international fatigue congress 2006. Atlanta, Georgia, USA.: Elsevier; 2006. May.
[33] Dai DN, Nowell D, Hills DA. Eigenstrain methods in 3-D crack problems; an alternative integration procedure. J Mech Phys Solids Struct 1993;41(6):1003–17.
[34] Atkinson HV, Shi G. Characterization of inclusions in clean steels: a review including the statistics of extreme methods. Prog Mater Sci 2003;48:457–520.
[35] Coles S. An introduction to statistical modeling of extreme values, 3rd ed. Springer Series in Statistics, London, 2001.
[36] Anderson CW, Coles SG. The largest inclusions in a piece of steel. Extremes 2002;5:237–52.
[37] Anderson CW, de Maré J, Rootzén H. Methods for estimating the sizes of large inclusions in clean steels. Acta Mater 2005;53(8):2295–304.
[38] Sakai T, Sato Y, Nagano Y, Takeda M, Oguma N. Effect of stress ratio on long life fatigue behaviour of high carbon chromium bearing steel under axial loading. Int J Fatigue 2006;28(11):1547–54.
[39] Shi G, Atkinson HV, Sellars CM, Anderson CW. Application of the generalized Pareto distribution to the estimation of the size of the maximum inclusion in clean steels. Acta Mater 1999;47(5):1455–68.
[40] Shi G, Atkinson HV, Sellars CM, Anderson CW. Comparison of extreme value statistics methods for predicting maximum inclusion size in clean steel. Ironmak Steelmak 1999;26(4):239–46.
[41] Beretta S, Murakami Y. Statistical analysis of defects for fatigue strength prediction and quality control of materials. Fatigue Fract Engng Mater Struct 1998;21(9):1049–65.

Please cite this article in press as: Fjeldstad A et al., Simulation of fatigue crack growth in components with ..., Eng Fract Mech (2007), doi:10.1016/j.engfracmech.2007.04.006

Paper 8

A reanalysis of Frost's classical fatigue tests on self-arresting cracks at notches

A. Fjeldstad*, A. Wormsen and G. Härkegård.
Norwegian University of Science and Technology, Trondheim, Norway.

Abstract

In this paper, a short crack growth model is presented and used for predicting the arrest of cracks growing in stress gradient fields. The crack growth model makes use of an effective stress which can be interpreted as the stress that must be applied to the corresponding smooth semi-infinite cracked plate to obtain the same value of the stress intensity factor as for the considered notched configuration. The short crack growth model has been used for predicting the conditions, under which crack initiation, crack arrest and failure are expected to occur. These predictions have been compared with experimentally obtained data for notched specimens of mild steel. The predictions are found to be in good agreement with the experimental data.

Keywords: short crack growth model, effective stress, crack arrest.

NOTATION

a	crack depth
a'	crack depth at transition between shallow and deep crack asymptotes
a_0	intrinsic crack depth
C	coefficient of crack growth law
d	notch depth
F_0	geometry factor for a crack emanating from a smooth surface
K	stress intensity factor
ΔK_{th}	threshold stress intensity range
ΔK_{eq}	equivalent stress intensity range
K_{t}	gross stress concentration factor $= \sigma_{\max}/\sigma_\infty$
m	exponent of crack growth law
ρ	notch root radius
σ_{A}	intrinsic fatigue limit
σ_∞	remote gross stress
$\bar{\sigma}$	effective stress

1 Introduction

In the late fifties, Frost [**1**] carried out a celebrated series of fatigue tests on notched specimens of mild steel. He noticed that cracks, which initiated at the root of the notch, either continued to grow to failure or arrested at some depth below the notch. Thus, in agreement with later observations by Kitagawa and Takahashi [**2**] on *smooth* specimens, cracks were consistently observed in specimens, where the notch strss amplitude exceeds the ordinary, 'intrinsic' fatigue limit, σ_{A}. However, in severely notched specimens, Frost observed that fatigue cracks were arrested and became 'non-propagating', when the applied stress amplitude fell below some critical level. By plotting the fatigue limit of a *smooth* specimen with a (short) surface crack against the depth of the crack, Kitagawa and Takahashi [**2**] found the fatigue limit to be a steadily decreasing function of the depth, with the intrinsic fatigue limit given by the short crack asymptote. The results by Kitagawa and Takahashi are in good qualitative agreement with a fracture mechanics model by El Haddad et al. [**3**] for a through-crack in a homogeneous stress field. According to El Haddad et al., the long crack asymptote is given by the threshold for crack growth, ΔK_{th}.

In an attempt to understand the mechanisms behind Frost's observations, Smith and Miller [**4**]used ΔK_{th} to predict the critical level, below which a fatigue crack becomes non-propagating. This gave acceptable agreement for relatively deep cracks ($a > 1.3$ mm) investigated by Frost. However, for smaller cracks, with a depth approaching the intrinsic crack depth, the direct use of ΔK_{th} would overpredict the critical level. Moreover, since fatigue crack *growth* was not modelled by Smith and Miller, they could not explicitly treat the transition from initial crack growth to crack arrest.

In [**5**], the present authors generalised El Haddad's model to cover the case of a crack of arbitrary shape in an inhomogeneous stress field, e.g., a semi-elliptic crack at the root of a notch. In conjunction with the fatigue-crack-growth law by Klesnil and Lukas [**6**], the generalised model was found to agree well with the growth of short (and long) surface cracks observed in a steel and in an aluminium alloy. In the following it will be shown that the short-crack-growth model of [**5**] is able to model the transition from initial crack growth to crack arrest.

*Corresponding author: Department of Engineering Design and Materials, Norwegian University of Science and Technology, Richard Birkelandsvei 2B, Trondheim, NO-7491 , Norway; email: Arne.Fjeldstad@ntnu.no

Predictions of crack initiations and crack arrest will be compared with the results from the classical fatigue tests by Frost [**1**].

2 Modelling the arrest of fatigue cracks

2.1 A model for the growth of short fatigue cracks

The use of stress intensity factors was extended to fatigue problems by Paris and Erdogan [**7**], who suggested a power-law relationship between the crack growth rate $\mathrm{d}a/\mathrm{d}n$ and the stress intensity range ΔK. Klesnil and Lukáš [**6**] suggested the following equation to extend Paris' law into the near-threshold region:

$$\frac{\mathrm{d}a}{\mathrm{d}n} = C(\Delta K^m - \Delta K_{\mathrm{th}}^m). \tag{1}$$

C and m are material parameters, and ΔK_{th} is the threshold stress intensity range. For a crack in a homogeneous, normal stress field, σ, the stress intensity factor may be expressed in terms of the crack depth, a, and the geometry, F_0, as

$$K = F_0 \sigma \sqrt{\pi a}. \tag{2}$$

A compilation of fatigue tests by Kitagawa and Takahashi [**2**] clearly shows that the fatigue limit of a cracked solid can be determined by means of the threshold of the stress intensity range, ΔK_{th}, for long cracks only. Thus, for short cracks, the fatigue limit asymptotically approaches the ordinary fatigue limit, $\Delta\sigma_{\mathrm{A}} = 2\sigma_{\mathrm{A}}$, as determined by means of a smooth specimen. Both the long and the short crack fatigue limits are asymptotically satisfied by an equation proposed by El Haddad et al. [**3**] for $F_0 = 1$, and generalised by Härkegård [**8**] to an arbitrary geometry factor F_0, viz.

$$\Delta\sigma = \frac{\Delta K_{\mathrm{th}}}{F_0\sqrt{\pi(a+a_0)}} = \frac{\Delta\sigma_{\mathrm{A}}}{\sqrt{1+a/a_0}}. \tag{3}$$

The characteristic crack length, a_0, which signifies the transition between short cracks, $a < a_0$, and long cracks, $a > a_0$, is defined by

$$a_0 = \frac{1}{\pi}\left(\frac{\Delta K_{\mathrm{th}}}{F_0\Delta\sigma_{\mathrm{A}}}\right)^2. \tag{4}$$

One may interpret a_0 as an 'intrinsic' crack length, which should be added to the length of the real crack to yield an 'equivalent' crack length.

Based on the observation [**9, 10**] that short cracks grow faster than long cracks at a given stress intensity level, El Haddad et al. [**3**] introduced an equivalent stress intensity range that accounts for the elevated crack growth rate of short cracks, viz.

$$\Delta K_{\mathrm{eq}} = F_0\Delta\sigma\sqrt{\pi(a+a_0)} \tag{5}$$

Strictly speaking, equations (3) and (5) are only valid for a crack growing in a homogeneous stress field. It would therefore be of great interest to extend the theory by El Haddad et al. to handle crack growth in inhomogeneous stress fields. This can be done by replacing the homogeneous stress range $\Delta\sigma$ with an effective stress range, $\Delta\bar{\sigma}$. This is defined as the stress range that must be applied to the corresponding smooth semi-infinite plate to obtain the same stress intensity range as that of the crack at the root of the notch, cf. Fig. 1. The effective stress range is defined as

$$\Delta\bar{\sigma} = \frac{\Delta K}{F_0\sqrt{\pi a}}. \tag{6}$$

For a shallow edge through-crack, $F_0 = 1.122$ [**11**], and for a semi-elliptic surface crack with aspect ratio $a/c = 1$, the geometry factor at the deepest point of the crack front has the value $F_0 = 0.663$ [**12**].

The preceding equations explicitly depend on the characteristic crack length, a_0, which, in its turn, depends on the crack geometry factor, F_0. The latter will not be constant, if the crack shape changes. This inconvenience can be avoided by substituting $F_0^2 a_0$ and $F_0^2 a$ from equations (6) and (4), respectively, into equation (5). After some rearrangement, one obtains

$$\Delta K_{\mathrm{eq}} = \Delta K_{\mathrm{th}}\left[\left(\frac{\Delta K}{\Delta K_{\mathrm{th}}}\right)^2 + \left(\frac{\Delta\bar{\sigma}}{\Delta\sigma_{\mathrm{A}}}\right)^2\right]^{1/2}. \tag{7}$$

By replacing ΔK in equation (1) by the equivalent stress intensity range of equation (7), one obtains a crack-growth law that accounts for the growth of a short crack in an inhomogeneous stress field, viz.

$$\frac{\mathrm{d}a}{\mathrm{d}n} = C\Delta K_{\mathrm{th}}^m\left[\left\{\left(\frac{\Delta K}{\Delta K_{\mathrm{th}}}\right)^2 + \left(\frac{\Delta\bar{\sigma}}{\Delta\sigma_{\mathrm{A}}}\right)^2\right\}^{m/2} - 1\right]. \tag{8}$$

This equation predicts a finite crack-growth rate as soon as $\Delta\bar{\sigma} > \Delta\sigma_{\mathrm{A}}$, even for a crack of vanishing depth. Using equation (8), Fjeldstad et al. [**5**] were able to unify $\mathrm{d}a/\mathrm{d}n$-data for long and short crack in a low-alloy steel [**13**] and in an aluminium alloy [**14**].

2.2 Crack arrest at notches

The stress field decreases rapidly ahead of a notch and may cause a decreasing crack growth rate for a propagating crack. Fig. 2 shows the normalised equivalent stress intensity factor, $\Delta K_{\mathrm{eq}}/\Delta K_{\mathrm{th}}$, against the normalised crack depth, a/d, for a circumferentially notched specimen subject to tension-compression. The effective stress range $\Delta\bar{\sigma}$ has been calculated as [**15**]

$$\Delta\bar{\sigma} = \Delta\sigma_\infty\sqrt{1+\frac{d}{a}\left[1-\exp\left(-\frac{a}{a'}\right)\right]}, \tag{9}$$

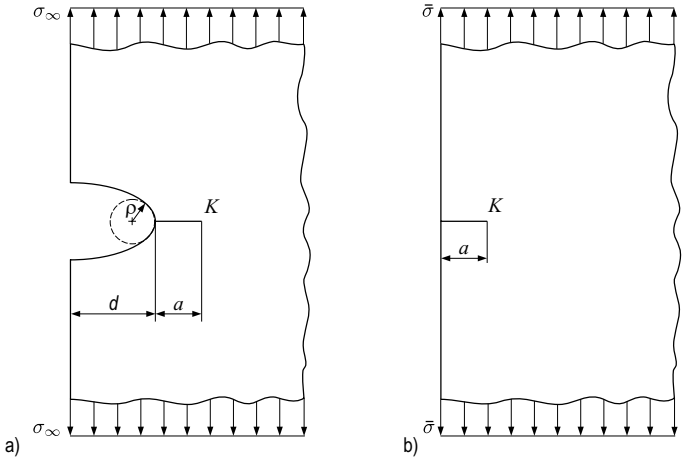

Figure 1: When subjected to the effective stress, $\bar{\sigma}$, the edge-crack of the smooth plate (b) has the same stress intensity factor, K, as that of the crack of the notched plate (a) subjected to the remote stress σ_∞.

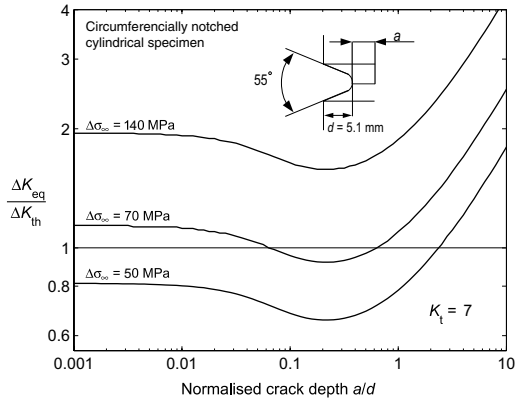

Figure 2: $\Delta K_{\rm eq}/\Delta K_{\rm th}$ versus a/d at three different stress ranges. The curves are obtained by using $\Delta\sigma_{\rm A} = 430$ MPa and $\Delta K_{\rm th} = 13$ MPa$\sqrt{\rm m}$ for $R = -1$.

where the transition crack depth a' is defined by

$$a' = \frac{d}{K_{\rm t}^2 - 1};\ K_{\rm t} = \frac{\sigma_{\max}}{\sigma_\infty}. \tag{10}$$

The stress intensity range, ΔK, is then found by means of equation (6) using $F_0 = 1.122$, i.e., assuming a circumferencial crack of constant depth. In Fig. 2, $\Delta K_{\rm eq}/\Delta K_{\rm th}$ has been presented for three different stress ranges. The upper curve illustrates a situation, where the crack starts to grow from the notch root and continues to grow until final failure. The intermediate curve shows crack initiation and growth, until $\Delta K_{\rm eq}$ falls below $\Delta K_{\rm th}$ and the crack arrests. The lower curve corresponds to a situation, where no crack is initiated.

3 Analysis of Frost's classical fatigue test data

3.1 Comparison of predictions with test data

The existence of crack arrest for short cracks growing from the root of a notch has been experimentally confirmed by Frost [**1**]. The experimental data reported in [**1**] will be compared with predictions from equation (8). The mild steel specimens tested are shown in Fig. 3. The specimen in Fig. 3(a) was subjected to fully reversed tension-compression, while the specimen in Fig. 3(b) was subjected to rotating bending. Both specimens were machined with different notch root radii in order to obtain different $K_{\rm t}$ values. The plain tension-compression fatigue limit of the mild steel was reported to be $\Delta\sigma_{\rm A} = 430$ MPa [**1**]. According to Smith and Miller [**4**], the threshold stress intensity range, $\Delta K_{\rm th}(R = -1)$, for the mild steel considered is 13 MPa$\sqrt{\rm m}$. Based

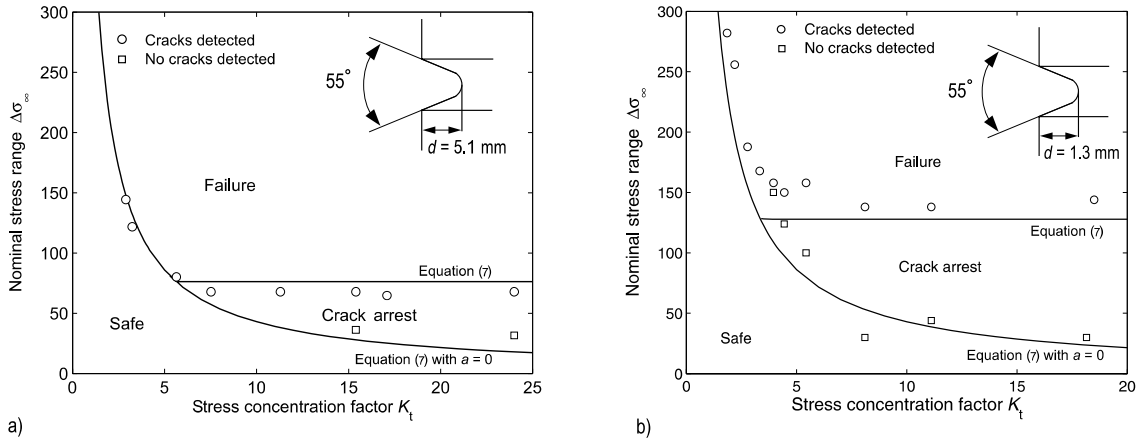

Figure 4: Fatigue regimes in notched components according to the short crack growth model [equation (8)]. The experimental data are from cylindrical specimens of mild steel with notch depth (a) $d = 5.1$ mm [Fig. 3(a)] and (b) $d = 1.3$ mm [Fig. 3(b)] **[1, 16]**.

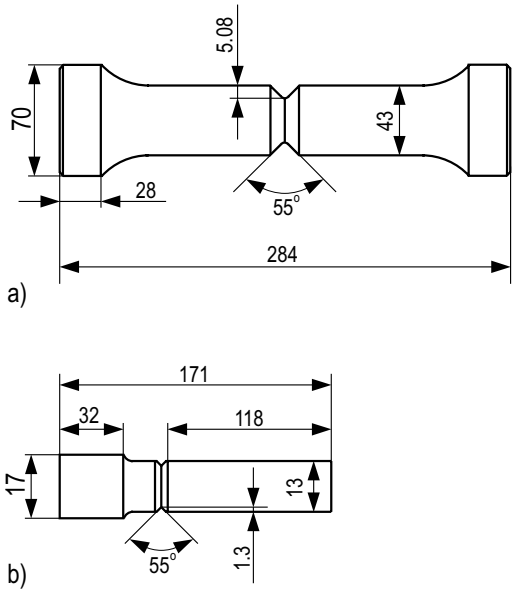

Figure 3: Cylindrical fatigue test specimens subjected to (a) fully reversed tension-compression and (b) rotating bending **[1, 16]**.

on a metallographic examination, Frost **[1]** found that the cracks initiated with an approximately uniform depth around the complete periphery for both types of specimens. Frost's data **[1]** are presented in Fig. 4 together with curves predicted by equation (8). The predictions are carried out by assuming a crack of constant depth around the complete periphery. Fig. 4 is divided into three regions **[4]**: (*i*) one in which no crack will be formed, (*ii*) one in which crack arrest will occur, and (*iii*) one in which a crack will be formed and propagate to failure. As can be seen, the proposed crack growth model agrees very well with the experimental data. Moreover, the crack growth model reveals the change in fatigue limit of notched specimens of the same notch depth d but different notch root radii ρ. Note that the stress level separating the propagation and crack arrest regimes is independent of the stress concentration factor K_t above a certain value of K_t. It is clearly seen that the threshold stress level, at which no crack arrest will occur, is higher for the specimen with notch depth $d = 1.3$ mm than for the specimen with $d = 5.1$ mm.

3.2 Some remarks

The peak stress level needed to form a crack at the root of the notch is low and the degree of notch root plasticity is therefore so small that it could be neglected.

The solid line that defines the boundary between crack arrest and complete failure in Fig. 4 has been obtained by neglecting the effect of notch root plasticity.

The following points summarises the present Section:

- Crack arrest can be predicted by the short crack growth model.

- A crack emanating from the root of a notch, below a certain stress concentration factor, will propagate to failure if the stress range exceeds the fatigue limit.

- Above a certain K_t value the stress level separating the propagation and crack arrest regimes are nearly independent of the stress concentration factor.

- Although no effect of notch plasticity is taken into account in the analysis, the crack growth predictions agrees very well with Frost's experimental data.

4 Conclusions

A short crack growth model has been used to predict the conditions for crack initiation, crack arrest and failure for notched cylindrical specimens of mild steel. The crack growth model uses an effective stress, which is interpreted as the stress that must be applied to the corresponding semi-infinite cracked plate to obtain the same stress intensity factor value as for the notched configuration considered. These analyses show that crack arrest is expected to occur below a certain stress range, which depends on the notch geometry. The predictions are found to be in good agreement with experimental data reported by Frost [**1**].

Acknowledgments

The authors gratefully acknowledge the research support for this work provided by the Research Council of Norway (NFR) and the industrial participants within the NorLight project, and GE Energy (Norway) AS.

References

[1] **Frost, N. E.** A relation between the critical alternating propagation stress and crack length for mild steels. *Proceedings of the Institution of Mechanical Engineers*, 173:811–827, 1959.

[2] **Kitagawa, H.** and **Takahashi, S.** Applicability of fracture mechanics to very small cracks or the cracks in early stage. In *Proceedings of the Second International Conference on the Mechanical Behaviour of Materials*, pages 627–631, Boston, Ma., 1976.

[3] **El Haddad, M. H.**, **Topper, T. H.**, and **Smith, K. N.** Prediction of non-propagating cracks. *Engineering Fracture Mechanics*, 11(3):573–584, 1979.

[4] **Smith, R. A.** and **Miller, K. J.** Prediction of fatigue regimes in notched specimens. *International Journal of Mechanical Sciences*, 20(4):201–206, 1978.

[5] **Fjeldstad, A.**, **Wormsen, A.**, and **Härkegård, G.** Simulation of fatigue crack growth in components with random defects. *Engineering Fracture Mechanics*, doi:10.1016/j.engfracmech.2007.04.006, 2007.

[6] **Klesnil, M.** and **Lukáš, P.** Influence of strength and stress history on growth and stabilisation of fatigue cracks. *Engineering Fracture Mechanics*, 4(1):77–92, 1972.

[7] **Paris, P. C.** and **Erdogan, F.** A critical analysis of crack propagation laws. *Journal of Basic Engineering*, 85:528–534, 1963.

[8] **Härkegård, G.** An effective stress intensity factor and the determination of the notched fatigue limit. In J. Bäcklund, A. F. Blom, and C. J. Beevers, editors, *Fatigue thresholds: fundamentals and engineering applications, volume II*, pages 867–879. Engineering Materials Advisory Services Ltd, 1982.

[9] **Pearson, S.** Initiation of fatigue cracks in comercial aluminium alloys and the subsequent propagation of very short cracks. *Engineering Fracture Mechanics*, 7(2):235–247, 1975.

[10] **Dowling, N. E.** Crack growth during low cycle fatigue of smooth axial specimens. In *ASTM-STP 637*. American Society for Testing and Materials, ASTM, 1978.

[11] **Tada, H.**, **Paris, P. C.**, and **Irwin, G. R.** *The stress analysis of cracks handbook*. Professional Engineering Publishing Limited, Bury St. Edmunds and London, 3rd edition, 2000.

[12] **Newman, Jr. J. C.** and **Raju, I. S.** An empirical stress-intensity factor equation for the surface crack. *Engineering Fracture Mechanics*, 15(1-2):185–192, 1981.

[13] **Breat, J. L.**, **Murdy, F.**, and **Pineau, A.** Short crack propagation and closure effects in A508 steel. *Fatigue of Engineering Materials & Structures*, 6(4):349–358, 1983.

[14] **Mann, T.**, **Härkegård, G.**, and **Stärk, K.** Short fatigue crack growth in aluminium alloy 6082-T6. *International Journal of Fatigue*, doi: 10.1016/j.ijfatigue.2007.01.002, 2007.

[15] **Wormsen, A.**, **Fjeldstad, A.**, and **Härkegård, G.** The application of asymptotic solutions to a semi-elliptical crack at the root of a notch. *Engineering Fracture Mechanics*, 73(13):1899–1912, 2006.

[16] **Frost, N. E.** and **Dugdale, D. S.** Fatigue tests on notched mild steel plates with measurements of fatigue cracks. *Journal of the Mechanics and Physics of Solids*, 5(3):182–188, 1957.